CHEMICAL VAPOR INFILTRATION IN SIC FIBER PREFORM: A STUDY OF EFFECT OF PORE ORIENTATION

by
Rajagopalan Balaji

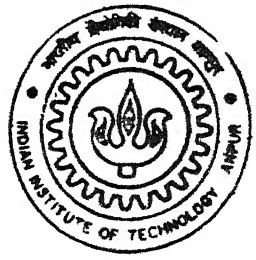

DEPARTMENT OF MATERIALS AND METALLURGICAL ENGINEERING
INDIAN INSTITUTE OF TECHNOLOGY KANPUR

January, 2000

Dedicated

to

My Parents

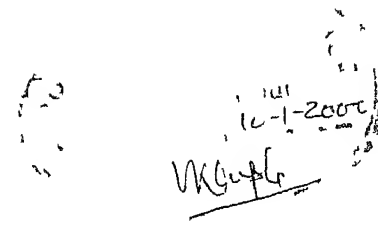

CERTIFICATE

It is certified that the work contained in the thesis titled CHEMICAL VAPOR INFILTRATION IN SiC FIBER PREFORM: A STUDY OF EFFECT OF PORE ORIENTATION by Rajagopalan Balaji has been carried out under my supervision and this work has not been submitted elsewhere for a degree.

Dr Deepak Gupta
Asstt.Professor
Deptt.of Materials & Metallurgica
Engineering
Indian Institute of Technology,
Kanpur-208016

TABLE OF CONTENTS

ABSTRACT

Ceramic matrix composites are promising materials for applications in a wide temperature range, from ambient to a very high temperature Many of such composites are known for their excellent mechanical and chemical properties at an elevated temperature In addition, these materials are light weight and retain their mechanical strength at high temperatures

In the recent past, chemical vapor infiltration (CVI) has emerged as a promising method for processing ceramic matrix composites, in which the matrix is chemical vapor deposited in a fibrous preform

Processing of ceramic matrix composites depends upon many process variables, such as temperature, temperature gradient, pressure, flow rate of precursor gas, structure of preform (that is, nature of pore network), and concentration of precursor gas

In the present work a model is developed for diffusion in porous media and it is applied to study the effect of pore orientation in the deposition of SiC preform by SiC matrix

The model uses the Dusty gas model for describing diffusion which takes into account binary diffusion, Knudsen flow, and viscous flow The concept of orientation averaging for diffusion of species in a porous media is applied The porous medium is divided into many elemental volume each containing pores oriented in a specified direction and by applying the orientation averaging method the porous medium is represented by a piece wise homogeneous medium

We consider four cases of pores orientations at angles of $\phi = 0^0$, 45^0, 90^0 and 135^0 and the various combinations included pores in single, two, three and four

directions The studies are carried out at a temperature of 1200 K for the initial pore radius of 2 5 μm The initial porosity for different pore orientations ranged from 0 3 to 0 45

The results show that open-ended pore and pores inclined to the surface of the preform enhance the densification of the preform

ACKNOWLEDGEMENTS

I would like to express my deep sense of gratitude to Dr Deepak Gupta for his invaluable guidance throughout my M Tech programme It is because of his constant encouragement and motivation, I could accomplish some fruitful results in my thesis work I am always grateful to him for sparing his precious time and providing valuable suggestions at each point

I would like to pay my sincere regards to Dr R K S Rathore, Dr M Katiyar and Dr B Deo for providing motivation and encouragement during the thesis work

I am thankful to all my senior especially Mr Kaliprasad, Mr S B Rao and Mr alok Srivastava for giving me proper guidance and support whenever I needed it I also thanks my classmates, especially Prabhanjan, Murali, Girija, Kaushik and Pavitda for giving me a good company and making my stay, at IIT Kanpur, a pleasant and memorable one

lastly, I Thank Anshu for rescuing me in my last days by editing my work and sparing his valuable time for me I am really indebted to him for sparing his valuable time for me

Rajagopalan Balaji

LIST OF FIGURES

CHAPTER 1

INTRODUCTION

Ceramic matrix composites are promising material for applications in a wide temperature range, from ambient to a very high temperature Many of such composites are known for their excellent mechanical and chemical properties at an elevated temperature In addition, these materials are light weight and retain their mechanical strength at high temperatures Thus, they find applications in heat generators, turbines and space systems[1]

Processing of ceramic matrix composites can be classified into two categories In the first category, the fiber-matrix preform is prepared by slurry infiltration or sol-gel method and then the preform is either hot pressed or sintered In the other category, the composites are prepared by melt infiltration or chemical vapor infiltration (CVI)

In the slurry infiltration method, the fiber tow is passed through a slurry mixture, constituting of a carrier liquid, matrix powder and a binder, which is usually an organic compound The tow is subsequently dried, cut and stacked one above the other in a desired configuration Then, the composite is made by sintering or hot pressing the stack In the sol-gel process, the fiber is dispersed in the sol The gel material is allowed to dry to form a porous ceramic, which is then densified by sintering Both the methods suffer from serious problems A major disadvantage of the slurry process is damage to the fiber during hot pressing, where the temperature is high On the other hand, sol-gel processing involves a large volume shrinkage during drying and also during densification firing stage Furthermore, the yield of ceramic material is low

These disadvantages can be overcome by processing ceramic composites by melt infiltration or chemical vapor infiltration However, melt infiltration is of a limited utility in producing ceramic matrix composites, because it requires melting of the matrix material, which in most cases melts at a very high temperature

In the recent past, chemical vapor infiltration (CVI) has emerged as a promising method for processing ceramic matrix composites In this process, the matrix is chemical vapor deposited in a fibrous preform Thus, the process is a specialized form of chemical vapour deposition (CVD) process, except that here, instead of gas flow over the surface, the precursor gases, diffuse into a porous preform made up of fibers Chemical reaction at the pore wall leads to the deposition of the matrix material

The chemical vapor infiltration process has many advantages over the other processes Fabricating composites using this process requires only atmospheric pressure and low temperatures compared to other processes, thus minimizing damage to the fibrous preform

1 1 LITERATURE REVIEW

From here on we focus on fabrication of SiC fiber-SiC matrix composites by CVI This composite has a high strength and elastic modulus, and exhibits good mechanical strength associated with high strain-to-failure Also, SiC composites are resistant to high temperatures, and have high thermal conductivity, and low thermal expansion, which provides good thermal shock resistance[2, 3]

Trichloromethylsilane (TMS) is used as a precursor gas in fabricating SiC/SiC composites[3, 4] The matrix is deposited by thermal decomposition of TMS in excess of hydrogen[5] The decomposition reaction proceeds according to

CH_3SiCl_3 (g) = SiC (s) + 3HCl (g) (in excess of H_2)

Chemical vapor infiltration process for fabricating SiC/SiC composites can be classified into four categories[1]

Isothermal chemical vapor infiltration (ICVI)[4, 6]

Thermal gradient chemical vapor infiltration[7]

Forced flow chemical vapor infiltration (FCVI)[8, 9]

Pulse flow chemical vapor infiltration[10]

In isothermal chemical vapor infiltration (ICVI), the preform is maintained at a uniform temperature in a chamber and the precursor gas is flown over the preform[4] The major disadvantage in this process is that, at high temperatures, a preferential deposition occurs on the surface layer, leaving behind a large internal porosity In order to reduce the residual porosity, if the process is conducted at a lower temperature, it takes longer time to densify the preform

This difficulty is overcome in thermal gradient CVI, where a temperature gradient is applied across the thickness of the preform, and the gases diffuse through the low temperature end[7] This procedure allows densification such that deposition front move from high temperature end to the low temperature end

In FCVI[8], the precursor gas is forced through the preform in which a temperature gradient is also maintained In yet another process, as in the previous case called pulse flow CVI, pulsed flow of precursor gas is caused by cyclic evacuation of the reaction chamber and back filling with precursor gas[10]

Despite the mentioned disadvantages for ICVI, it is frequently used because a large number of parts of different sizes and shapes can be easily made and also very irregular shapes can be fabricated using this process This process is commercially used in the fabricating high performance brakes for aerospace applications[1]

In the following, I review various models for diffusion in porous media and chemical vapor infiltration process related to SiC composites The models for diffusion of species in porous media can be broadly classified into two approaches, discrete and continuum In the first approach, the porous media is treated as a discrete collection of objects, such as voids and grains In the continuum models, porous media is treated as a continuum were temperature, concentration, and solid species concentration vary smoothly with respect to position and time[11]

Among the discrete approaches, use of percolation theory is common Reyes and Jenson[12] simulated pore related properties in porous media using the concept of percolation theory on a bethe lattice They evaluated effective transport coefficients without introducing a tortousity factor Their model inherently accounted for narrow necks, tortuous path and dead ends

Another approach called "Effective medium approximation (EMA)," was originally applied by Landauer[13] to find the effective electrical conductivity of a bimetal-strip Subsequently, Kirckpatrick[14] used this theory to find electrical conductivity of a random resistor network

Burganos and Storichos[16] applied EMA (or EMT) to find the effective conductance of the pore network and, by assuming that network of pores satisfies the smooth field approximation (SFA), they applied these conductivities to find effective diffusivity in the pore network Sotirchos[17] further developed the model by adding convection along with diffusion in a porous media Pedro et al [18] then extended the EMA theory for anisotropic lattice structures

Two main approaches used in continuum models are dusty gas model and capillary model In "dusty gas model"[19-21], the solid is treated as another heavy immobile gas, which is uniformly distributed in the medium By treating the medium

as a heavy immobile gas, transport properties are calculated by applying the kinetic theory to all the gas species including the "dust gas" The binary diffusion coefficient between the dust gas and another gas particles is equivalent to Knudsen diffusion coefficient Further the viscous flow arising from pressure build up is also included in the mass flux expression Thus, the flux expression includes all, the multicomponent ordinary diffusion, Knudsen diffusion and viscous flow Therefore, the model applies well to diffusion in the transition regime However, the effect of structure of the porous medium is included only as empirical parameters in molecular, Knudsen and viscous flow

Though dusty gas model gives satisfactory results, its ability to deal with the structure of porous medium is not fully developed

Another important model in the continuum approach is Feng and Stewart's[21-22] capillary model They represented the medium by a network of pore, which is thoroughly cross linked By assuming the species concentration and pressure to vary smoothly with respect to position and time, they evaluated the flux of a species for a fraction of all pores aligned in a particular orientation and of a given radius Then, the total flux for a species was calculated by integrating the flux over all orientations and radii However, the flux expression was based on dusty gas model and, in addition, the model also included surface diffusion in the flux expression Thus, Feng and Stewart's model was the first attempt to include the effect of pore network in the dusty gas model

Apart from capillary model, grain model is also used where solid phase consists of spherical particles or grains Evangelos et al [23] modeled a gas-solid reaction with partially overlapping grains, each consisting of a hard core and a soft shell in which fluid could penetrate or diffuse Only the soft shells were allowed to

overlap with each other as the reaction proceeded This approach was verified their model by comparing with the experimental data for the reaction of ZnO particles with 0 5% H_2S in N_2 at 600^0C

Another model involves volume averaging of transport properties over a domain involving solids and voids Using the volume-averaging model Jin et al [24] studied the phenomenon of diffusion in the media consisting of glass sphere, mica particle and disks made of mylar sheets

Another frequently used model to describe porous media is pore network model Hollewand and Gladden[25] modeled a random network of pore to study the problem of diffusion and reaction occurring simultaneously in a porous catalyst Tortuosity is a common parameter in modeling a porous media and result from this model suggests that the tortuosity obtained under strong diffusion control cannot be applied to the condition where both diffusion control as well as reaction control is important In another work the same authors compared random and regular network using percolation and finite scaling theory[26] and found that random pore model had greater percolation threshold They also developed a random micro and macro pore network by connecting the micropore to macropore and obtained experimentally matched tortuosity Reckmann and Keil[27] modeled a three dimensional pore network with predefined pore radii, connectivity and porosity for any type of reaction Dusty gas model was used for calculating mass transport in a pore Fuertes and Marben[28] used random pore model, incorporating percolation phenomenon to analyze gasification reaction when percolation takes place simultaneously Zhang and Seaton[29] compared the diffusion coefficient obtained by continuum model to that from pore network model to investigate the effectiveness of using continuum diffusion –reaction model to describe diffusion and reaction in pore network When

the pore network was very close to percolation threshold, the continuum diffusion-reaction model failed

Pavol and Yang[30] used bethe lattice to represent the porous media They used percolation model of mass transport in the network and applied effective medium theory to find the effective diffusivity of condensable vapor in porous media, where condensation and adsorption-desorption hysteries occurred

In addition to various models to treat transport in a porous media, we now provide a review on modeling of chemical vapor infiltration of SiC Gupte and Tsamapoulos[31] modeled mass transport and deposition of SiC by chemical vapor infiltration, in a single pore Their model predicts negligible effect of pressure on deposition as long as the pressure is below 0 5 atm and a temperature less than 1000^0C, if isothermal chemical vapor infiltration is used The authors also modeled deposition using temperature gradient and found that small temperature gradient enhances the densification process

Lu[32] studied the effect of a structural parameter and theile module on densification using a random pore structure model In that work, the structural parameter is a non-dimensional quantity which depends on surface area of the pore, porosity and total pore length He found that a smaller value of theile module leads to more uniform deposition, whereas pore plugging occurrs at high theile module and structural parameter Further, substance having wide pore distribution was found to offer more resistance to diffusion as deposition proceeds (that is after initial deposition)

Chung and smith[33] modeled deposition of SiC by chemical vapor infiltration on a sample of overlapping fibrous preform Their model assumed diffusion to occur in channels formed between the fibers, space between stacked mats and channel

formed due to stacking of mats one on top of another Comparing two cases in model, where in one channels are aligned straight and are staggered in the other, the former alignement leads to a lower porosity

Deepak and Evans[34] modeled deposition of SiC from trichloromethylsilane in a porous preform in which thermal gradient was achieved by microwave heating Dusty gas model was used for describing mass transport in the preform They suggest that at least one dimension of the preform should be short for gas to diffuse through the preform Lower temperature, and larger pore size favored uniform deposition of matrix material, but required longer time for densification Also temperature gradient favors more densification in less time Kawasi[35] et al fabricated SiC whisker reinforced alumina composite by chemical vapor infiltration technique, where the core was heated to 1100^0C at a total pressure of 3 3-13 kpa Preform surface was cooled by radiation as well as convection due to gas flowing around the preform surface The authors also modeled isothermal and thermal gradient CVI by employing cubic array of whiskers Pore plugging occurred in both the cases, but isothermal process had premature pore plugging compared to thermal gradient process Comparing both the cases, thermal gradient process greatly reduced the processing time

Chang et al [36] studied the effect of reaction mechanism in the chemical vapor infiltration for production of SiC composites by considering different reaction model for deposition of SiC They inferred that first-order kinetic model is not correct for predicting the infiltration process by showing influence of chlorine containing by-products in delaying the infiltration time Use of alternate method of precursor chemistry, which avoids chlorine containing by-products, was suggested for minimizing infiltration time Tai et al [37] also considered the influence of deposition

mechanism in FCVI Two different reaction mechanisms were considered for deposition A Zero-order reaction mechanism with activation energy of 188 kJ/mol and a first –order reaction mechanism with activation enrergy of 120 kJ/mol were adopted for comparision The deposition mechanism was found to effect the density distribution in the preform More uniform densification was observed when first – order reaction mechanism was considered, but rapid densification occurred for the case of zero-order mechanism They concluded that assumption of reaction mechanism affects not only the infiltration time, but also the theoretical matrix deposition

Ofori and Sotrichos[38] studied the effect of multicomponent mass transport on the densification of SiC/SiC composites, using dusty gas model for describing transport in the fibrous preform They compared various variation of dusty gas model by neglecting the interaction of TMS, HCl, and H_2 for two cases, one by including viscous flow and the other by neglecting the viscous flow The study showed that interaction of HCl with TMS influences the deposition, as diffusion of TMS into the preform is impeded by diffusion of HCl out of the preform It was also demonstrated that full dusty gas model should be used unless both temperature and pressure are low The same authors also simulated 2-D, 3-D CVI models for densification of preform with uniform porosity and an anisotropic preform (Fibers oriented in one or two dimensions) for studying the effect of preform anisotropy, aspect ratio and shape of the preform[39] They observed difference in deposition for anisotropic structure (having cubic shape) in different direction when it reached percolation threshold For large aspect ratio of the preform, deposition in the preform was influenced by gases diffusing through the small sides of the preform, whereas the gases diffusing along the longer length of the preform effected only the outer surface Shape of the preform

also influenced the deposition of the gas in the preform, more uniform deposition was seen in regular shape(Like cube) Thus they favored multidimensional model to be used for simulation unless mass transport is identified to be occurring in a dominant direction

The effect of pore structure during densification of SiC/SiC composites was also studied by Ofori and Sotirchos[40] Two models were considered, one in which pores were represented as cylindrical capillaries randomly oriented in all the three directions and another the solid phase was represented by fibers oriented in one, two and three dimensions In the later case fiber orientation and direction of diffusion were found to effects the overall diffusion coefficients and percolation threshold(that is minimum porosity left which cannot be filled) For the case were capillary were used to model the porous media, the deposition rate was dependent on the pore size distribution The model suggested that use of bi-modal capillary structure (that is, two different sizes of capillaries were used to represent porous media) is more applicable for simulating a chemical vapor infiltration process The effect of mass transport on optimal pressure and temperature pair that can be used for minimum infiltration time was also studied by the same authors[41] The optimal pressure for CVI under condition of diffusion driven transport was found to be larger than that used in the industrial CVI process Optimal pressure was found to be located at the molecular diffusion regime, and as a result, it tends to increase with decreasing pore size It was found that optimal temperature for densification decrease significantly with increasing deposition uniformity in the final product, final conversion level at the external surface, reverse rate constant and the preform size Mole fraction of the precursor gas also was found to have a strong influence on processing time

1 2 OBJECTIVE OF THE PRESENT STUDY

Processing of ceramic matrix composites depends upon many process variables, such as temperature, temperature gradient, pressure, flow rate of precursor gas, structure of preform (that is, nature of pore network), concentration of precursor gas Optimizing these process variables not only reduces the infiltration time, but also affects the structure of matrix material deposited, ultimately affecting the properties of the composite

Preform for fabrication of composite material consists of pores, which are to be filled by CVI Although at microscopic level, the diffusion is isotropic, but at this level it is not possible to model diffusion and deposition because this scale is shorter than the pore radius Therefore, models are built at a scale much larger than the pore radius However, then at this scale, the effect of pore network make diffusion apparently anisotropic

In the present work, I propose to model a porous medium by representing the pore network as a piece wise homogeneous medium The basic idea is to use orientation averaging method, similar to that by Feng and Stewart[22] But this model differs from the model of Feng and Stewart in the way the porous media has been represented Feng and stewart represented the whole domain as a homogeneous medium, whereas I will be dividing the porous medium into a number of smaller units and by performing orientation averaging in each volume element I will represent the pore network as a piece wise homogeneous medium As an application of the model developed, I apply the model to a SiC/SiC system

The objective of the present study is to

- Represent a porous media consisting of network of pores aligned in various orientation by an effective homogeneous media consisting of finite number of elemental volume
- Study the effect of orientation of network of pores on the deposition of SiC in a SiC preform by chemical vapor infiltration

- Represent a porous media consisting of network of pores aligned in various orientation by an effective homogeneous media consisting of finite number of elemental volume
- Study the effect of orientation of network of pores on the deposition of SiC in a SiC preform by chemical vapor infiltration

CHAPTER 2

MODEL FOR CHEMICAL VAPOR INFILTRATION FOR SiC COMPOSITES

This chapter discusses mass transport and chemical reaction in a porous media constituting of a capillary network by orientation averaging method The method is used with a goal to represent a porous medium with an effective homogenous medium In this model orientation averaging is done on a second phase (pores in porous media) and an effective equivalent homogenous medium is represented through an anisotropy tensor developed in the following sections

2 1 DIFFUSION IN A HOMOGENOUS MEDIA

Consider diffusion of v gaseous components in a homogenous volume β If we define diffusion velocity of species i in an arbitrary coordinate system as,

$$\mathbf{V}_i = \mathbf{v}_i - \mathbf{v}_0 \tag{1}$$

The expression for $\mathbf{V}_i$, based on Chapman-Enskog theory of gases [42] is derived to be,

$$\mathbf{V}_i = \frac{n^2}{n_i \rho} \sum_{j=1}^{v} m_j D_{ij} \mathbf{d}_j \tag{2}$$

in which thermal diffusion is neglected and where the quantity $\mathbf{d}_j$ is defined as,

$$\mathbf{d}_j = \nabla x_j + \left(\frac{n_j}{n} - \frac{n_j m_j}{\rho} \right) \nabla \ln P - \frac{n_j m_j}{P\rho} \left(\frac{\rho}{m_j} \mathbf{F}_j - \sum_k n_k \mathbf{F}_k \right) \tag{3}$$

Further, we can write the mass diffusion flux from equation (2) as,

$$\mathbf{J}_i = \frac{n^2 m_i}{\rho} \sum_j m_j D_{ij} \mathbf{d}_j \tag{4}$$

Coupled with an equation for total momentum balance (such as the Navier-Stokes equation) and an appropriate boundary condition on $\partial\beta$, the fluxes can be determined in the volume β. However, the problem is much more complicated when the volume β consists of pores rather than a homogenous medium because the diffusion occurs preferentially along the direction of the pores. But, it is still possible to solve equation (4) if the structure of the porous media were known in complete detail. Unfortunately, it is not always practical to solve the fluxes on the same dimensional scale as the pores.

Therefore, the purpose of the following development is to piece wise homogenize the porous media occupying volume, in order to account for the anisotropic nature of the diffusion caused by the structure of the porous media.

2.2 MATHEMATICAL DEVELOPMENT

Consider a volume β which is riddled with cylindrical pores, where a pore is defined as a void with one dimension much longer than the other two. We subdivide the volume β into N smaller regions β_α, such that,

$$\beta = \sum_{\alpha=1}^{N} \beta_\alpha$$

and the radii of the pores in each volume element is same, while in order to take advantage of homogenization, variation in the pore radius is allowed from one element to another

We define two coordinate systems [x] and [x′], related to each other through rotation of axes by an angle θ and ϕ as described in Appendix (A) [x] is the global coordinate system in which the diffusion flux is expressed after homogenization (averaging) Now, consider a pore in β_α with its longest dimension (length) along $[x_3']$ Thus, [x′] is the local coordinate system associated with a pores and, hence, molecular diffusion flux given by equation (4) can be easily expressed in this coordinate system Since the other two dimensions $(x_1' \text{ and } x_2')$ of the pores are short, it is reasonable to neglect the gradients of mole fractions, and pressure in these directions

Thus, equation (4), the diffusion flux in a pore is expressed as,

$$J_i^{'p} = \frac{n^2 m_i}{\rho} \sum_j m_j D_{ij} \underline{\underline{L}} d'_j \tag{5}$$

where,

$$\underline{\underline{L}} = \begin{pmatrix} 0 & 0 & 0 \\ 0 & 0 & 0 \\ 0 & 0 & 1 \end{pmatrix}$$

and

$$d'_j = \nabla' X_j + \left(\frac{n_j}{n} + \frac{n_j m_j}{\rho} \right) \nabla' \ln P - \frac{n_j m_j}{P\rho} \left(\frac{\rho}{m_j} F'_j - \sum_k n_k F'_k \right) \tag{6}$$

Introducing $\underline{\underline{L}}$ allows for a non-zero flux only in the $[x_3']$ direction

The primed quantities are expressed in $[x']$ and the superscript p on the diffusion flux is used to designate that this flux is only in one pore

We now transform the vector quantities expressed in the local coordinate system of the pore, $[x']$, to the global coordinate system $[x]$ Thus, according to the transformation, equation (5) is written as

$$\mathbf{J}_i^p = \underline{\underline{\mathbf{M}}}^T \left[\frac{n^2 m_i}{\rho} \sum_j m_j D_{ij} \underline{\underline{\mathbf{L}}}\,\underline{\underline{\mathbf{M}}}\,\mathbf{d}_j \right]$$

or,

$$\mathbf{J}_i^p = \underline{\underline{\mathbf{M}}}^T \underline{\underline{\mathbf{L}}}\,\underline{\underline{\mathbf{M}}} \left[\frac{n^2 m_i}{\rho} \sum_j m_j D_{ij} \mathbf{d}_j \right] \tag{7}$$

and $\mathbf{d}_j$ is now expressed in $[x]$, and the mass diffusion flux, $\mathbf{J}_i^p$, represents the diffusion of a component i in a pore oriented in the (θ,ϕ) direction (subsequently called direction g) In the following section, a procedure based on orientation averaging is developed to add the contribution, weighted over an orientation distribution function, from many pores such that β_α can be treated as an effective homogenous media

We now represent the mass flux in the Cartesian coordinate system Thus, it is reasonable to take β_α as a cuboid with L_1, L_2 and L_3 as the length of the three sides along the $x_1, x_2,$ and x_3 direction and A_1, A_2 and A_3 as the area of the faces perpendicular to these three axes, respectively Furthermore, suppose there are $dN(g,\ell)$ pores in orientation $[g, g+dg]$ and of length $[\ell, \ell+d\ell]$ Then, the rate of mass diffusion is, $\mathbf{J}_i^p(g,\ell)\,a\,dN(g,\ell)$, where 'a' is the cross sectional area of each pore

Thus, the mass diffusion flux, expressed over the superficial area of a volume element, is given by

$$d\mathbf{J}_i(g,\ell) = a\, dN(g,\ell)\,\ell \begin{pmatrix} \frac{1}{L_1 A_1}\frac{L_1}{\ell} & 0 & 0 \\ 0 & \frac{1}{L_2 A_2}\frac{L_2}{\ell} & 0 \\ 0 & 0 & \frac{1}{L_3 A_3}\frac{L_3}{\ell} \end{pmatrix} \mathbf{J}_i^p(g,\ell) \qquad (8)$$

Where, ℓ is the length of the pores in the orientation g Also, since $L_1A_1 = L_2A_2 = L_3A_3$ is the volume of β_α equation (8) is therefore, rewritten as,

$$d\mathbf{J}_i(g,\ell) = d\varepsilon(g,\ell)\underline{\underline{\mathbf{P}}}\,\mathbf{J}_i^p(g,\ell) \qquad (9)$$

where,

$$\underline{\underline{\mathbf{P}}} = \begin{pmatrix} \frac{L_1}{\ell} & 0 & 0 \\ 0 & \frac{L_2}{\ell} & 0 \\ 0 & 0 & \frac{L_3}{\ell} \end{pmatrix}$$

is a dyad which accounts for reduced (increased) diffusion due to longer (shorter) pores

In writing this equation, we have assumed that a pore both begin and ends at $\partial\beta_\alpha$ Thus only those pore are considered which are connected

2 3 ORIENTATION AVERAGING

We define an orientation distribution function such that $f(g,\ell)dgd\ell$ is the fraction of porosity in dg oriented along g and of length between ℓ and $\ell+d\ell$ Expressing it mathematically, we have

$$\frac{d\varepsilon(g,\ell)}{\varepsilon}=\frac{1}{4\pi}f(g,\ell)dgd\ell \tag{10}$$

and since the distribution function is normalized, therefore, it satisfies the following equation

$$\frac{1}{4\pi}\int_0^{2\pi}\int_0^{\pi}\int_0^{\ell} f(\theta,\phi,\ell)\sin\theta\, d\ell d\theta\, d\phi = 1 \tag{11}$$

Thus, using equation (9), we write the total flux in β_α expressed over its superficial area as,

$$\mathbf{J}_i=\varepsilon\int_0^{2\pi}\int_0^{\pi}\int_0^{\ell}\underline{\underline{\mathbf{P}}}\,\mathbf{J}_i^p(\theta,\phi)f(\theta,\phi,\ell)\sin\theta\, d\ell d\theta\, d\phi \tag{12}$$

In order to evaluate the integral in equation (12), we make an assumption that in β_α the term, d_j appearing in equation (7) is constant Thus, an upper limit on the size of β_α is determined by ensuring the validity of this assumption However, it must be noted that the flux is calculated this way only in a β_α and that these fields may vary from one volume element to another Further, after combining equation (7) and (12), the mass diffusion flux in the homogenized volume is given by

$$\mathbf{J}_i^p=\langle\underline{\underline{A}}\rangle\left[\frac{n^2 m_i}{\rho}\sum_j m_j D_{ij}\,\mathbf{d}_j\right] \tag{13}$$

where,

$$\langle \underline{\underline{A}} \rangle = \frac{\varepsilon}{4\pi} \int_0^{2\pi} \int_0^{\pi} \int_0^{\ell} \underline{\underline{P}} \left(\underline{\underline{M}}^T \underline{\underline{L}} \underline{\underline{M}} \right) f(\theta, \phi, \ell) \sin\theta \, d\ell d\theta d\phi \tag{14}$$

is the anisotropy tensor

The anisotropy tensor, which is expanded in appendix (B) and the mass diffusion flux in an effective homogenous volume, derived in equation (13), applies to any β_α Hence equation (13) and (14) represent the transformation of mass flux in a porous media to piece-wise homogenous media of dimension L_1, L_2 and L_3 along the three respective axes An advantage of this procedure is obtained when the scales L_1, L_2 and L_3 are much larger than the spacing between the pores Yet a β_α must be kept small to the extent that the concentration gradient remain constant within the β_α

The multicomponent diffusion coefficients in equation (13) are a spatially dependent quantities Moreover, the value of diffusivity reported in literature is generally for the binary diffusion coefficient Although the two diffusion coefficients are related, because of the reasons, given above, it is often inconvenient to use equation (13)

Hirschfelder et al [42] have shown that the equation (4), even in the presence of non-isobaric diffusion can be manipulated to obtain a set of generalized stefan-maxwell equation, which contains the binary diffusion coefficient instead of the multicomponent diffusion

Similarly in presence of $\langle \underline{\underline{A}} \rangle$, equation (13) becomes,-

$$\frac{1}{n} \sum_j \frac{1}{m_i m_j \vartheta_{ij}} \left(X_i m_i \mathbf{J}_j - X_j m_j \mathbf{J}_i \right) = \langle \underline{\underline{A}} \rangle \mathbf{d}_i \tag{15}$$

The equation above represents (v - 1) independent equation in the mass fluxes J and describe multicomponent molecular diffusion in a porous media However, when the pore radius is small, in addition to the molecular diffusion, the viscous flow originating from a pressure buildup and the Knudsen flow are important A model that includes mass transport by these mechanisms is "dusty gas model" An equation similar to the dusty gas model can also be obtained after orientation averaging Following the same method as observed by Mason and Malinauskas[20], from equation (15), we obtain

$$\frac{1}{n}\sum_{j=1}^{v}\frac{1}{\vartheta_{ij}}\left(\frac{X_i J_j}{m_j}-\frac{X_j J_i}{m_i}\right)-\frac{J_i}{nm_i D_{ik}}+\frac{X_i J_v}{\rho D_{ik}}=\langle\underline{\underline{A}}\rangle\left[\nabla X_i+X_i\nabla\ln P-\frac{n_i}{P}\mathbf{F}\right] \tag{16}$$

Also, after using a procedure similar to orientationally averaging the diffusion flux, the viscous flux, based of fully developed Poiseuille flow, is given as

$$J_v=-\langle\underline{\underline{A}}\rangle\frac{\rho R^2}{8\eta}\left(\nabla P-\sum_{j=1}^{n}n_j F_j\right) \tag{17}$$

2 4 APPLICATION TO CHEMICAL VAPOR INFILTRATION

This section deals with two-dimensional modeling of chemical vapor infiltration (CVI) for production of SiC/SiC composites Orientational averaging method discussed in the previous chapter with "dusty gas model" is used to express the molar fluxes

First a porous preform made up of largely SiC fibers is assumed Then the preform is densified by CVI, where in, the gaseous reactant, trichloromethylsilane(TMS), and the carrier gas, H_2 diffuse into the pores Following chemical decomposition of TMS according to equation (18),

$$CH_3SiCl_3(g) = SiC\ (s) + 3HCl\ (g) \qquad (\text{in excess } H_2) \qquad (18)$$

SiC is deposited on the pore walls The product gas HCl, diffuses out of the pores

In Fig 2 1, we show that a two dimensional region is divided into many volume (area) elements β_α of dimension L_1 and L_2 in x and y direction, respectively Because we model two dimensional arrangement of pores, the third dimension, L_3, could be of any magnitude β_α contains a network of pores of specified orientation, and volume of pores over which chemical reaction takes place is related to volume of β_α ($V_\alpha = L_1 \times L_2 \times L_3$) as

$$V_\alpha^p(t) = \varepsilon_\alpha(t) V_\alpha \qquad (19)$$

And the surface area over which the reaction takes place is given by,

$$S_\alpha = \frac{2\varepsilon_\alpha(t) V_\alpha}{R_\alpha} \qquad (20)$$

In writing equation (20), we have assumed purely cylindrical pores, neglecting the effect of pore intersections

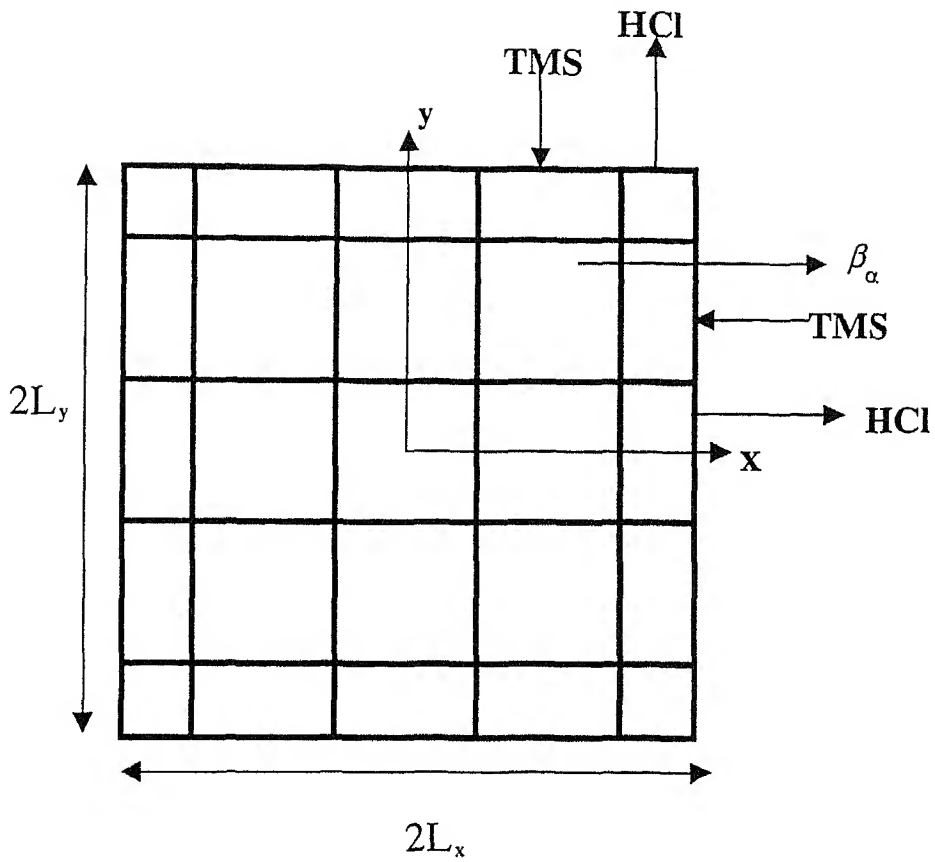

Fig 2 1 Schematic diagram of a preform divided into elemental volume

As the deposition in SiC is described by first-order, heterogeneous kinetics, the deposition of SiC on pore walls in a β_α occurs according to,

$$\frac{1}{-S_\alpha}\frac{dN_{SiC}}{dt} = kcX_1, \qquad (21)$$

where $k = k_0 e^{-E_A/R_gT}$ and the subscript 1 stands for TMS

Making use of equation (4) in a mass balance on TMS we get

$$N^{s}_{1y}L_1L_3 + N^{w}_{1x}L_2L_3 - N^{n}_{1y}L_1L_3 - N^{e}_{1x}L_2L_3 = S_{\alpha}kcX_{1P} \qquad (22)$$

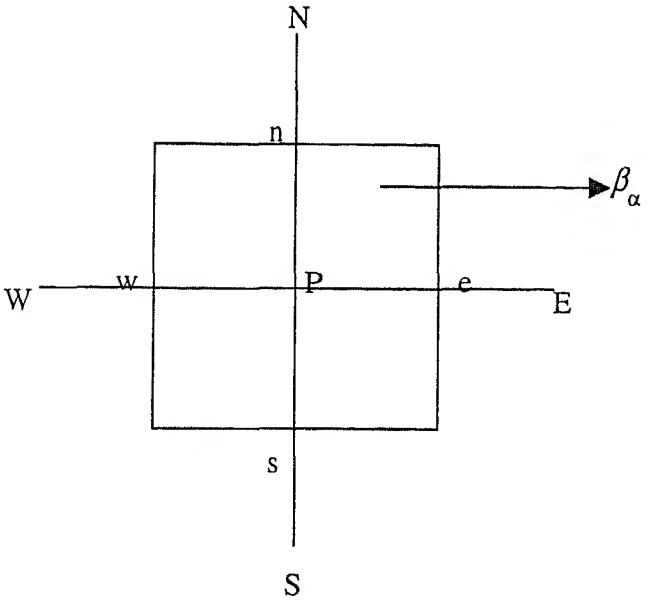

Fig 2 2 Schematic sketch of a control volume

Where L_1, L_2 and L_3 are length, width and the height of the control volume respectively and N_1 is molar flux of TMS The superscript indicates the location at which flux is considered (see Fig 2 2) The equation (22) is solved using the finite difference method

The multicomponent diffusion flux at the points such as p is given according to the dusty gas model, which includes ordinary diffusion, viscous flow and Knudsen flow Detail of this flux expression is available in monograph on the Dusty gas model[20]

In the present analysis, the contribution of thermal diffusion is considered negligible In that case, the dusty gas model based expression for flux for the effective medium in equation (16) is converted to molar fluxes and that reads

$$\frac{1}{c}\sum\frac{1}{\vartheta_{ij}}\left[\, X_j N_i - X_i N_j \,\right] + \frac{N_i}{cD_{ik}} = \langle A \rangle \left[-\nabla X_i - X_i \left[\frac{1}{P} + \frac{R^2}{8\eta D_{ik}} \right] \nabla P \right] \quad (23)$$

for i,j =1,2,3

where the subscript 1, 2 and 3 is reserved for TMS, HCl and H_2, respectively, and D_{ik} is the Knudsen diffusion coefficient for species i The quantities ϑ_{ij}, D_{ik} and η are estimated by the formulae given in Appendix (C)

With an assumption of an ideal gas, the following equation of state holds

$$P = cR_gT \quad (24)$$

Furthermore, from chemical reaction in eq (18), for every one mole of TMS consumed, 3 moles of HCl is produced Therefore in quasi–steady state, we have

$$N_2 = -3N_1 \quad (25)$$

As H_2 does not take part in the reaction , H_2 is stationary and hence

$$N_3 = 0 \quad (26)$$

After explicitly writing eq (22) for species 1, 2 and 3 and then substituting eqs (25) and (26), we get three equations, which are

$$\left[\frac{3X_1}{\vartheta_{12}} + \frac{X_2}{\vartheta_{12}} + \frac{X_3}{\vartheta_{13}} + \frac{1}{D_{1k}} \right] N_1 = \langle A \rangle \left[-c\nabla X_1 - \frac{X_1}{R_gT} \left[1 + \frac{R^2P}{8\eta D_{1k}} \right] \nabla P \right] \quad (27)$$

$$-\left[\frac{3X_1}{\vartheta_{12}} + \frac{X_2}{\vartheta_{12}} + \frac{3X_3}{\vartheta_{23}} + \frac{3}{D_{2k}} \right] N_1 = \langle A \rangle \left[-c\nabla X_2 - \frac{X_2}{R_gT} \left[1 + \frac{R^2P}{8\eta D_{2k}} \right] \nabla P \right] \quad (28)$$

$$\left[\frac{3X_3}{\vartheta_{23}} - \frac{X_3}{\vartheta_{13}}\right] N_1 = \langle A \rangle \left[-c\nabla X_3 - \frac{X_3}{R_g T}\left[1+\frac{R^2 P}{8\eta D_{3k}}\right]\nabla P\right] \quad (29)$$

Where,

$$X_1 + X_2 + X_3 = 1 \quad (30)$$

The eqs (22), (24), and (27)-(30) constituting a system of partial differential equations in variable X_1, X_2, X_3, P and c are solved subject to the boundary conditions discussed below

For a preform symmetrical with respect to **x** and **y** axis, calculation are reduced to only the first quadrant and the boundary conditions are,

at $\mathbf{x} = L_x$ or $\mathbf{y} = L_y$

$X_1 = X_1^0$,
$X_1 = X_2^0$,
$X_3 = X_3^0$,
$c = c^0$,
$P = P^0$

Also, the boundary condition at **x**=0 is $N_v = 0$, and similaraly, the boundary condition at $\mathbf{y} = 0$, is $N_x = 0$

When the entire preform is considered due to lack of symmetry, the boundary conditions are,

At $\mathbf{x} = -L_x$ and L_x or $\mathbf{y} = -L_y$ and L_y,

$X_1 = X_1^0$,
$X_1 = X_2^0$,
$X_3 = X_3^0$,
$c = c^0$,
$P = P^0$

After modifying equation (21) and using equation (19 and 20), the rate of change of radius at any time t, in a control region is given by

$$-\frac{dR_\alpha}{dt}=\frac{M_{SiC}k c_{1\alpha}X_{1\alpha}}{\rho_{SiC}} \qquad (31)$$

where, $R_\alpha = R_0$ at time $t = t_0$ and the subscript α represents the concentration and mole fraction of TMS in the β_α respectively

With the radius in each β_α at a given time, the pore volume $\mathbf{V}_\alpha^p(t)$ is computed and accordingly porosity is obtained by using equation (19)

First the system of equation is solved for $X_1, X_2,$ and P, at each time step and then the radius and the porosity of the pores at each control volume is computed using equation (31) This process is continued till the radius of the pore at the edges and corner of the domain under consideration becomes zero

CHAPTER 3

RESULTS AND DISCUSSIONS

The system of equations (27)-(29), in the preceding chapter, contained five variables X_1, X_2, X_3, c and P The variable c and X_3 were eliminated from these using equations 24 and 30

Thus, the general form of flux expression is,

$$N=\langle A\rangle(\alpha_1\nabla X_1+\alpha_2\nabla X_2+\beta\nabla P),$$

in which the coefficients α_1, α_2 and β are dependent on the variables X_1, X_2, X_3, c and P First, we guessed the values for these variables to compute α's and β and then substituted the flux expression, linear in the gradient of X_1, X_2 and P in equation (22), to obtain a system of finite difference equations A self consistent solution is iteratively obtained when the values guessed to compute α and β are the same as the solution of the finite difference linear equations

Once the concentrations of all the gaseous species and pressure is computed everywhere at a given time, the deposition of SiC in a time step is computed by integrating equation 31 by the fourth order Runge-kutta method

Repeated calculations of concentrations, and then marching forward in time determines the deposition profiles The process of densification ends when the radius of the pores at preform surface becomes zero

The list of properties used in the calculations[34] are given below

Table 1 List of properties used in calculations

Density of Silicon carbide, ρ, kg/m^3	3210
Activation energy, E_A, kJ/mole	120
Pre-exponential factor, k_0, m/s	2 62
Mole fraction of TMS, x_1^0	0 0452
Mole fraction of HCL, x_2^0	0
Pressure, P^0, Pa	$1\ 0133 \times 10^5$

However, the first step in calculations is determining the anisotropy tensor, $\langle A \rangle$, for all the volume elements

3 1 DETERMINATION OF ANISOTROPY TENSOR

As a sample calculation, consider a distribution of pores shown in Fig 3 1, where the bold lines define various β_α and the lighter lines are the pores, the radius of the pores is the same in a β_α but it is allowed to vary from one element to another

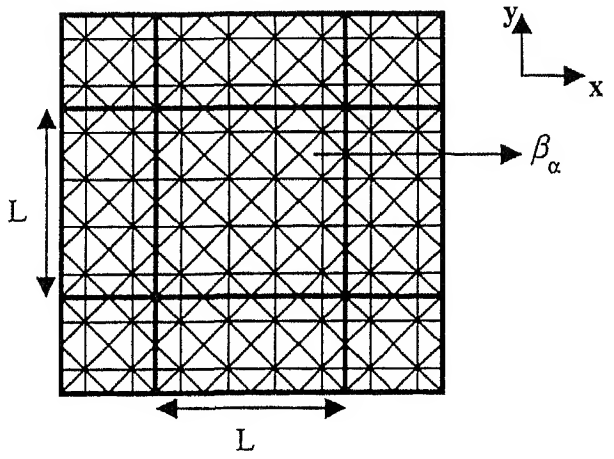

Fig 3 1 Preform with pores in four orientations and divided in smaller elements (β_α), $L_1=L_2=L$

Consider the β_α marked in the figure, where all pores lie in **x-y** plane Thus, for all pores $\theta=90^0$ and the pores are along $\phi = 0^0, 45^0, 90^0$, and 135^0 with respect to the **x**-axis If we define 'n' to be the number of pores, with $\phi = 45^0$ or 135^0, below the longest pore in β_α (n=3 in Fig 3 1), then the total volume of the pores is

$\mathbf{V}_\alpha^p = 2\left(1+\sqrt{2}\right)(n+1)\,\pi R^2 L$, where R the radius of pores

Hence the ODF for this pore arrangement is,

$$f(\theta,\phi,\ell)=\frac{4\pi}{2\left(1+\sqrt{2}\right)(n+1)L}\,\delta\left(\theta-\frac{\pi}{2}\right)$$

$$\left\{\begin{array}{l}\delta(\phi)\left[(n+1)\ell\,\delta(\ell-L)\right]+\delta\left(\phi-\frac{\pi}{2}\right)\left[(n+1)\ell\,\delta(\ell-L)\right]+\delta\left(\phi-\frac{\pi}{4}\right)\left[\ell\,\delta\left(\ell-\sqrt{2}L\right)+2\sum_{i=1}^{n}\ell\,\delta\left(\ell-\frac{\sqrt{2}i}{(n+1)}L\right)\right]+\\ \delta\left(\phi-\frac{3\pi}{4}\right)\left[\ell\,\delta\left(\ell-\sqrt{2}L\right)+2\sum_{i=1}^{n}\ell\,\delta\left(\ell-\frac{\sqrt{2}i}{(n+1)}L\right)\right]\end{array}\right\}$$

and then using this ODF in the equation (14) of chapter 2, the anisotropy tensor obtained is,

$$\langle A\rangle=\varepsilon\begin{pmatrix}\frac{(3n+2)}{2\left(1+\sqrt{2}\right)(n+1)} & 0\\ 0 & \frac{(3n+2)}{2\left(1+\sqrt{2}\right)(n+1)}\end{pmatrix}$$

where ε is the porosity of the element

Similarly, $\langle A\rangle$ is computed for all the elements, and although, in time, the ODF does not change, a change in porosity forces re-computing $\langle A\rangle$ in every time step

3 2 A TYPICAL CALCULATION

The preform dimension in all cases is 1cm × 1cm The third dimension, used only for calculation of porosity, is arbitrary and taken as 0 001 cm, ensuring that it is larger than the initial pore radii, R_0=2 5 μm For the cases in which the orientations of the pores were symmetrical both with respect to the **x**- and **y**-axes, the calculations are only in the first quadrant of the preform Accordingly, the preform is descretized into 51×51 node points and, when full preform is considered due to lack of symmetry, the number of node points is 101x101

Various computer subroutines like NAG, IMSL were used to solve the system of equation The direct subroutine using LU decomposition method, used from NAG consumed a lot of memory to solve the system of equations and, also, it took a long time The iterative subroutines were found to be faster Finally a Bi-congugate gradient method was used to solve the linear system of equations However, the convergence was severely dependent on the initial guessed values To overcome this problem, a direct method was used only at the start of computations to provide good guesses for the subsequent iterations A typical calculation with 51× 51 mesh size required 11-12 Hours in Pentium-2 machine with 192MB RAM

3 3 VALIDITY OF THE NUMERICAL APPROACH

In order to evaluate the accuracy of our calculations, we devised two tests In the first, we take a simple pore structure, all pores are parallel to the **x**-axis, along $\phi = 0^0$ This structure is the first among the total of 11 orientations considered in this work (see Appendix D) For this arrangement of pores, the evolution of instantaneous porosity of the preform normalized by the initial porosity is shown in Fig 3 2 (O1) However, since the pores are non-intersecting, and all of equal length, the results

should be the same whether we apply this orientation averaging method in calculation, or consider just an isolated pore Therefore, to validate our calculations, we wrote a completely different, albeit much simpler, computer program, which takes the original dusty gas flux expression (without any orientation averaging), computes mass transport and deposition in a single pore The curve O1 in Fig 3 2 was reproduced identically in this computation also

Second, we also compared our results with those by Deepak and Evans[44] for a specific case, where pores are aligned along both x- and y-axes (see O6 in Appendix D) The normalized porosity as a function of processing time computed by the model given here is compared with the results in [44] (see Fig 3 3) Clearly, the calculations are only slightly different at all times for all three temperatures The origin of difference lies in the manner the pore volumes have been taken

Deepak and Evans consider only a specific pore structure, in which there are 500 pores in both x- and y- directions in the first quadrant Because the pore structure if specified a priori, they are able to accurately include the volume of intersection of perpendicular pores and the total volume of the pores was $7\ 73 \times 10^{5}$ cm^3 Whereas, in the present work, since the model is for an arbitrary pore structure, we over-estimate the pore volume by counting volume of overlapping pores twice Thus, the initial pore volume for the same structure is $9\ 82 \times 10^{5}$ cm^3, greater than the actual volume In fact, this discrepancy will be even larger when the number of pore intersections is greater However, since a the error in computing initial volume is also introduced in calculating pore volume subsequent time steps, the representation of normalized porosity, that is, $\varepsilon(t)/\varepsilon_o$, is more accurate, accordingly, only a minor difference remains between the two calculations compared in Fig 3 3

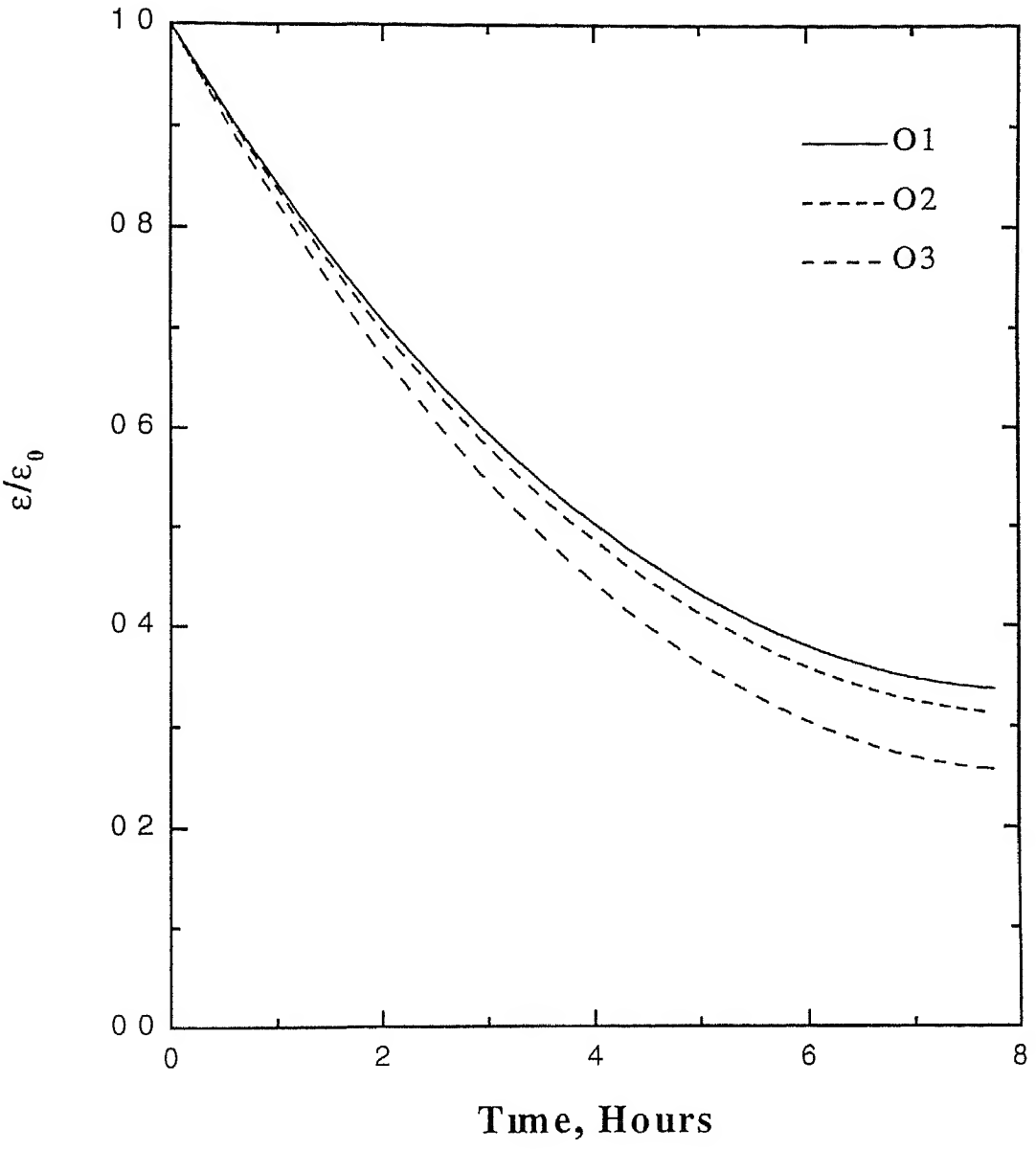

Fig 3 2 Evolution of porosity for pore structures O1, O2 and O3

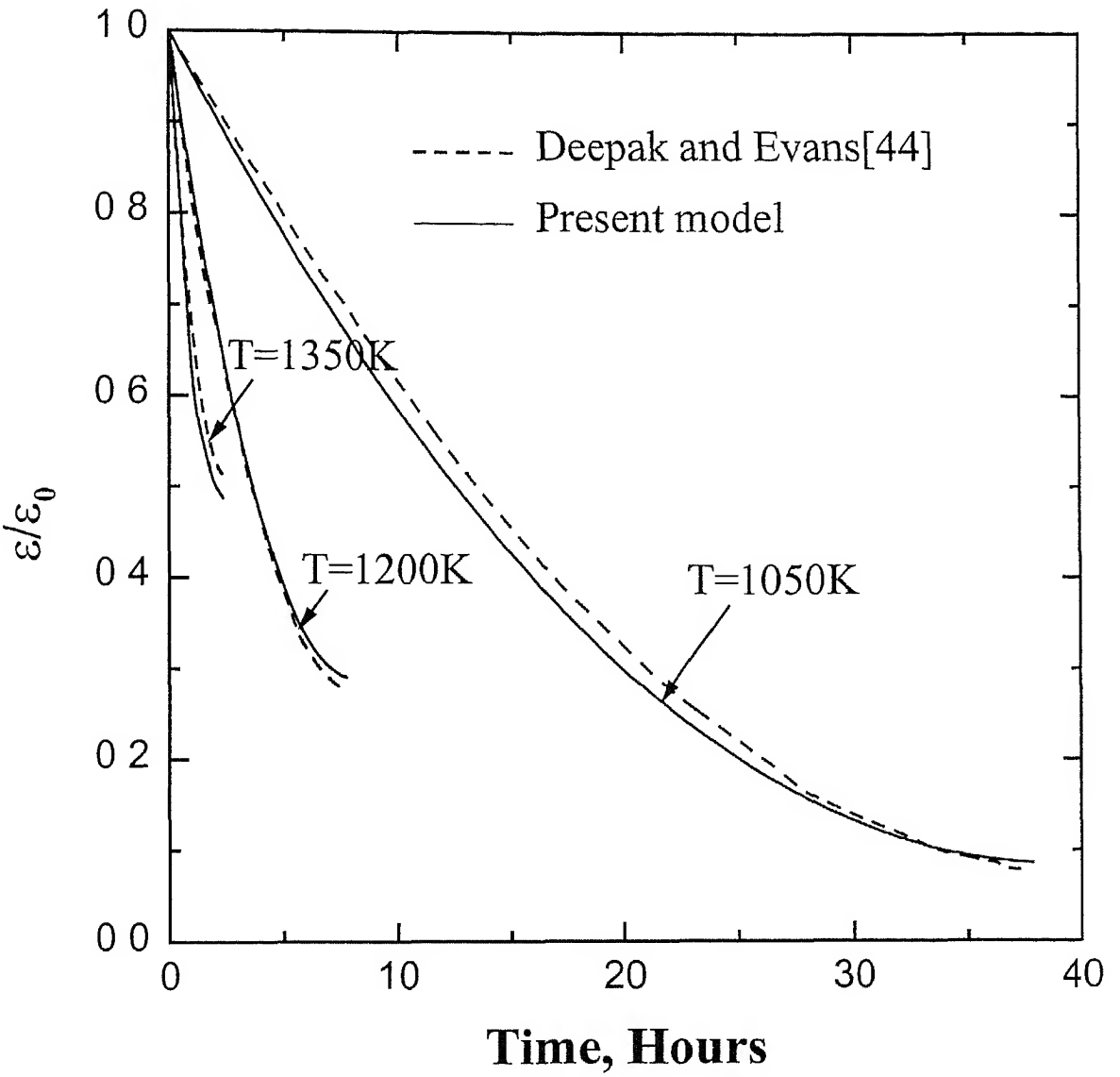

Fig 3 3 A comparison of this work with that of Deepak and Evans[44]

For this specific structure, if L_1 is the length of two intersecting pores associated with each intersection, then the ratio of actual porosity to that in this work is $\left(1-\frac{8}{3\pi}\frac{R}{L_1}\right)$ Thus, the error between the two approaches is less if the pore radius is small or the length associated with each intersection is large (that is, less number of intersections), both of these imply lower volume of intersection Nonetheless, for pore radius 2 5 μm and starting porosity of the preform approximately 0 4, as that considered in this work, the error in calculations due to overestimating volume of intersecting pores is minimal

3 4 EFFECT OF PORE ORIENTATION ON INFILTRATION

In this work we have considered pores in four different orientations, $\phi = 0^0$, 45^0, 90^0, and 135^0 The various combinations include pores only in one, two, three or all four directions In all, there are a total of 11 pore networks, as presented in Appendix E, where, in addition to the pore network, we have given the ODF and the initial porosity The expressions for ODF, and corresponding porosity, are derived in terms on an integer 'n' related to the number of pores The integer 'n' is always odd and when an even number of pores is required, we use n+1 pores A value of 'n' is selected which gives the initial porosity closest to 0 4 Thus, we find the initial porosity of the preform considered in this work varies between 0 33 and 0 45, as represented in Table 2

Table 2 A comparison of infiltration behaviour of pores in various orientations

Orientation number	Initial porosity (ε_0)	Final porosity (ε)	Final normalized porosity ($\varepsilon/\varepsilon_0$)
O1	0 393	0 133	0 337
O2	0 389	0 122	0 313
O3	0 389	0 100	0 257
O4	0 379	0 117	0 295
O5	0 379	0 102	0 269
O6	0 393	0 114	0 291
O7	0 333	0 082	0 246
O8	0 402	0 118	0 294
O9	0 402	0 110	0 274
O10	0 451	0 116	0 257
O11	0 379	0 108	0 284

3 4 1 PARALLEL PORES

First, we consider only the non-intersecting pores There are three such cases, O1–3 In the first case, the pores are only along the x-axis, and symmetry requires calculation only in the first quadrant Because the preform we consider is square in cross-section, an equivalent structure is obtained with all pores aligned along the y-axis In another case, the pores are along $\phi = 45^0$ However, when symmetry is assumed about both the axes, the structure (O2) is different from the case when calculations are on full preform (O3) The latter structure is also equivalent to $\phi = 135^0$

We compare the progress of infiltration for all three orientations in Fig 3 2 Clearly, the pores oriented 45^0 to the x-axis lead to greater densification Furthermore, a comparison of structures O2 and O3 intuitively suggest that the flux

directed to the center of preform in O2 will lead to a greater reduction of porosity than in O3 In Figs 3 4 and 3 5, we have compared the normalized radii for the two cases at the end of the process, and similarly, in Figs 3 6 and 3 7, the normalized local porosity, which is equivalent to ratio of square of local radius divided by square of initial radius of the pores We find, contrary to expectation, the local radii and porosity, and final porosity are all lower for orientation O3 For O3, in quadrant 2 and 4, this can be explained on the basis that flux is received in the pore from both the ends, as opposed to, only from one end in O2 However, when we compare Figs 3 8 and 3 9 with Figs 3 4 and 3 6, respectively, we find even in quadrant 1 and 3, where the pore structure is identical in the two cases, the infiltration is greater for O3 But, in O2, while the porosity is uniformly distributed in all quadrants, in O3, porosity is lower in quadrants 2 and 4 compared to that in quadrants 1 and 3 And, in all quadrants, porosity is lower for O3 than for O2

Finally, densification is greater when the pores are inclined to the preform surface, rather than perpendicular to it (compare O1 to O2 and O3)

3 4 2 PORES IN TWO ORIENTATIONS

First, we have taken pores along $\phi = 0^0$and 45^0 Assuming symmetry about both the axes, this structure is represented in O4, and if the structure is rotated by 90^0, it is equivalent to pores along $\phi = 45^0$ and 90^0 Also, as in the case with single orientation pores, we have removed the symmetry requirement, for pores shown in O5 In addition, we have considered pores that are either perpendicular (O6) or inclined to the axes (O7) In both cases, the structure is symmetric about the two axes

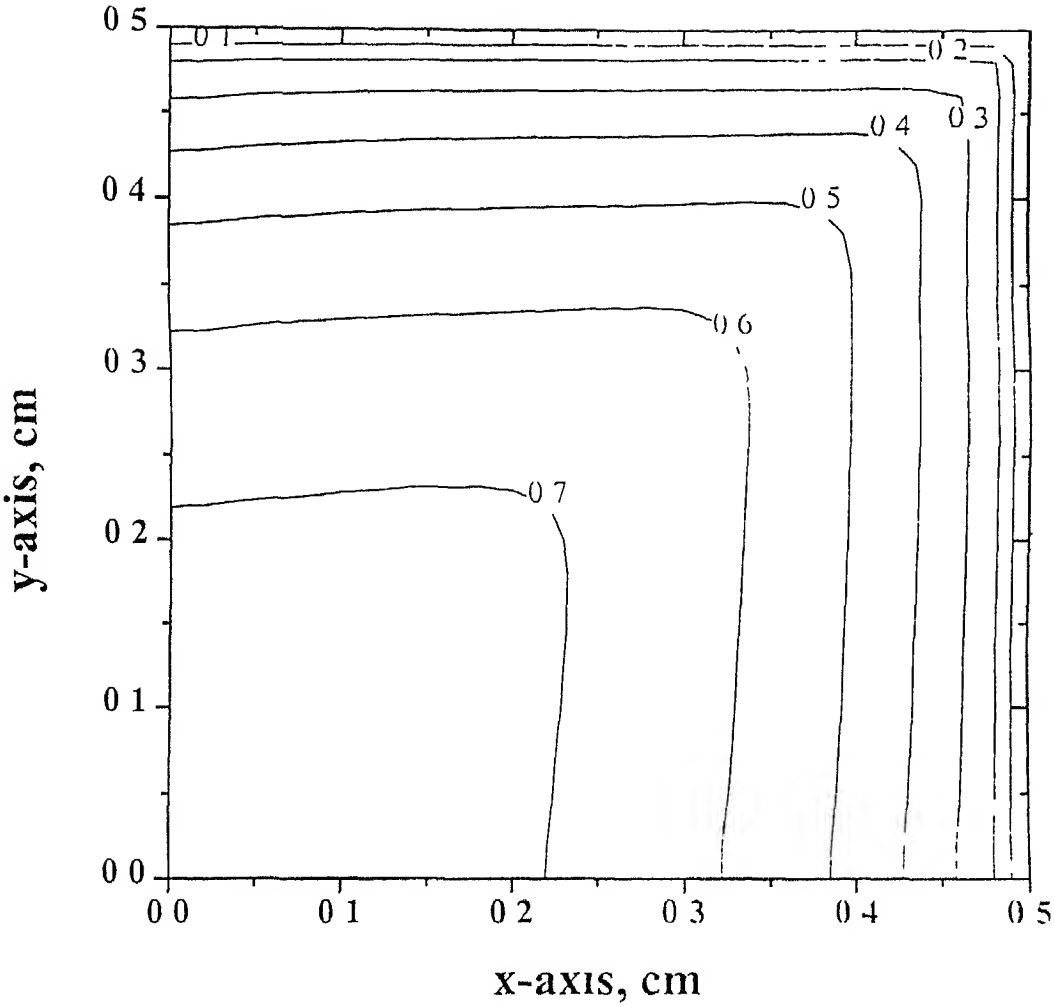

Fig 3 4 Final radius(R/R_0) at the end of infiltration for O2

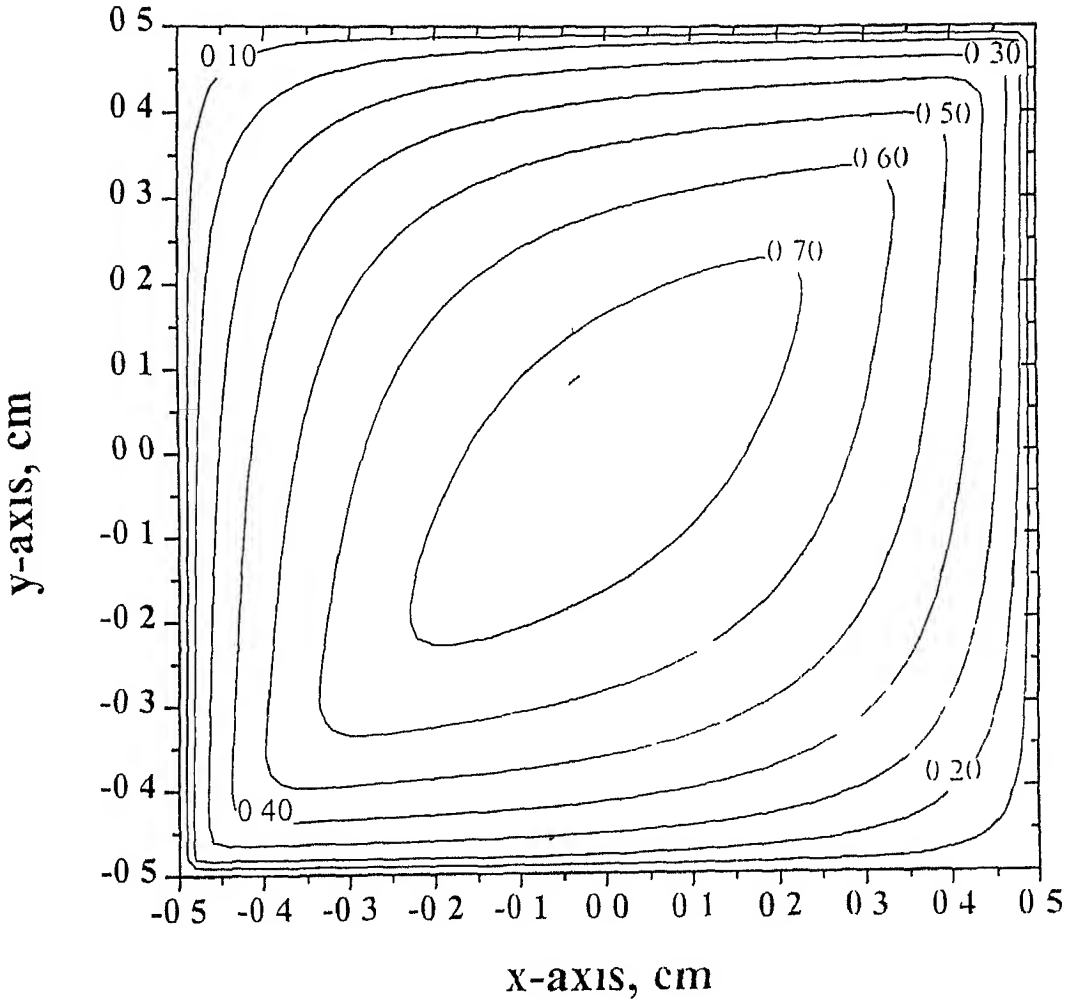

Fig 3 5 Final radius(R/R_0) at the end of infiltration for O3

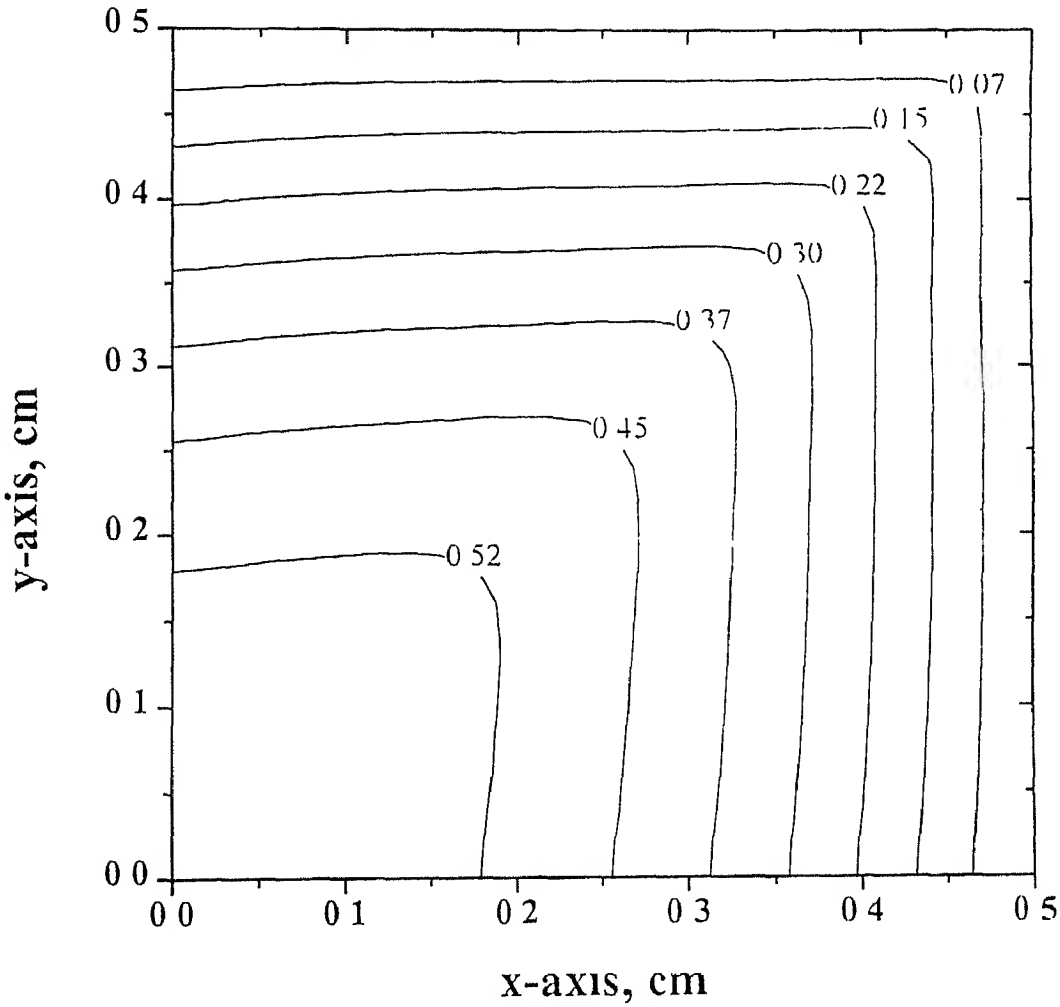

Fig 3 6 Final normalized porosity at the end of infiltration for O2

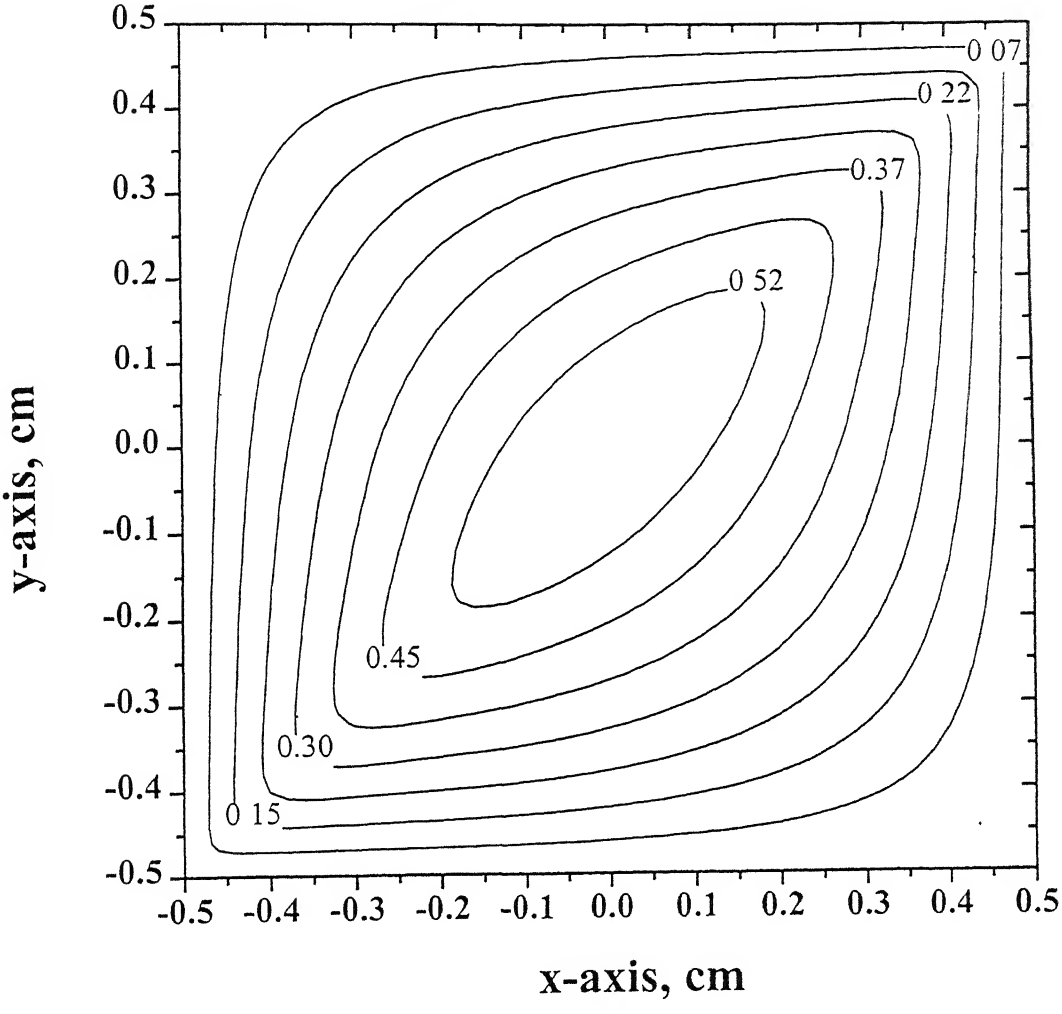

Fig. 3.7: Final normalized porosity at the end of infiltration for O3.

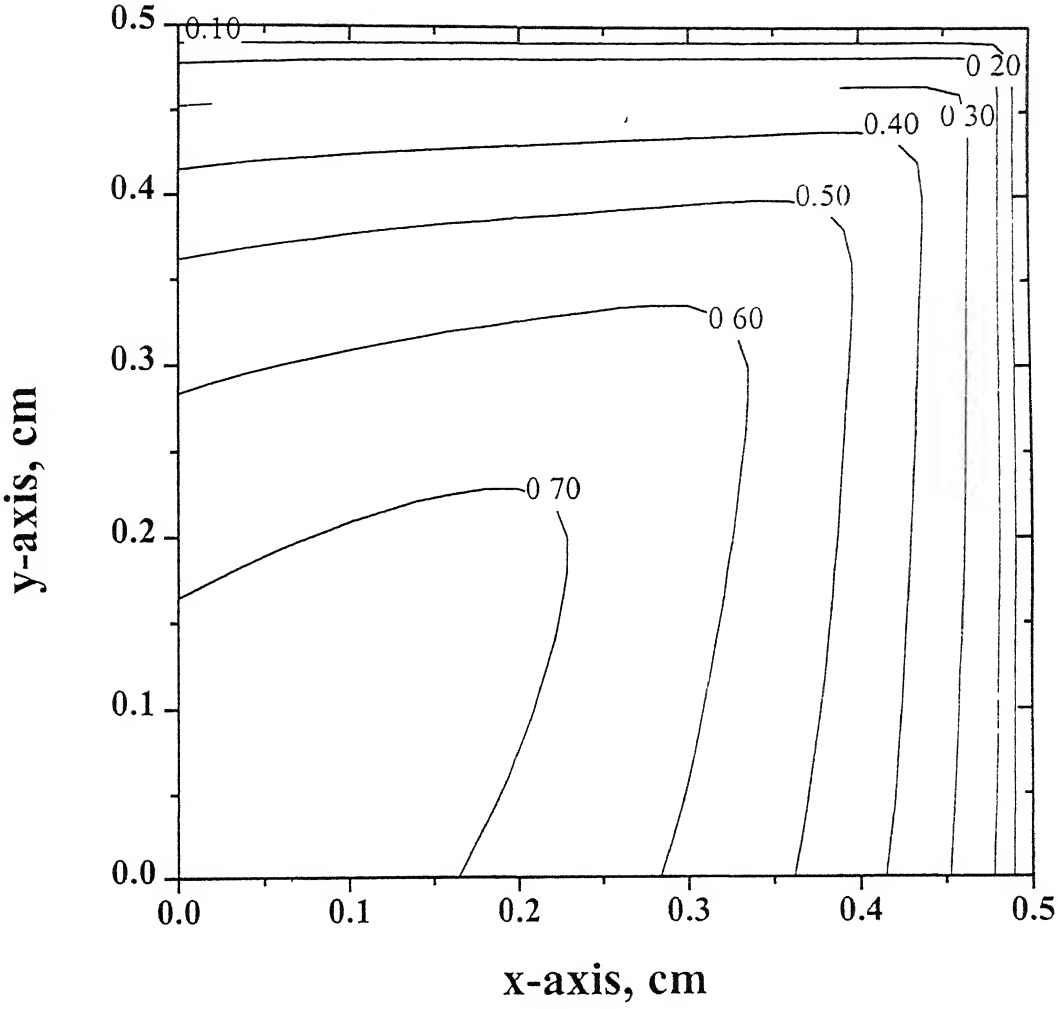

Fig. 3.8: Only the first quadrant of Fig. 3.5 for comparison with Fig. 3.4.

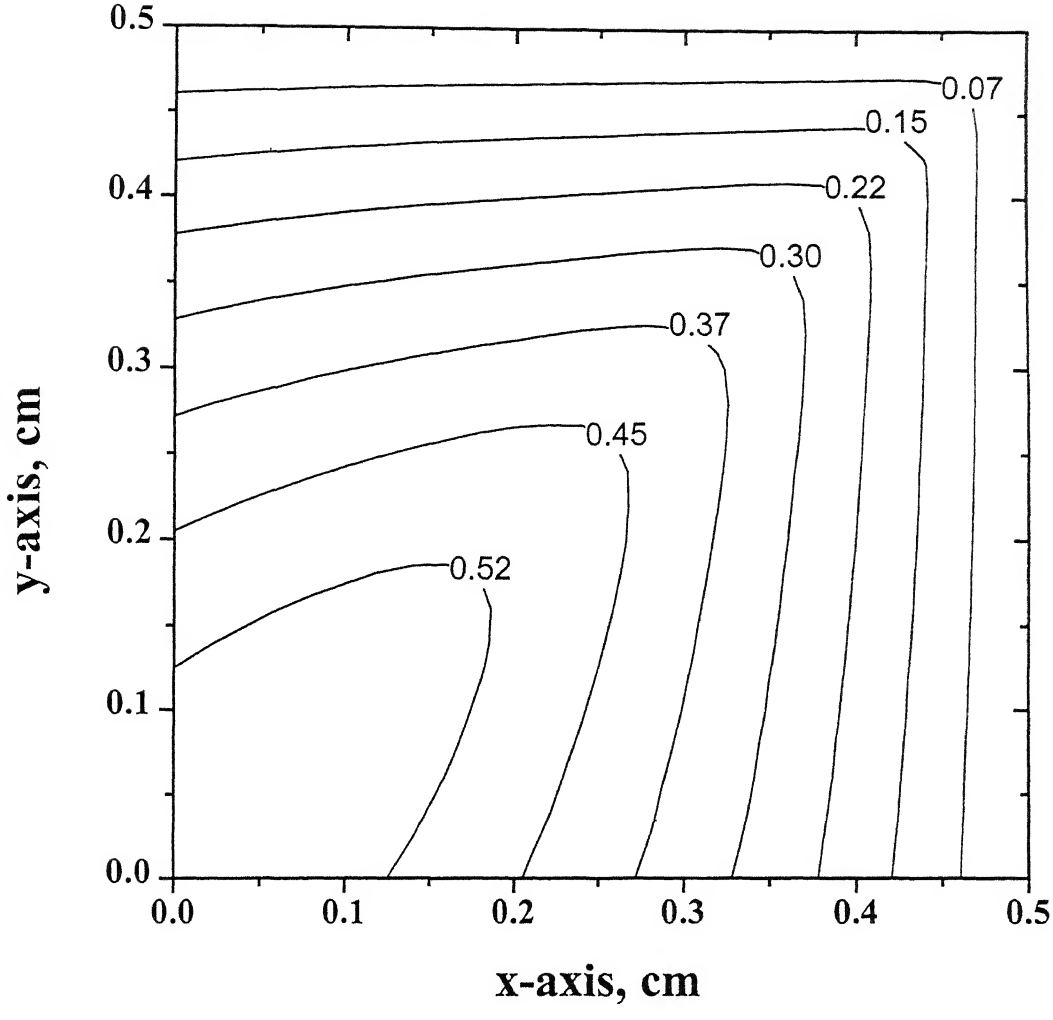

Fig. 3.9: Only the first quadrant of Fig. 3.7 for comparison with Fig. 3.6.

When evolution of porosity during infiltration is compared in Fig. 3.10, there is practically no difference in results for O4 and O6. Furthermore, lowest porosity is shown for O7

We also compare the local radii (Fig. 3.11-3.14) and porosity (Figs. 3.15-3.18) for the four orientations at the end of the process. For the same reason that causes greater infiltration in O3 compared to O2, a greater deposition occurs for O5 compared to O4, as illustrated in Figs. 3.11 and 3 12 and Figs. 3.15 and 3.16. Again, even in the first quadrant, radii and porosity are lower for O5 (see Figs. 3.19 and 3 20) However, the distribution of porosity in both O4 and O5 is not uniform across the area of the preform, whereas, in O6 and O7, the porosity contours are circular.

Also, greater infiltration occurs when both pores are inclined rather than perpendicular to the preform surface (compare Fig. 3.13 with 3.17 and Fig. 3.14 with 3.18). This, reinforces the fact that inclined pores lead to greater densification In other words, if fiber arrangement is such that it leads to perpendicular pores, then it may be prudent to carry out infiltration with pore structure as in O7. Then, after infiltration, rotate the preform by 45^0 and obtain the composite as in O6 by removing the extra triangular portions. This, of course, will take away the advantage of CVI, where near net shape composites can be processed.

Finally, comparing porosity results for O1 and O6, we find for the same initial porosity, final porosity is lower when half the pores are in one orientation and other half perpendicular to it, rather than all pores in a single orientation

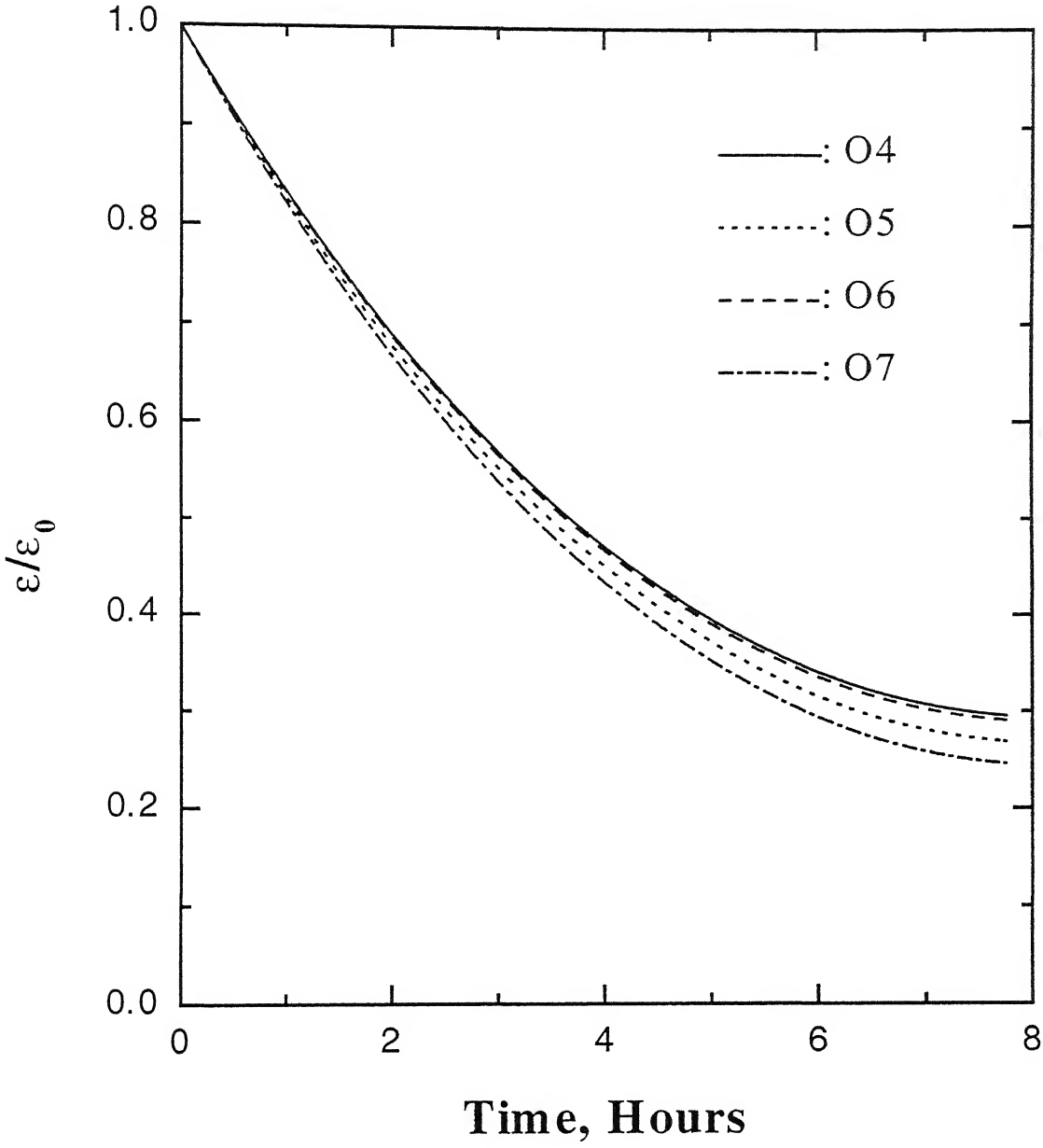

Fig 3 10: Evolution of porosity during densification of preform with pores in two orientations.

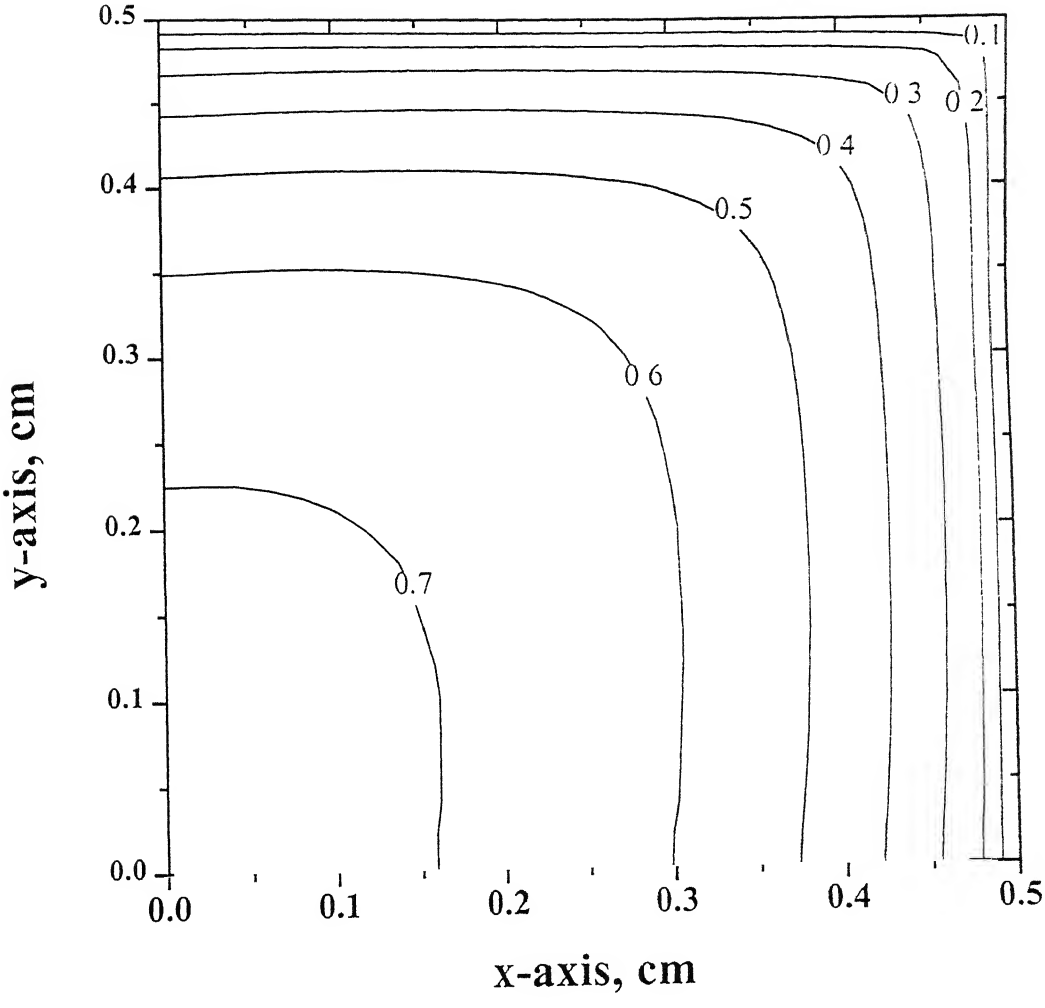

Fig. 3.11: Final normalized radius for two orientation pores -- O4

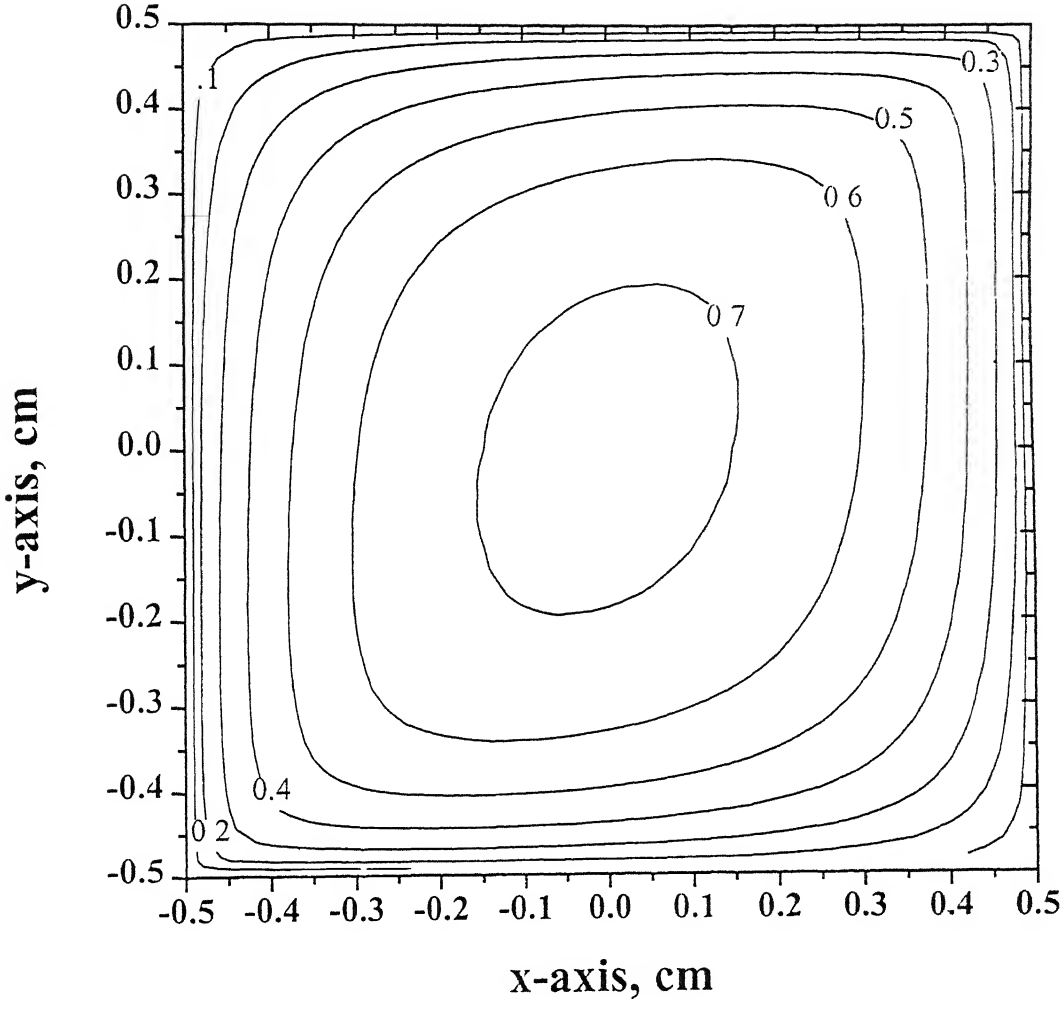

Fig. 3.12: Final normalized radius for two orientation pores – O5.

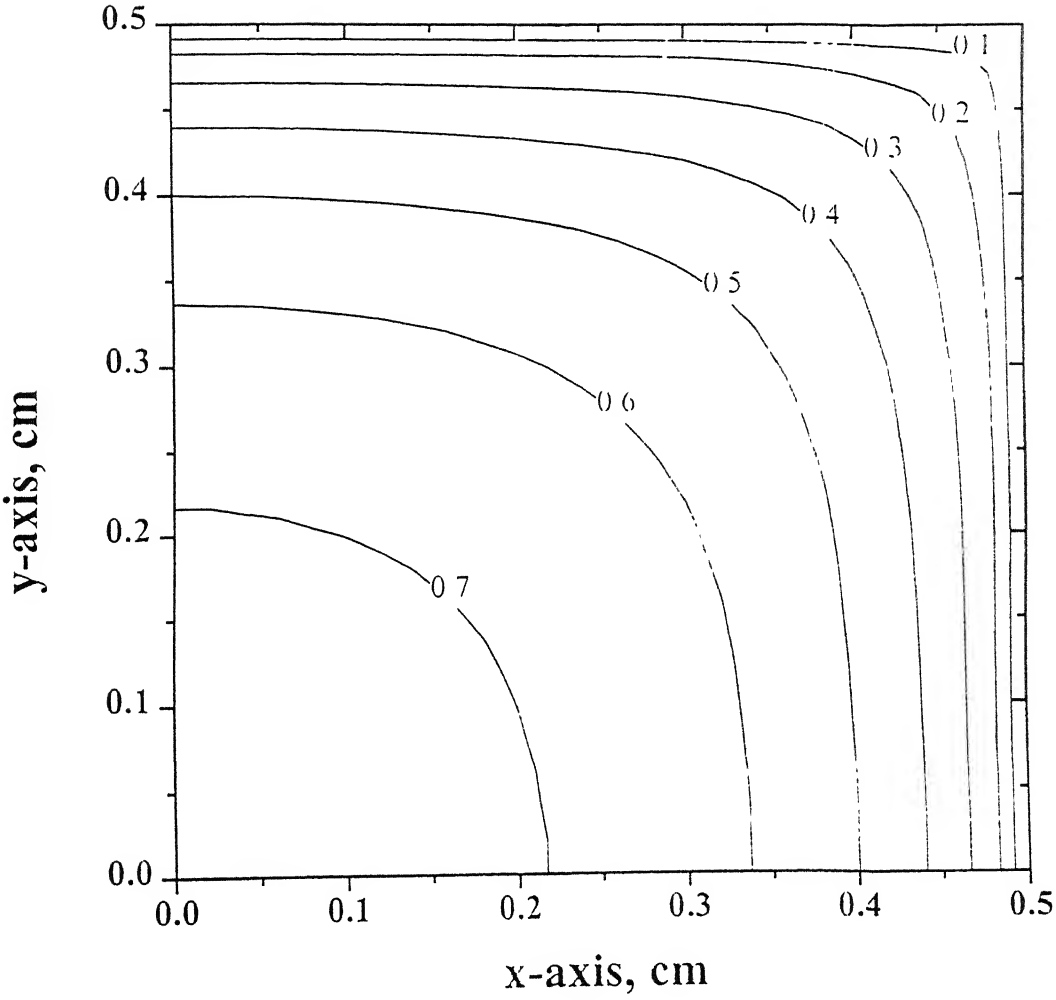

Fig. 3.13: Final normalized radius for two orientation pores – O6.

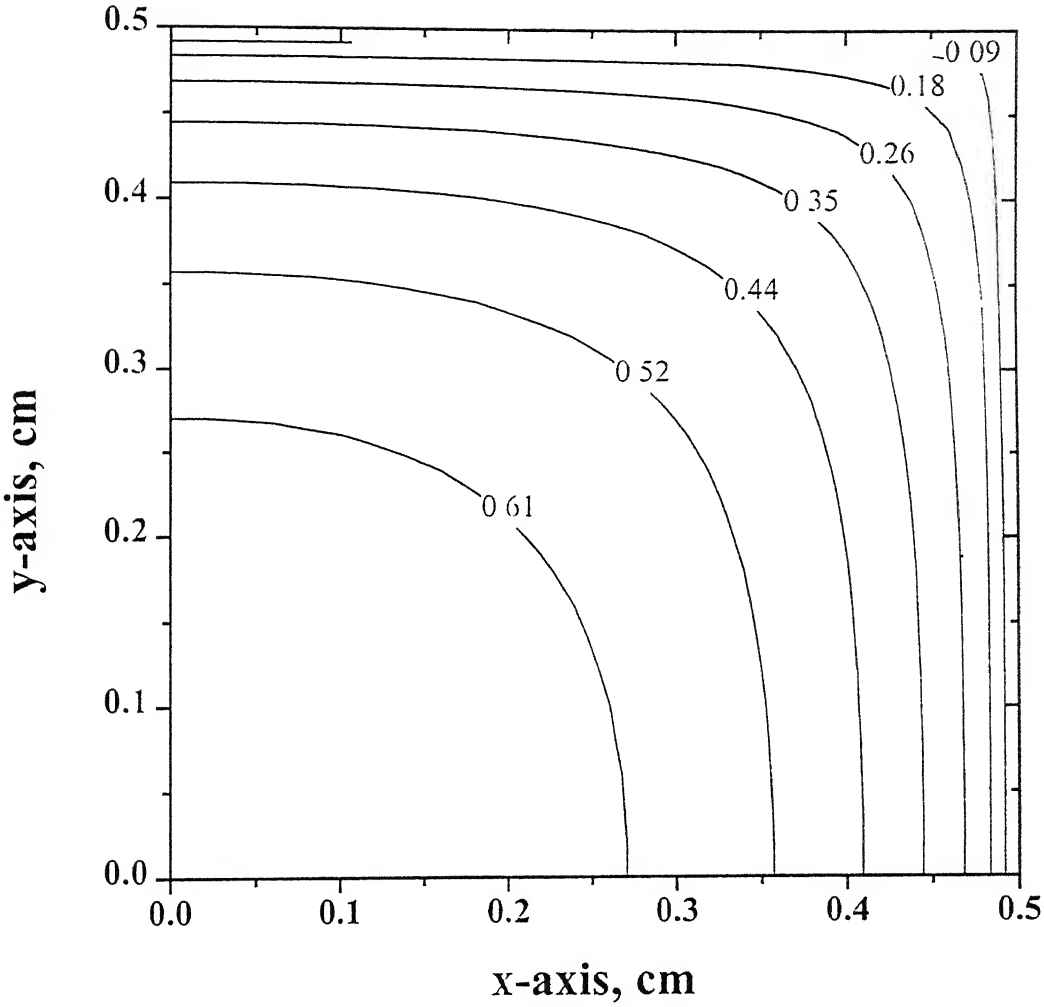

Fig. 3.14: Final normalized radius for two orientation pores – O7.

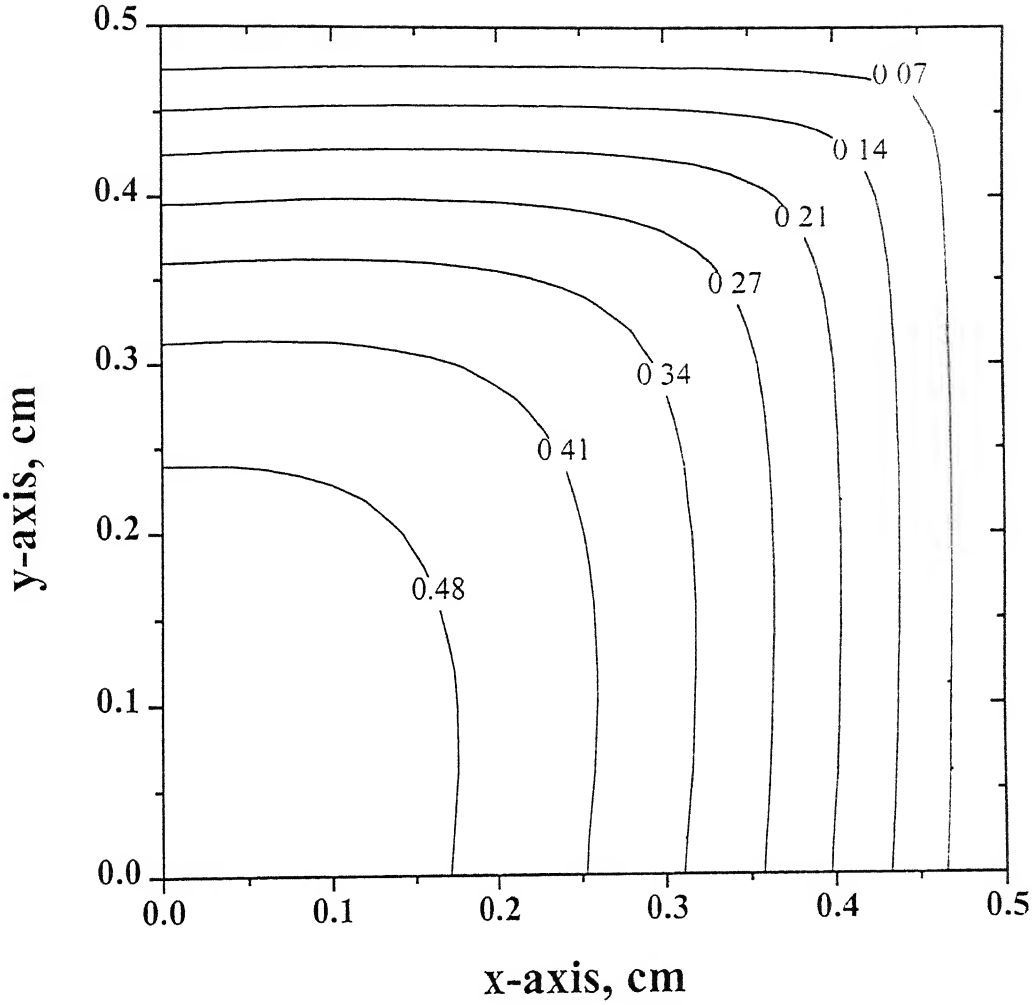

Fig. 3.15: Final normalized porosity for two orientation pores -- O4.

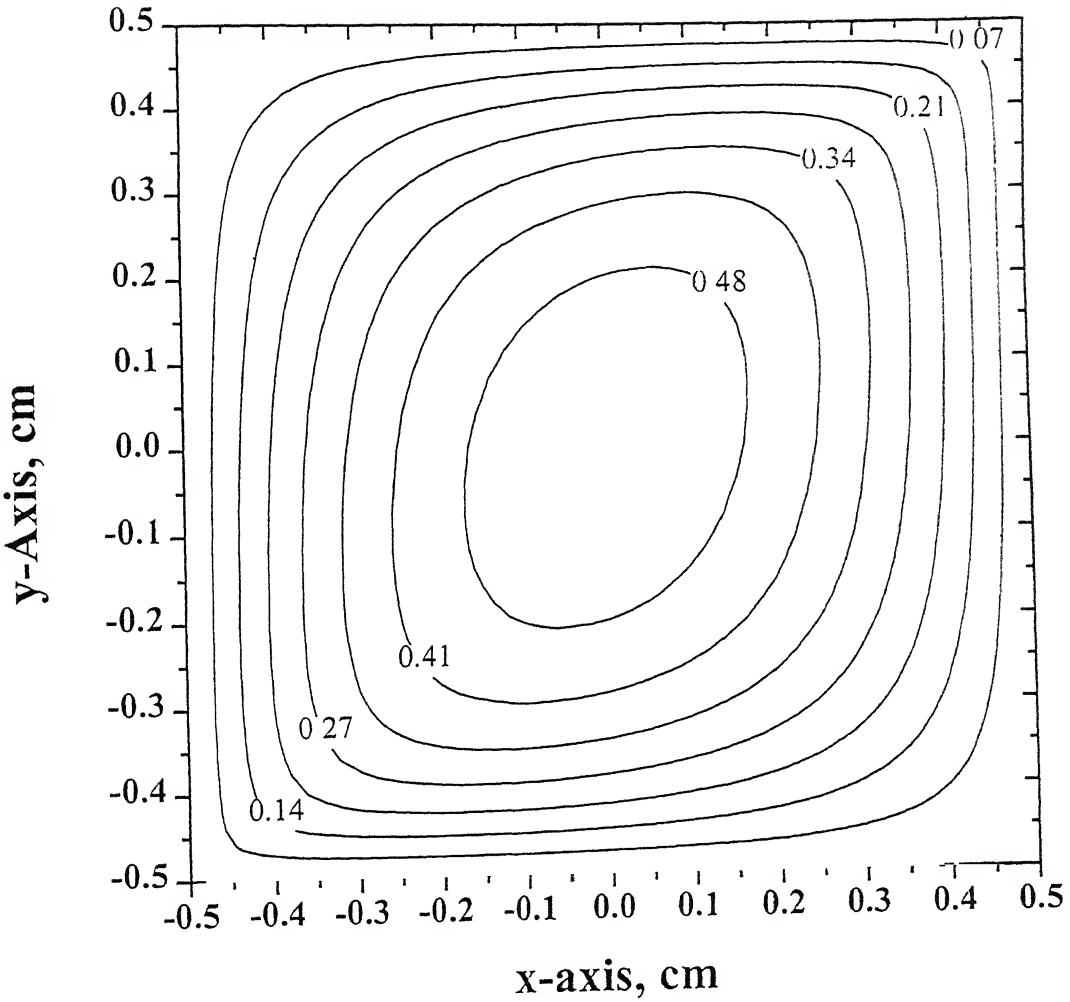

Fig. 3.16: Final normalized porosity for two orientation pores – O5.

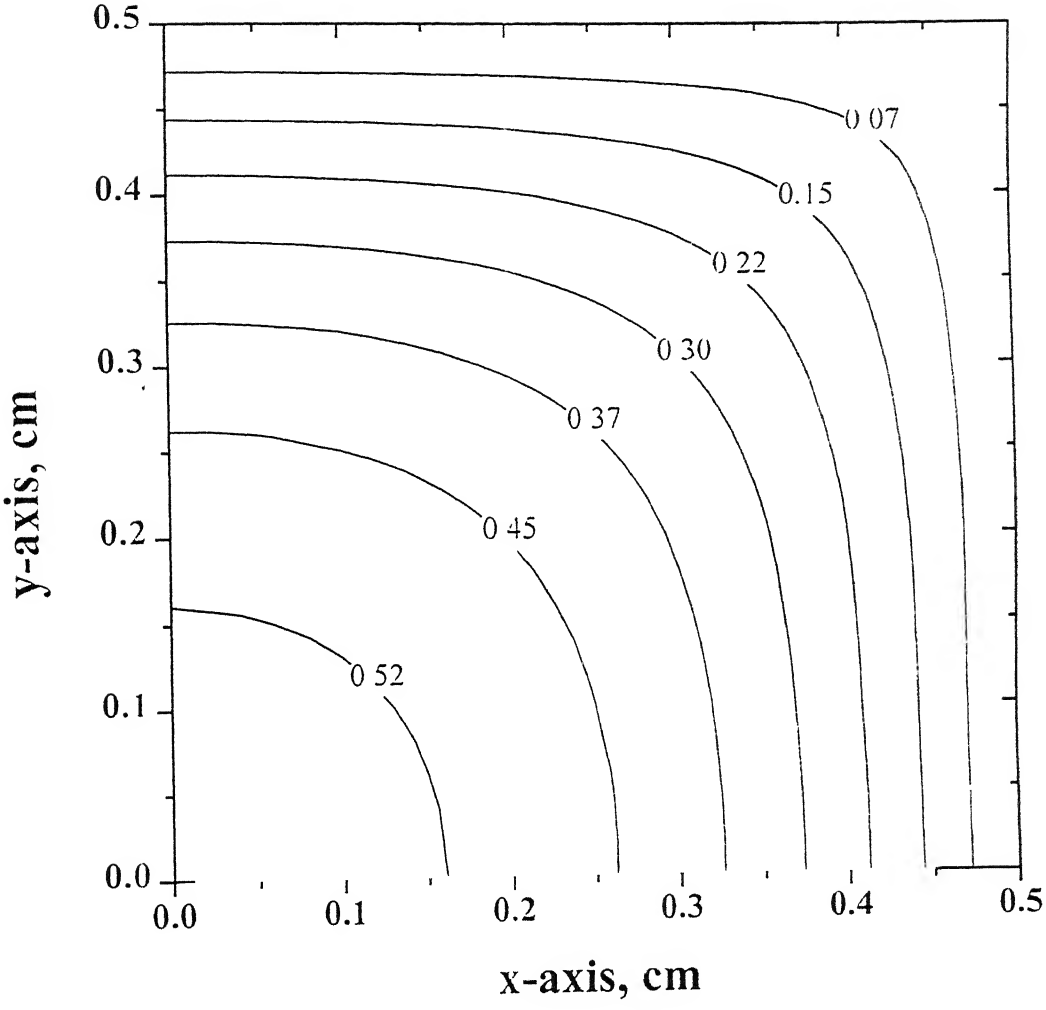

Fig. 3.17: Final normalized porosity for two orientation pores – O6.

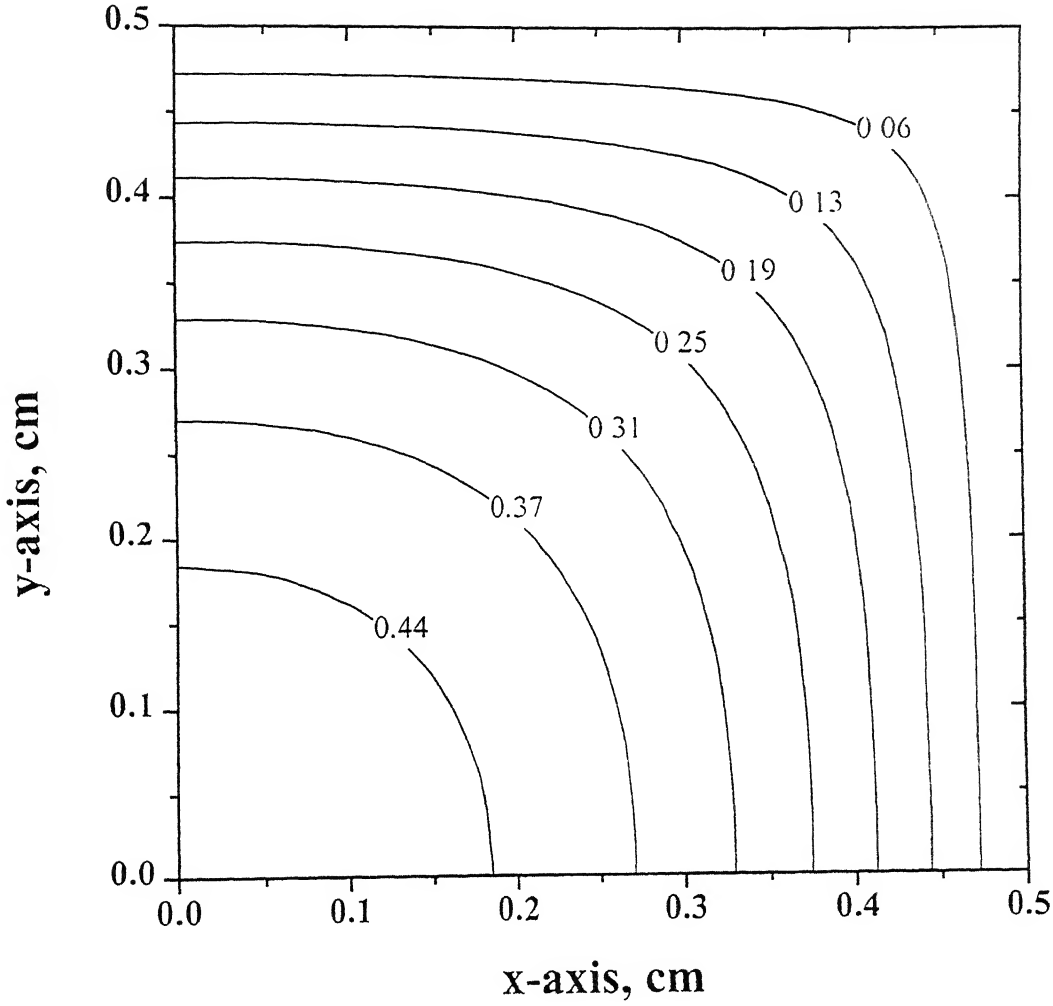

Fig. 3.18: Final normalized porosity for two orientation pores – O7.

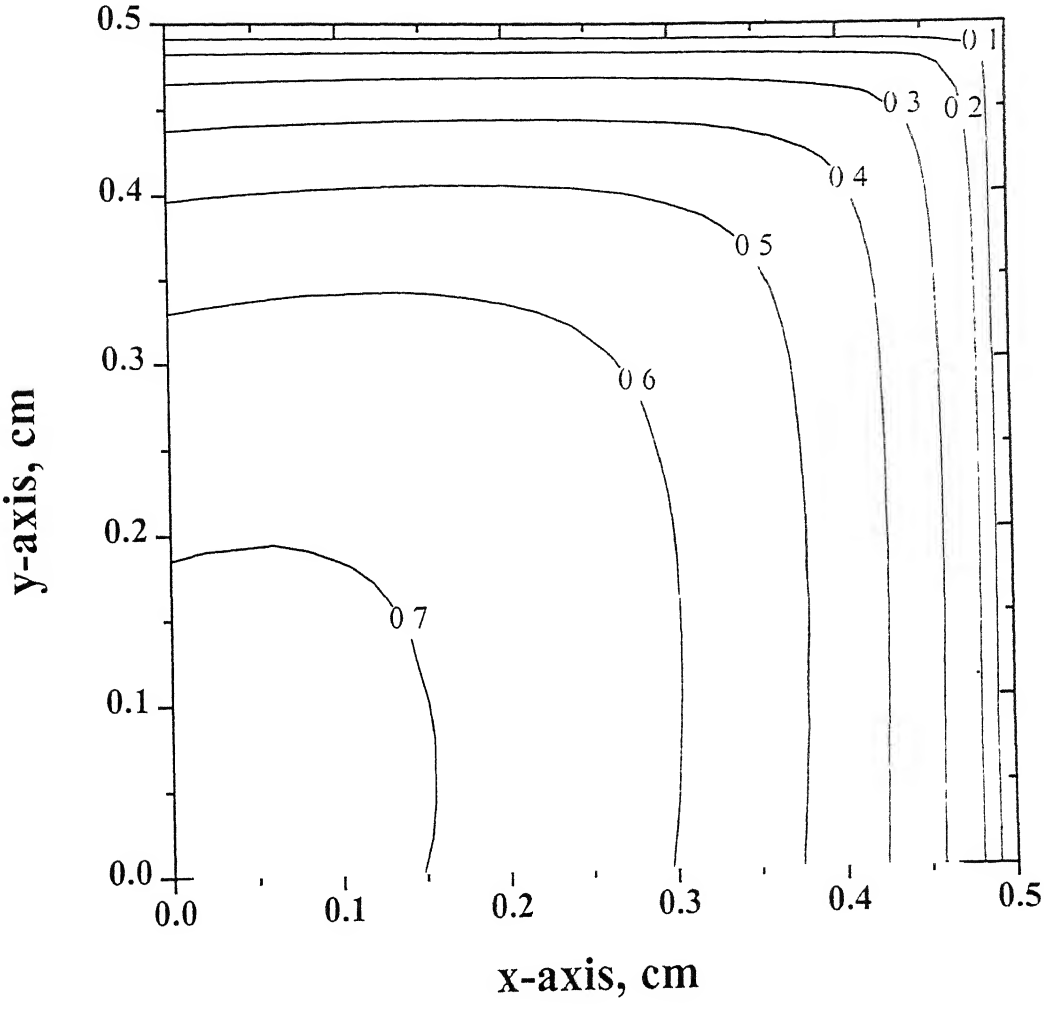

Fig. 3.19: Final normalized radius for O5 only the first quadrant.

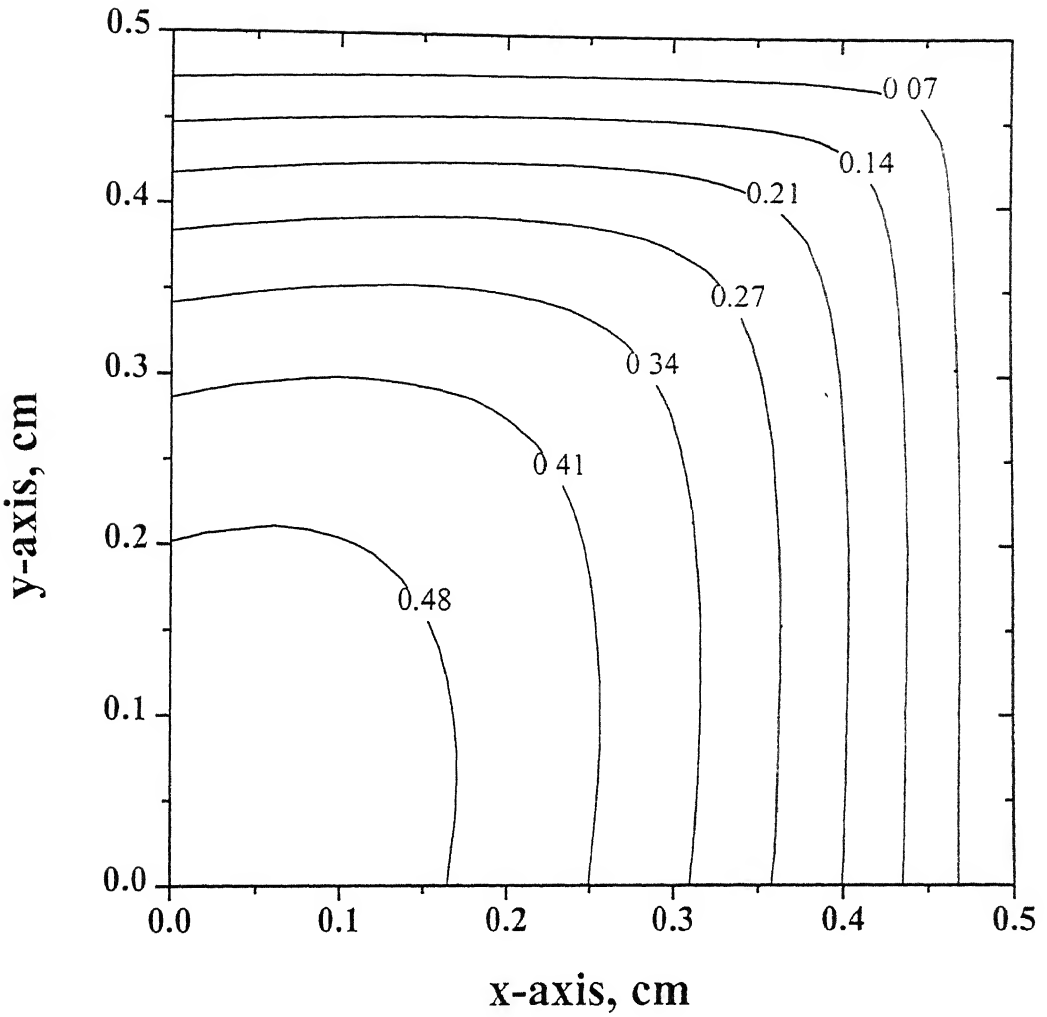

Fig. 3.20: Final normalized porosity for O5 only the first quadrant

3.4.3 PORES IN THREE ORIENTATIONS

In addition to two orientations parallel to the axes, we also include pores oriented 45^0 to the x-axis With symmetry about both axes, the resulting structure is O8; without the requirement of symmetry, the structure is as in O9. From Figs 3.21 and 3 22, which are plots for local radii and, Figs. 3 23 and 3 24, for local porosity in O8 and O9, respectively, we again find greater infiltration for O9; the final normalized porosity of the composite for O8 is 0.293, whereas it is 0 274 for O9. Also, as before, although the structure in the first quadrant is the same for the two cases, the local radii and porosity are lower for O9 (compare Fig 3 21 with 3.25 and Fig 3.23 with 3.26).

Greater infiltration can be achieved by having more pores that are at an angle to the preform surface, rather than perpendicular to it. So, in O10, out of three, only one set of pores are parallel to the x-axis and other two are in orientations $45^0$and 135^0. This structure is equivalent to one when pores are oriented as $\phi = 45^0$, 90^0, and 135^0. According to results for local radii and porosity, in Figs. 3.27 and 3 28, respectively, the densification is greater than either O8 or O9. This fact is better illustrated in Fig. 3.29, where we show the evolution of porosity during the process.

3.4.4 PORES IN FOUR ORIENTATIONS

Finally, we present results (Figs. 3.30 and 3.31) for pores in all four orientations (O11). Here, for a similar initial porosity as in O7, a part of porosity is redistributed along the two axes. Therefore, the infiltration is not as good as in O8. In fact, we have compared the final normalized porosity for all cases (see Table 2) and find that O8 yields largest densification.

In summary, the infiltration with single orientation and pores perpendicular to the preform surface is poorest; whereas most densification is achieved when only both the inclined pores are present In between are the cases, where a part or all the initial porosity due to inclined pores is redistributed between one or both the perpendicular pores

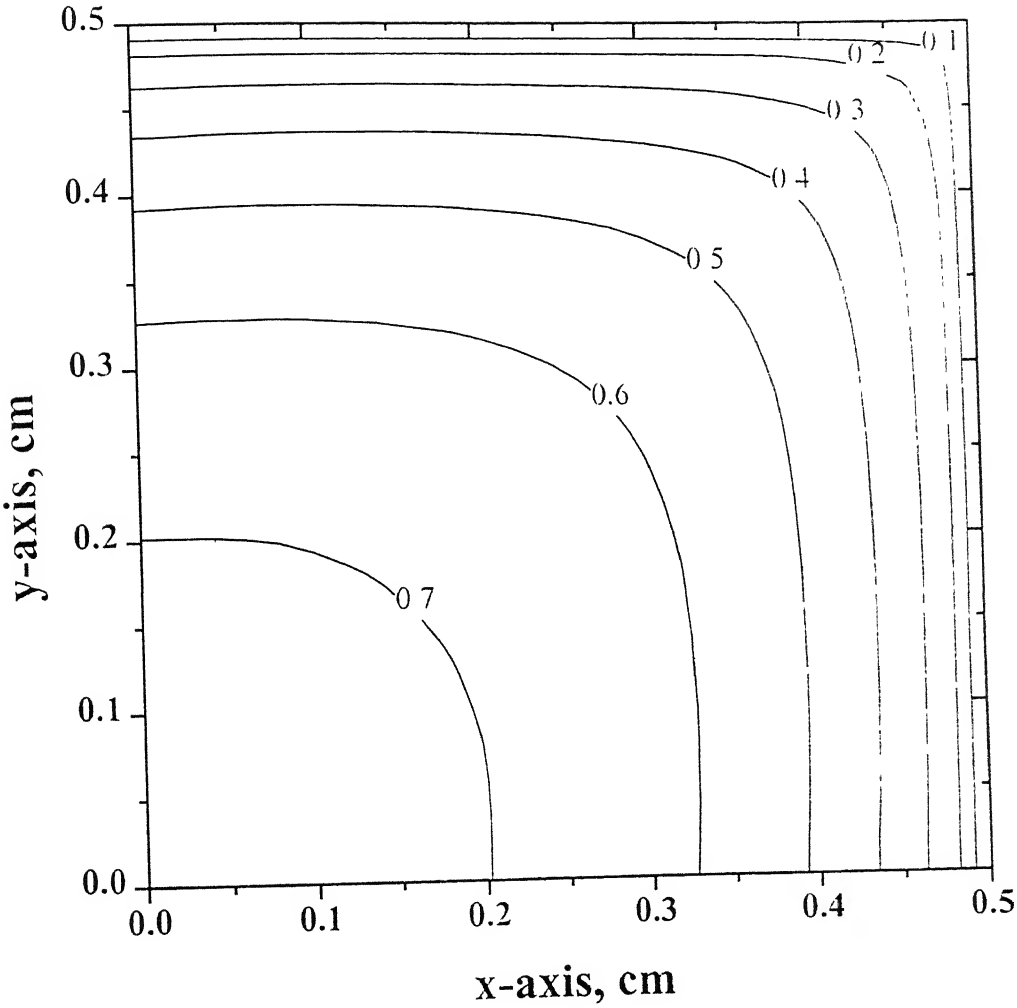

Fig:. 3.21· Final normalized radius for O8.

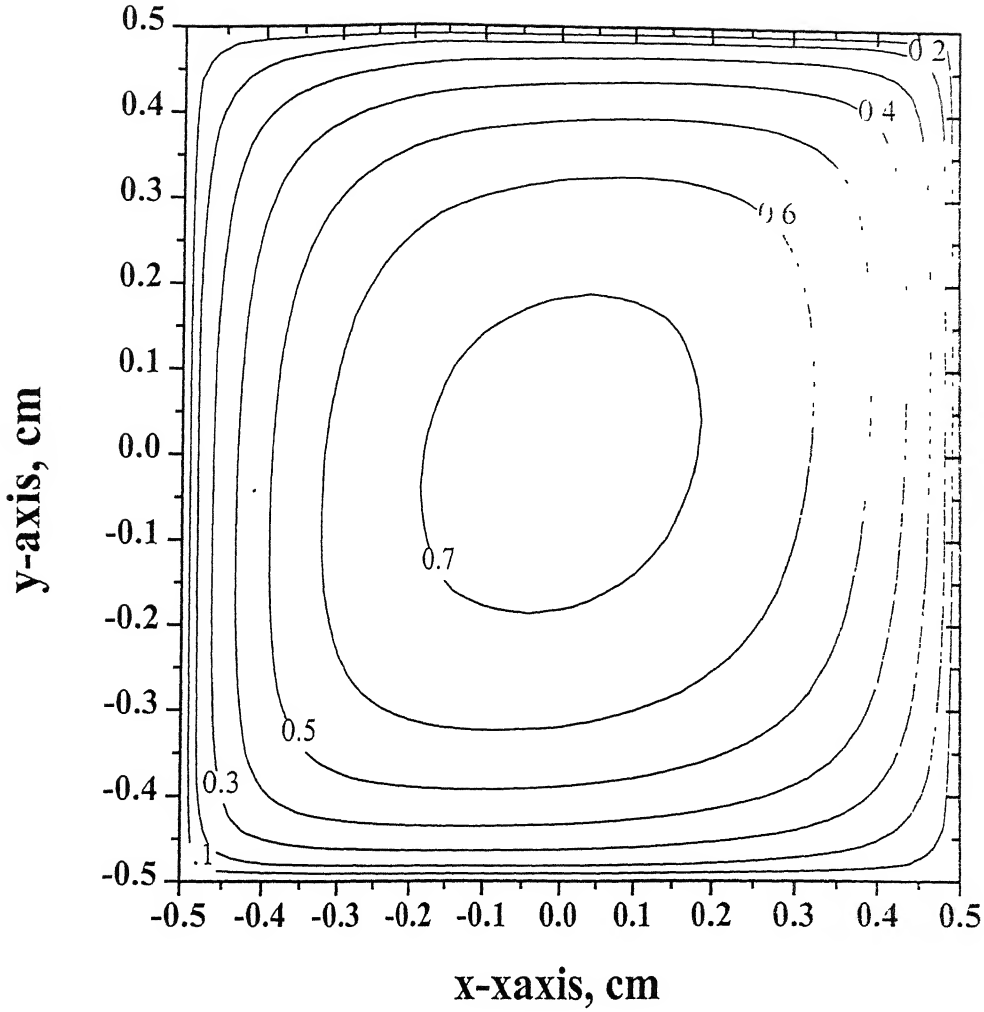

Fig. 3.22: Final normalized radius for O9

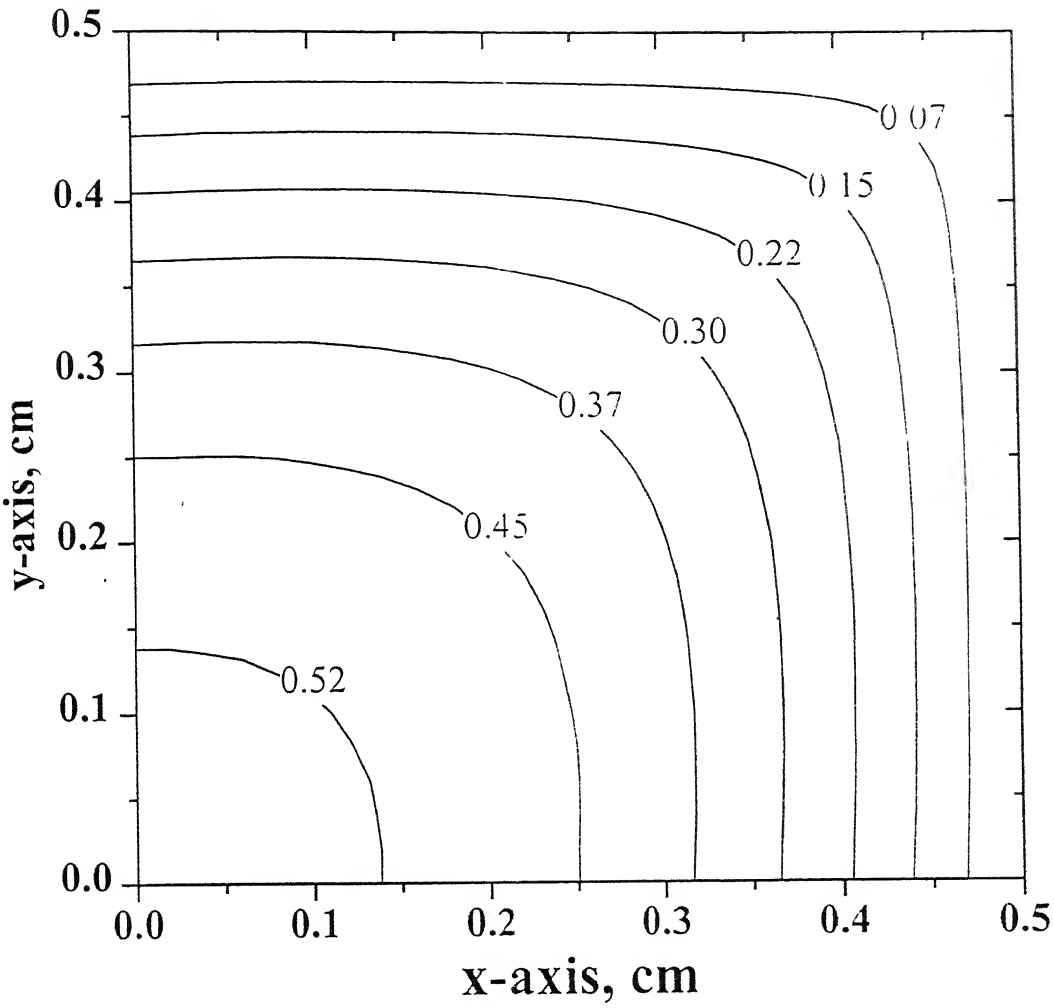

Fig. 3.23: Final normalized porosity for O8.

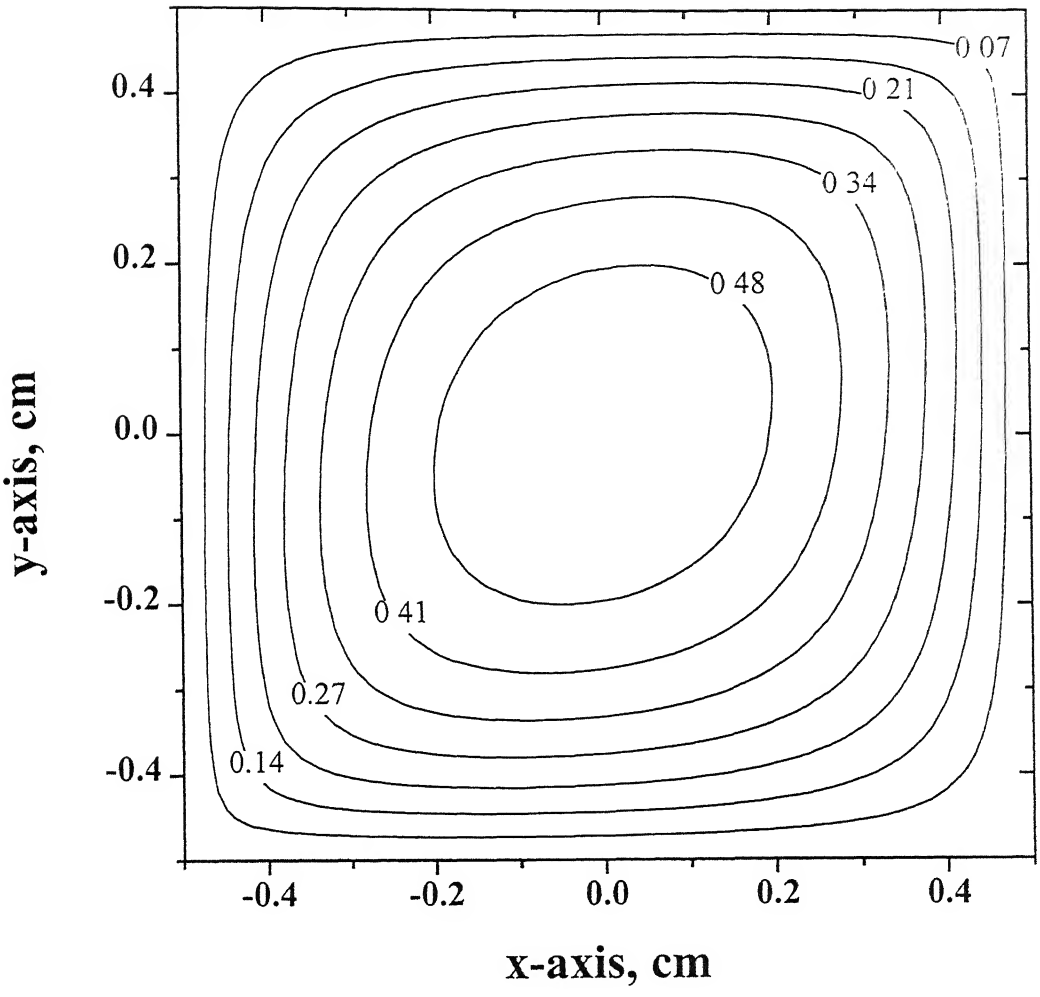

Fig. 3.24: Final normalized porosity for O9

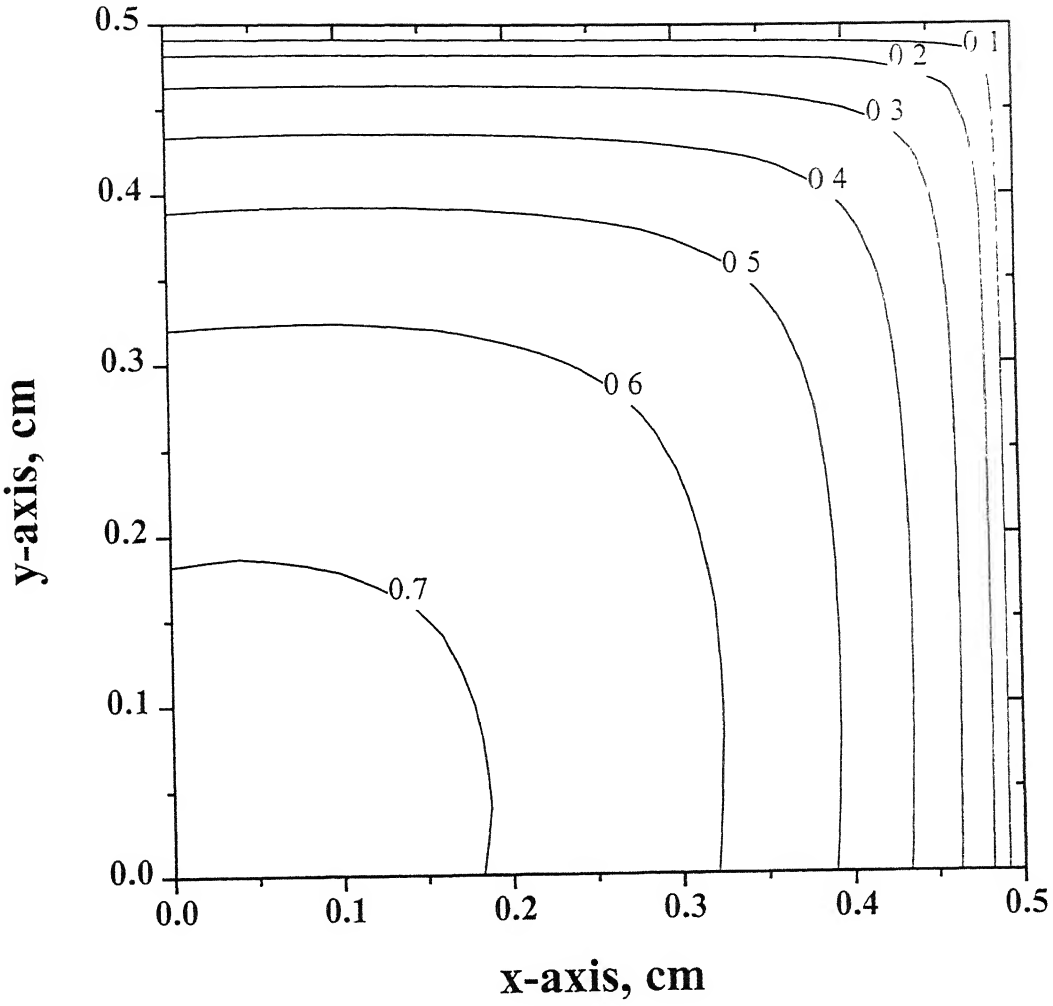

Fig. 3.25. First quadrant radii in O9 for comparison with Fig. 3.21

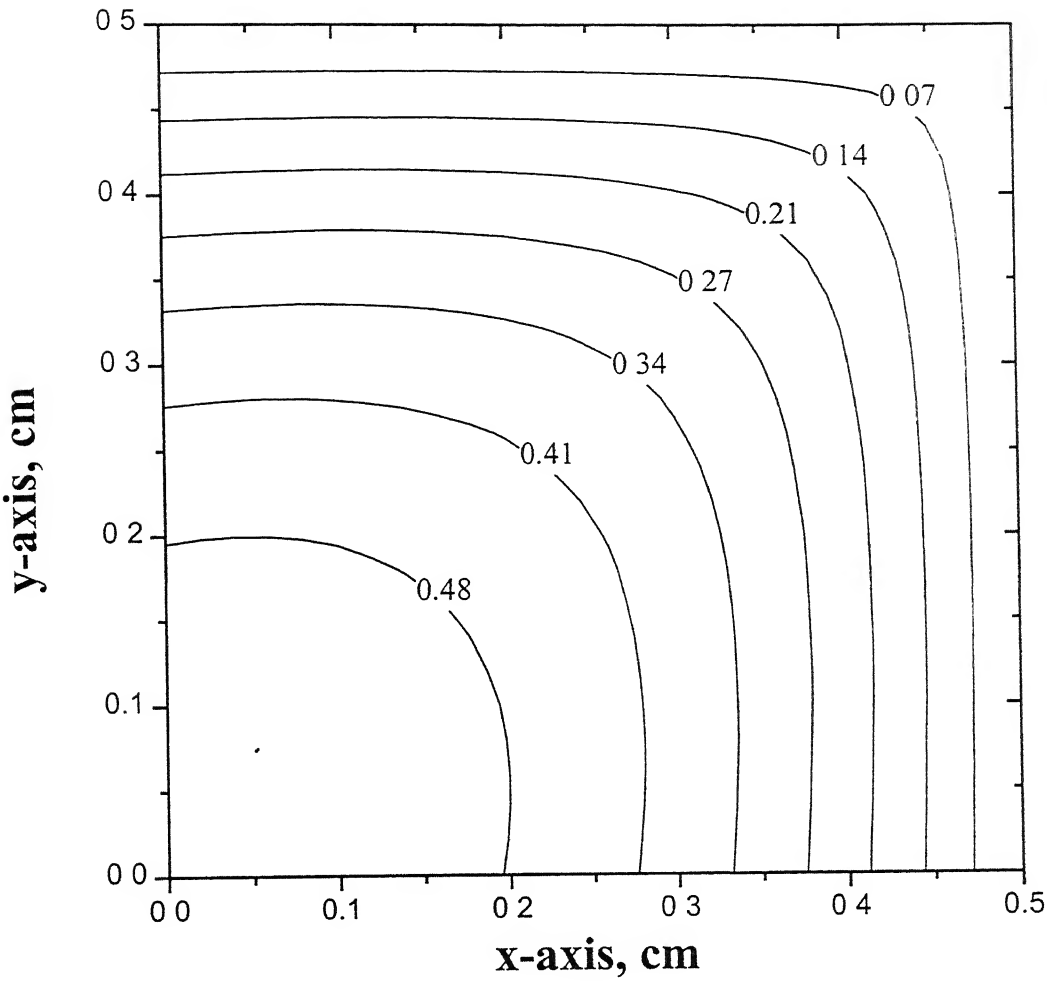

Fig. 3.26: First quadrant porosity in O9 for comparison with Fig. 3.23.

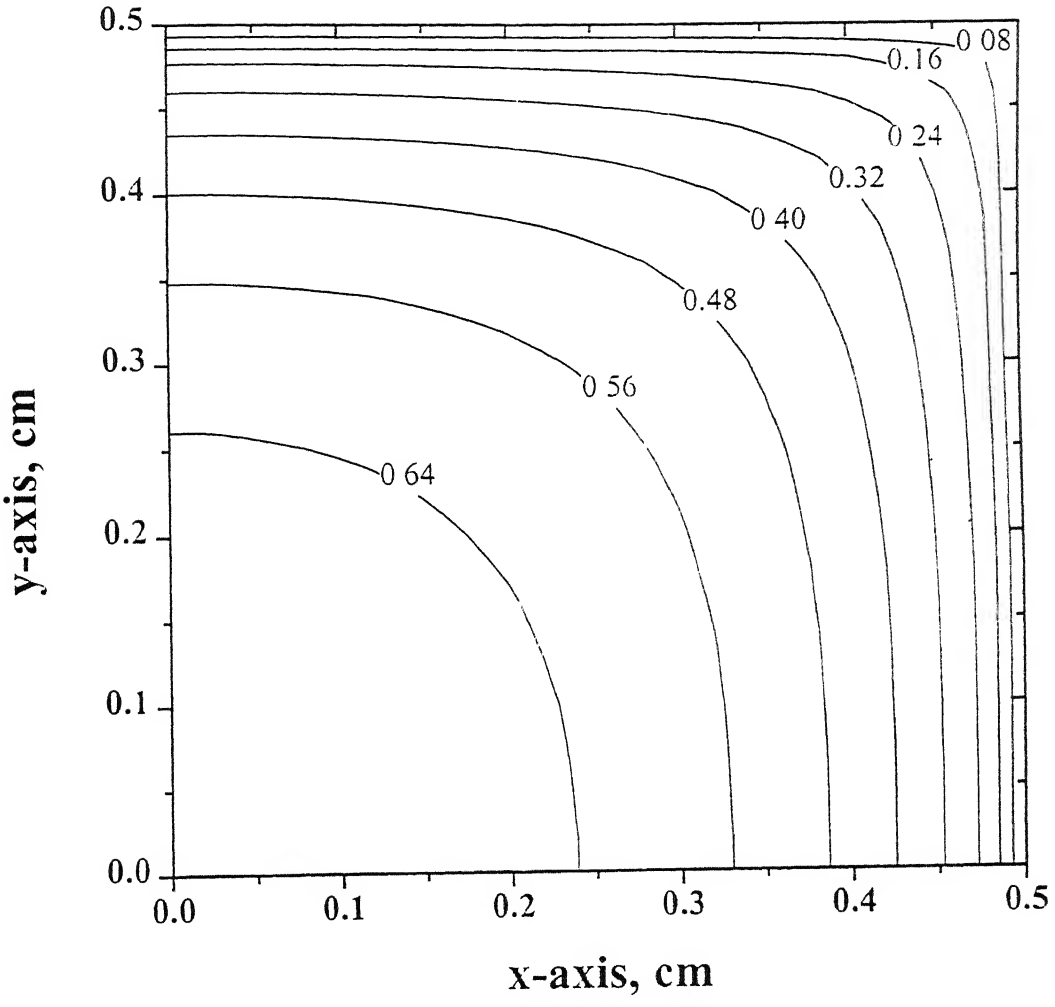

Fig 3.27: Final normalized radius for O10

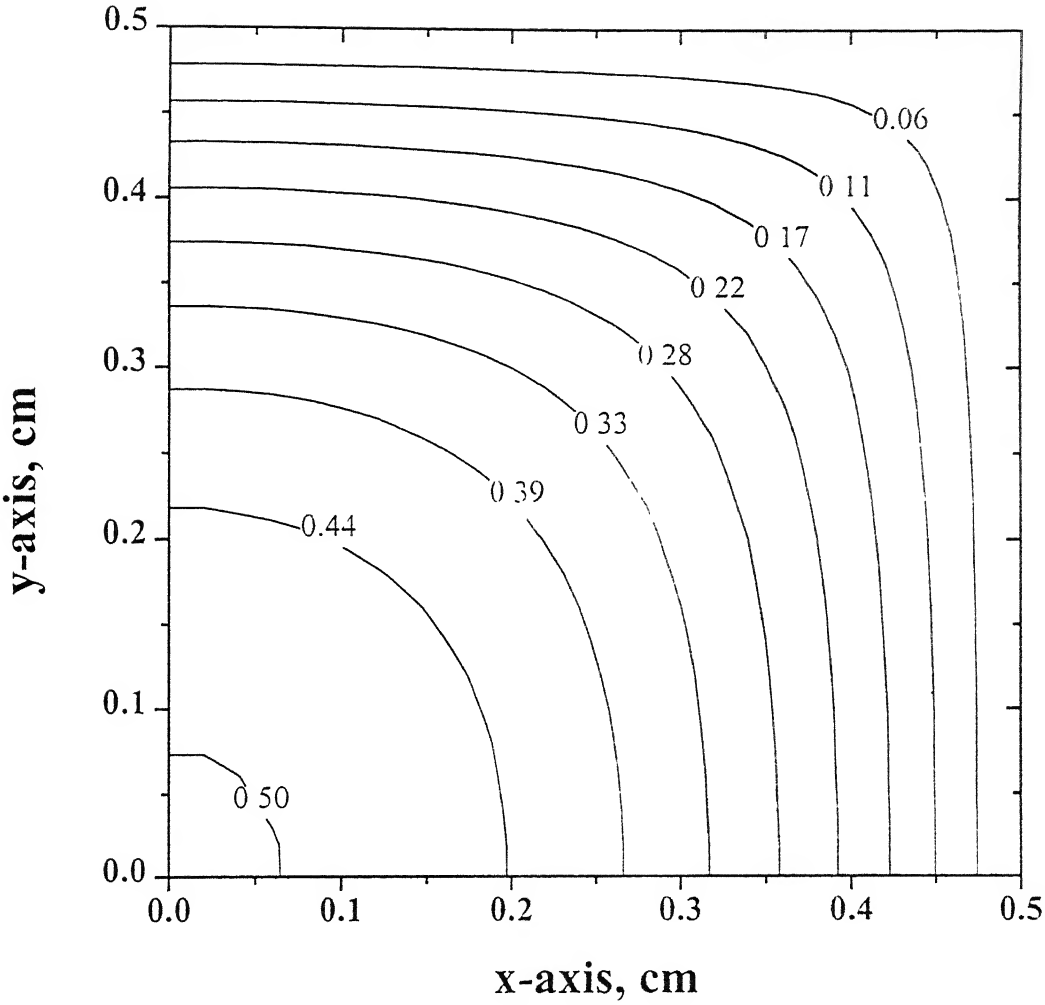

Fig. 3.28: Final normalized porosity for O10

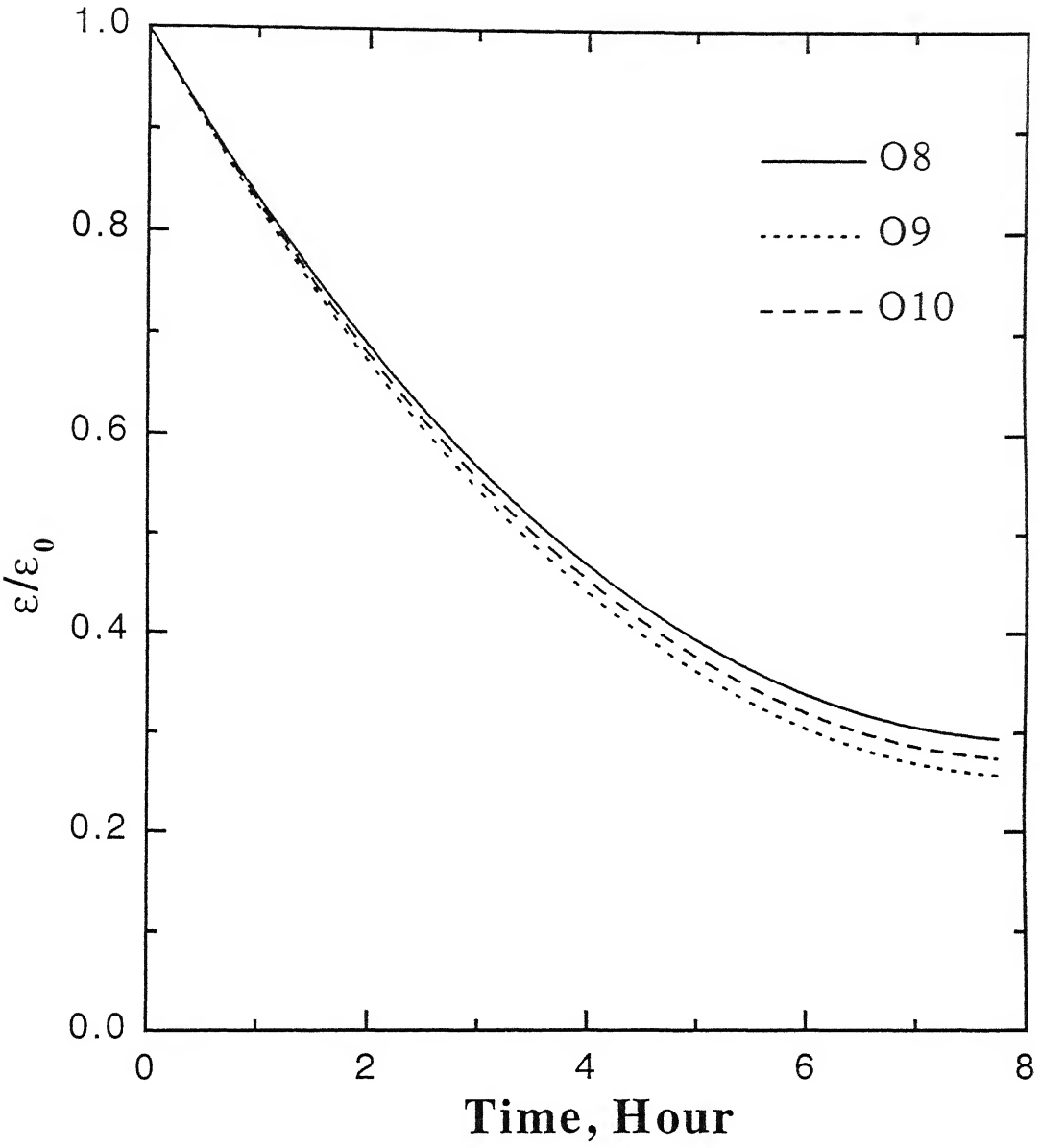

Fig. 3.29: Effect of three-pore orientations on densification of the preform.

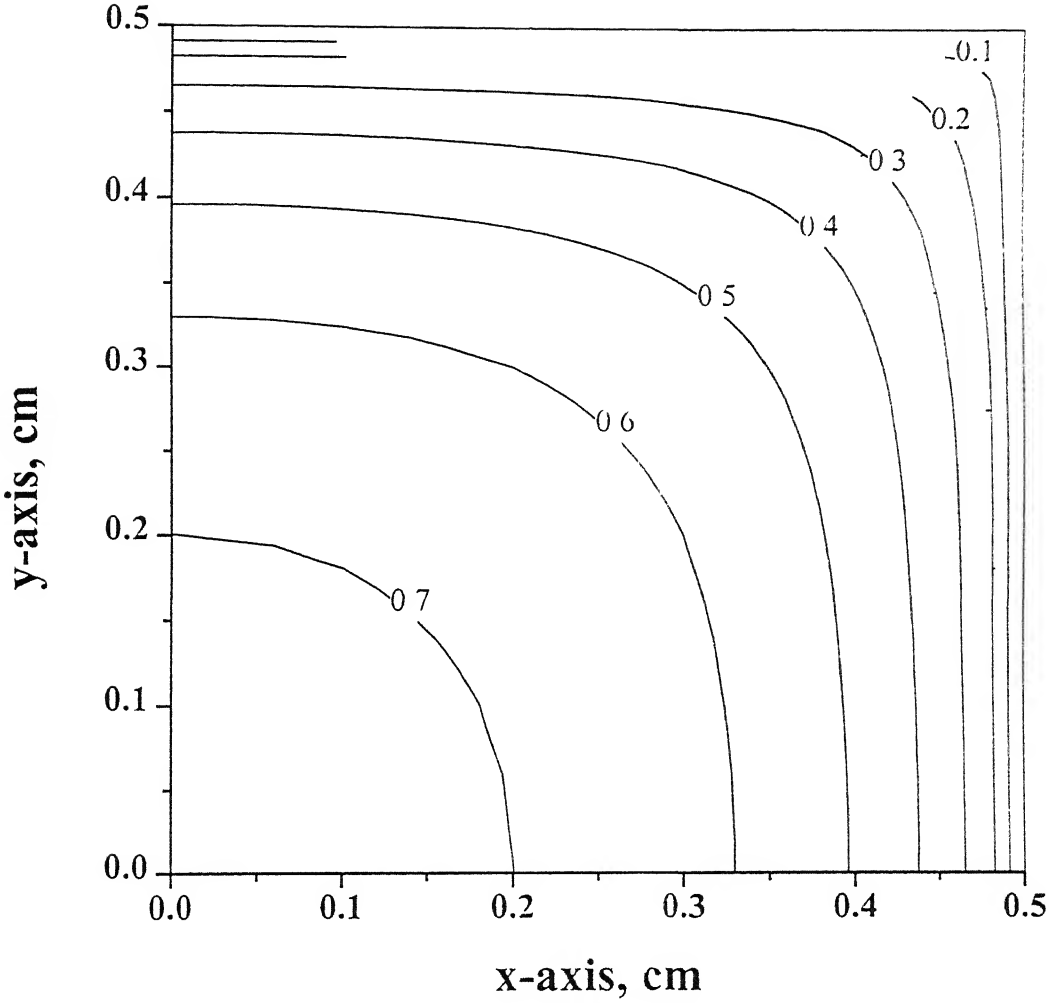

Fig. 3.30· Final normalized radius with pores in all four orientations.

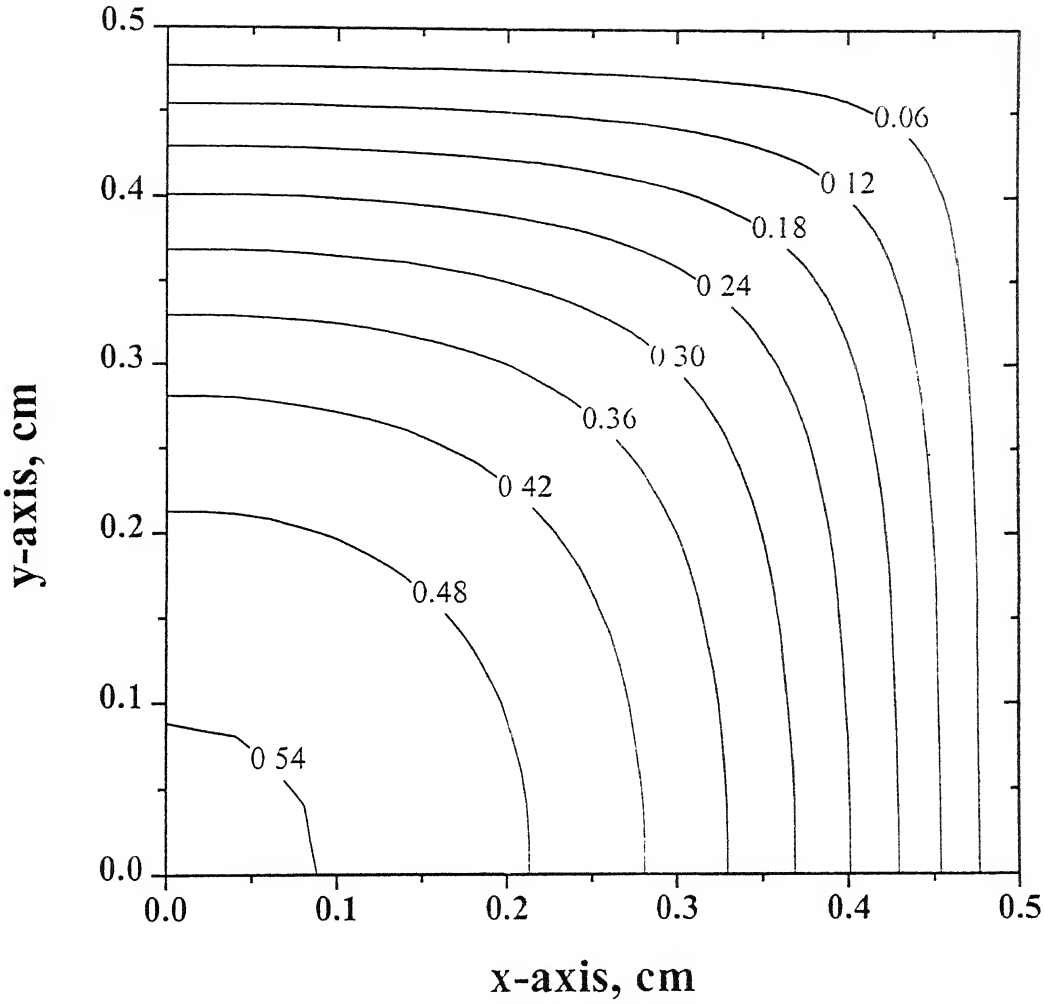

Fig. 3.31: Final normalized porosity with pores in all four orientations.

CHAPTER 4

CONCLUSIONS

In the present work, a model for diffusion in porous media is developed. The porous media consisting of pore network oriented in specific directions are divided into a number of elemental volumes and by orientation averaging on the pore network in each elemental volume, the porous media is represented as a piece wise homogeneous medium through an anisotropy tensor The flux are based on Dusty gas model for describing mass transport in the porous medium.

The present model is applied to study the effect of pore orientation on deposition of SiC in SiC preform by chemical vapor infiltration. The dusty gas based flux expression is used to generate a system of partial differential equations, containing variables mole fraction of TMS(X_1), mole fraction of HCl(X_2) and total pressure(P). The set of partial differential equations (PDE's) with appropriate boundary conditions are solved, using finite difference method. The equations are discretized in a uniform grid and are solved by bi-congugate gradient method.

The studies are carried out for pores oriented in four different orientations, ϕ = 0^0, 45^0, 90^0 and 135^0. The various combinations included pores only in one, two, three and all the four directions. Total of 11 cases of pore orientations is considered. An initial pore radius of 2.5 μm is taken and the simulations are carried out at a temperature of 1200 K.

For the pores oriented in only one direction, it is observed that the pores oriented at an angle of 45^0 through out the preform gives lowest porosity. Since for

this case, flux enters the pores from both the directions, as the pores are open in both the ends.

For the case when the pores are oriented in two directions, the preform is densified more when the pores are inclined at angles of $\phi = 45^0$ and 135^0 to the preform surface This clearly shows that, if the pores are open in both the end for the flux to enter through them and also if they are inclined, then more densification of the preform can be achieved. Comparing the deposition for the case when the pores are oriented in single direction and in two directions, it is seen that more densification can be achieved when the pores are oriented as in the latter case. Also uniform deposition is observed when the pores are oriented perpendicular to each other (as in the case when pores are oriented at angles of $\phi = 45^0$ and 135^0 or $\phi = 0^0$ and 90^0).

For the pores oriented in three directions and all four directions. The same trend was seen as in the previous cases, that is, densification of the preform was dependent on the population of the pores inclined to the surface of the preform and also on the number of open ended pores.

In brief it is seen that pores oriented perpendicular to the preform surface and in only one direction lead to higher porosity, whereas maximum densification occurred when the pores were inclined to the preform surface and oriented in two directions.

Based on our calculation, we suggest that preform should be placed such that there are more number of open ended and inclined pores for the optimum densification of the preform. Then the densified preform can be cut to the desired shapes for commercial purpose.

LIST OF SYMBOLS

$\langle A \rangle$	Anisotropy tensor
c	local gas concentration in moles per unit volume
ϑ_{ij}	binary diffusion coefficient between species i and j
D_{ik}	Knudsen diffusion coefficient of species i.
D_{ij}	multicomponent diffusion coefficient
E_A	activation energy
F	external force acting
$f(\theta, \phi \ell)$	orientation distribution function
$g(\theta, \phi)$	orientation of the pores
$\mathbf{j}_i$	mass diffusion flux with respect to mass average velocity
K	Boltzman constant
k_B	pre-exponential factor
k_0	half-thickness of ceramic slab in x and y direction
L_x, L_y	half-thickness of ceramic preform in **x** and **y** direction.
L_1, L_2, L_3	length, width and height of the elemental volume
$\underline{\underline{\mathbf{L}}}, \underline{\underline{\mathbf{M}}}, \underline{\underline{\mathbf{P}}}$	dyad used in the equation
ℓ	length of the pore
M_{SiC}	molecular weight of SiC
m_i	mass of a molecule of species i
n_i	number molecules of species i per unit volume
n	number of molecules per unit volume

N_i	molar flux of species i
N_{SiC}	moles of SiC
P	local pressure
R	instantaneous local radius
R_0	initial radius of the pores
R_g	universal gas constant
S_α	surface area of the pores in control region
t	time
T	temperature
$\mathbf{v}_i$	velocity of molecules of species i
$\mathbf{v}_0$	mass average velocity
$\mathbf{V}_i$	diffusion velocity of molecules of species i
$\mathbf{V}_\alpha$	volume of the control region
$\mathbf{V}_\alpha^p$	volume of the pores in control region
X_i	mole fraction of species i
η	viscosity of gas mixture
ρ	mass density of a gas
ρ_{SiC}	density of SiC
ε	porosity

APPENDIX A

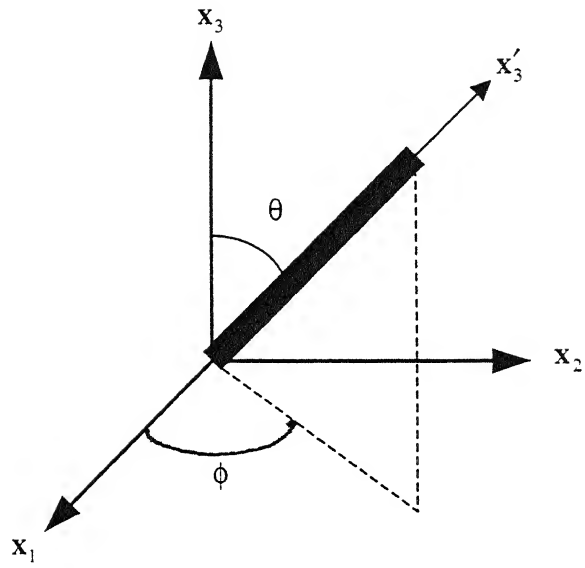

Figure A 1 The coordinates systems and pore orientation.

$$[x'] = \overrightarrow{M}\,[x]$$

$$[x] = \overrightarrow{M}^{T}\,[x']$$

$$\overrightarrow{M} = \begin{pmatrix} \cos\theta\cos\phi & \cos\theta\sin\phi & -\sin\theta \\ -\sin\phi & \cos\phi & 0 \\ \sin\theta\cos\phi & \sin\theta\sin\phi & \cos\theta \end{pmatrix}$$

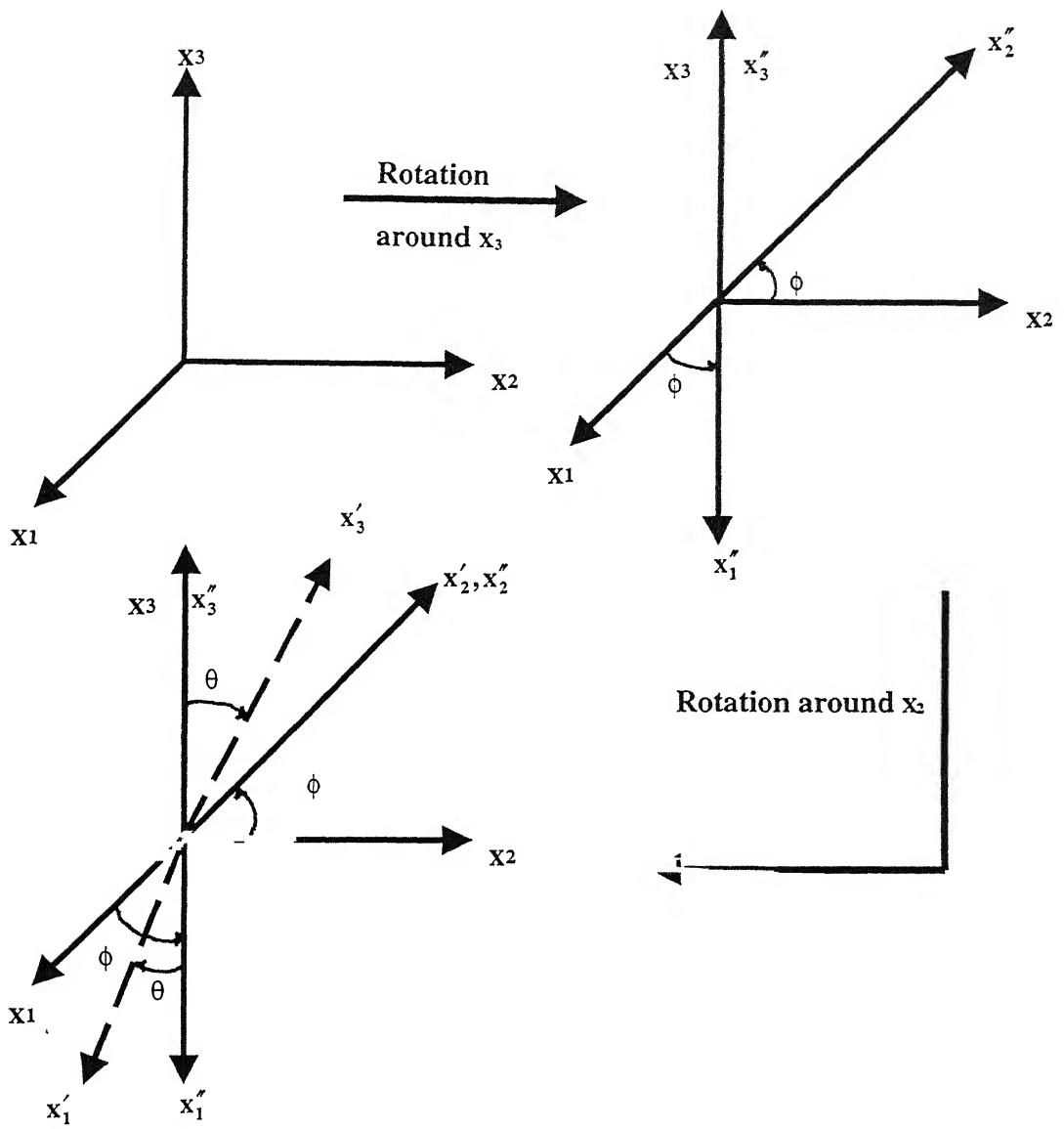

Fig. A.2: Schematic showing conversion from local to global coordinate system.

$$\begin{bmatrix} x_1' \\ x_2' \\ x_3' \end{bmatrix} = \begin{pmatrix} \cos\theta\cos\phi & \cos\theta\sin\phi & -\sin\theta \\ -\sin\phi & \cos\phi & 0 \\ \sin\theta\cos\phi & \sin\theta\sin\phi & \cos\theta \end{pmatrix} \begin{bmatrix} x_1 \\ x_2 \\ x_3 \end{bmatrix}$$

APPENDIX B

The anisotropy tensor $\langle A \rangle$ due to orientation of the pores, which accounts for anisotropy of the diffusion phenomenon due to the orientation as well as the geometry of the pore is derived as,

$$\langle \underline{\underline{A}} \rangle = \frac{\varepsilon}{4\pi} \int_0^{2\pi} \int_0^{\pi} \int_0^{\ell} \underline{\underline{P}} \left(\underline{\underline{M}}^T \underline{\underline{L}} \underline{\underline{M}} \right) f(\theta, \phi, \ell) \sin\theta \, d\ell \, d\theta \, d\phi$$

where the term $f(\theta, \phi, \ell)$ is orientation distribution function

The term $\underline{\underline{M}}^T \underline{\underline{L}} \underline{\underline{M}}$ is,

$$\begin{pmatrix} \sin^2\theta\cos^2\phi & \sin^2\theta\sin\phi\cos\phi & \sin\theta\cos\theta\cos\phi \\ \sin^2\theta\cos\phi\sin\phi & \sin^2\theta\sin^2\phi & \sin\theta\cos\theta\sin\phi \\ \sin\theta\cos\theta\cos\phi & \sin\theta\cos\theta\sin\phi & \cos^2\theta \end{pmatrix}$$

and

$$\underline{\underline{P}} = \begin{pmatrix} \frac{L_1}{\ell} & 0 & 0 \\ 0 & \frac{L_2}{\ell} & 0 \\ 0 & 0 & \frac{L_3}{\ell} \end{pmatrix}$$

For averaging at the region of control the delta functions were used, thus after averaging the anisotropy vector is calculated to be,

$$\langle \underline{\underline{A}} \rangle = \frac{\varepsilon}{4\pi} \int_0^{2\pi} \int_0^{\pi} \int_0^{\ell} \begin{pmatrix} \sin^3\theta\cos^2\phi\frac{L_1}{\ell} & \sin^3\theta\sin\phi\cos\phi\frac{L_1}{\ell} & \sin^2\theta\cos\theta\cos\phi\frac{L_1}{\ell} \\ \sin^3\theta\cos\phi\sin\phi\frac{L_2}{\ell} & \sin^3\theta\sin^2\phi\frac{L_2}{\ell} & \sin^2\theta\cos\theta\sin\phi\frac{L_2}{\ell} \\ \sin^2\theta\cos\theta\cos\phi\frac{L_3}{\ell} & \sin^2\theta\cos\theta\sin\phi\frac{L_3}{\ell} & \sin\theta\cos^2\theta\frac{L_3}{\ell} \end{pmatrix} f(\theta, \phi, \ell) \, d\ell \, d\theta \, d\phi$$

APPENDIX C

The Knudsen diffusion coefficient for species i is given by

$$D_{ik} = \frac{2}{3} R \sqrt{\frac{8 R_g T}{m_i \pi}}$$

where m_i is the molecular weight of gas species i

The formula for the viscosity of a gas species i, η_i, is derived from kinetic theory of gases[43]·

$$\eta_i = 2.6693 \times 10^{-5} \frac{\sqrt{m_i T}}{\sigma_i^2 \Omega^{22}(T^*)}$$

where η_i is in gm cm^{-1} s^{-1}, m_i is in gm, T in K and the lennard-jones parameter σ_i is in A^0. Ω^{22} is the collision integral tabulated as a function of dimensionless temperature, $T^* = \frac{k_B T}{\varepsilon_i}$, where ε_i is another Lennard-Jones parameter. Values of σ_i and ε_i for H_2 and HCl are known; but for TMS are not available in the literature. Therefore, they are estimated from emperical relationships[34],

$$\frac{\varepsilon}{k_B} = 0\ 77 T_c$$

$$\sigma = 0.841 V_c^{1/3}$$

where the critical volume V_c is in $cm^3/mole$, the critical temperature , T_c is in K and computed $\frac{\varepsilon}{k_B}$ and σ are in K and A, respectively.

Values of σ_i and ε_i used in the computations are presented in Table B-1

Table B-1· Lennard-Jones parameters for TMS, HCl and H_2

σ, H_2, A^0	2.915
ε/k_B, H_2, K	38
σ, HCl, A^0	3.305
ε/k_B, HCl, K	360
σ, TMS, A^0	5.913
ε/k_b, TMS, K	398

The viscosity of the gas misture is given by Wilke's semi-emperical formula

$$\eta=\sum_{i=1}^{i}\frac{\eta_i}{\sum_{j=1}^{i}X_j\varphi_{ij}}$$

where $\varphi_{ij}=\frac{\sqrt{2}}{4}\left[1+\left(\frac{\eta_i}{\eta_j}\right)^{1/2}\left(\frac{m_j}{m_i}\right)^{1/4}\right]^2\left(1+\frac{m_i}{m_j}\right)^{-1/2}$

The expression for the binary diffusion coefficient is also based on the kinetic theory of gases

$$\vartheta_{ij}=1.8583\times10^{-3}\frac{\sqrt{T^3\left(\frac{1}{m_i}+\frac{1}{m_j}\right)}}{P\sigma_{ij}^2\Omega^{11}(T_{ij}^*)}$$

where ϑ_{ij} is in cm^2/s, T in K, m_i, in gm, P in atm, $\sigma_{ij}\left(\frac{\sigma_i+\sigma_j}{2}\right)$ in A^0 and $T_{ij}^*=\frac{k_BT}{\varepsilon_{ij}}$

where $\varepsilon_{ij}=\sqrt{\varepsilon_i\varepsilon_j}$.

APPENDIX D

ODF AND ANISOTROPY TENSOR

ORIENTATION 1 (O1)

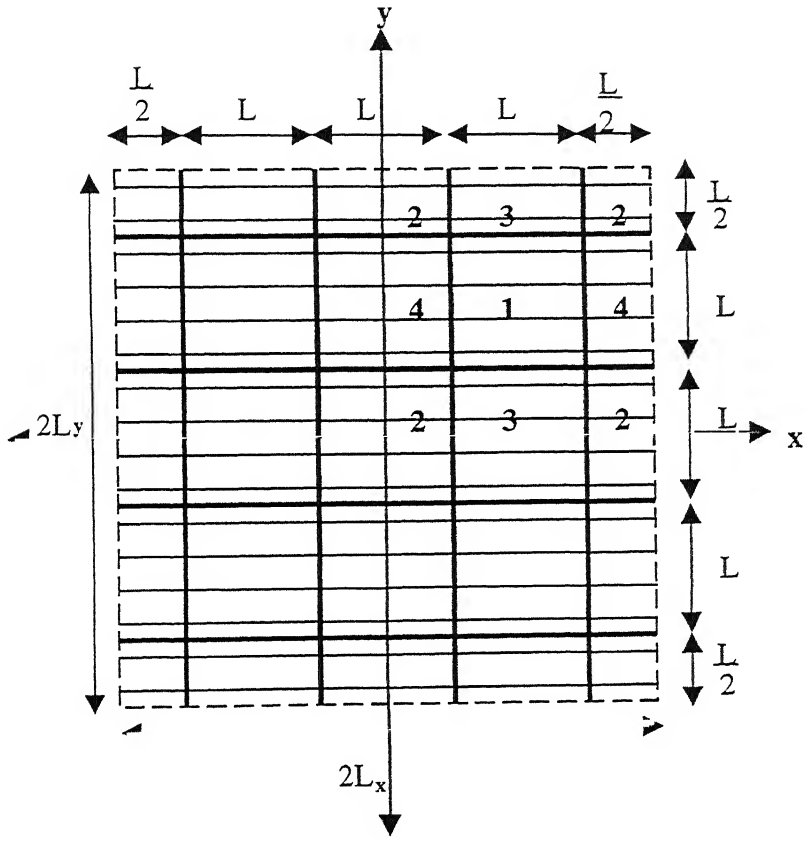

Fig. D.1: Schematic diagram of alignment of pore network in O1

Fig. D 1 represents pore network for the case, when the pores are aligned perpendicular with respect to **z**-axis ($\theta = 90^0$) and at an angle of 0^0 with respect to **x**-axis ($\phi = 0^0$). The preform is divided into different elemental volume β_{α}^{i}, where i can be 1, 2, 3 or 4. The number 1, 2, 3, and 4 represents the elemental volume at the interior, corners, lower and upper edges, and side edges of the preform respectively.

The dimension of the preform in the z-direction is taken as W for all the orientations.

Anisotropy tensor for β_α^1

Volume of the elemental volume is $V_\alpha = L \times L \times W$ and total volume of the pores inside the elemental volume is, $V_\alpha^p = \pi R^2 (n+1)L$, where (n+1) represents number of pores in the element

The ODF for the above pore network in the internal elemental volume is,

$f(\theta,\phi,\ell) = \frac{4\pi}{(n+1)L}\delta\left(\theta - \frac{\pi}{2}\right)\{\delta(\phi)[(n+1)\ell\,\delta(\ell - L)]\}$ Thus, the anisotropy tensor for the above pore network is,

$\langle A \rangle = \varepsilon\begin{pmatrix} 1 & 0 \\ 0 & 0 \end{pmatrix}$, where $\varepsilon = \frac{(n+1)\pi R^2}{L \times W}$

Anisotropy tensor for β_α^2

Volume of the element: $V_\alpha = \frac{L}{2} \times \frac{L}{2} \times W$

Total volume of the pores inside the elemental volume $V_\alpha^p = \pi R^2 (m+1)\frac{L}{2}$, for

$m = \frac{n-1}{2}$

The ODF: $f(\theta,\phi,\ell) = \frac{4\pi}{\frac{(m+1)}{2}L}\delta\left(\theta - \frac{\pi}{2}\right)\left\{\left[\delta(\phi)(m+1)\ell\,\delta\left(\ell - \frac{L}{2}\right)\right]\right\}$

The anisotropy tensor $\langle A \rangle = \varepsilon\begin{pmatrix} 1 & 0 \\ 0 & 0 \end{pmatrix}$, where $\varepsilon = \frac{(m+1)\pi R^2}{L/2 \times W} = \frac{(n+1)\pi R^2}{L \times W}$

Anisotropy tensor for β_α^3

Volume of element $V_\alpha = L \times \frac{L}{2} \times W$

Total volume of the pores: $V_\alpha^p = \pi R^2 (m+1) L$, where $m = \frac{n-1}{2}$.

The ODF is: $f(\theta,\phi,\ell) = \frac{4\pi}{(m+1)L} \delta\left(\theta - \frac{\pi}{2}\right) \{\delta(\phi)[(m+1)\ell\delta(\ell - L)]\}$

The anisotropy tensor. $\langle A \rangle = \varepsilon \begin{pmatrix} 1 & 0 \\ 0 & 0 \end{pmatrix}$, where, $\varepsilon = \frac{(m+1)\pi R^2}{L/2 \times W} = \frac{(n+1)\pi R^2}{L \times W}$

Anisotropy tensor for β_α^4

Volume of the element: $V_\alpha = L \times \frac{L}{2} \times W$

Total volume of the pores: $V_\alpha^p = \pi R^2 (m+1) L$, where $m = \frac{n-1}{2}$

The ODF $f(\theta,\phi,\ell) = \frac{4\pi}{(m+1)L} \delta\left(\theta - \frac{\pi}{2}\right) \left\{\delta(\phi)\left[2(m+1)\ell\delta\left(\ell - \frac{L}{2}\right)\right]\right\}$

The anisotropy tensor $\langle A \rangle = \varepsilon \begin{pmatrix} 1 & 0 \\ 0 & 0 \end{pmatrix}$

Where, $\varepsilon = \frac{(m+1)\pi R^2}{L/2 \times W} = \frac{(n+1)\pi R^2}{L \times W}$

ORIENTATION 2 (O2)

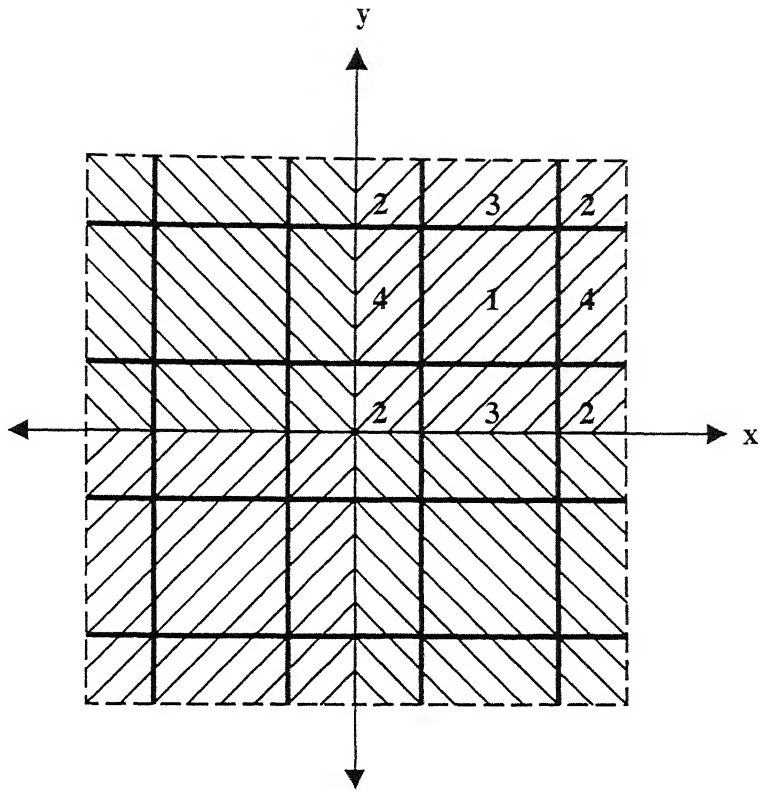

Fig. D.2: Schematic diagram of alignment of pore network in O2, $\phi = 45^0$.

Anisotropy tensor for β_α^1

Volume of the element is $V_\alpha = L \times L \times W$ and total volume of the pores inside the elemental volume is $V_\alpha^p = \sqrt{2}\pi R^2 (n+1) L$, where n represents the number of pores oriented at an angle of $\phi = 45^0$ below the diagonal and is always odd.

The ODF:

$$f(\theta,\phi,\ell) = \frac{4\pi}{\sqrt{2}(n+1)L}\delta\left(\theta - \frac{\pi}{2}\right)\delta\left(\phi - \frac{\pi}{4}\right)\left[\ell\delta\left(\ell - \sqrt{2}L\right) + 2\sum_{i=1}^{n}\ell\delta\left(\ell - \frac{\sqrt{2}i}{(n+1)}L\right)\right]$$

The anisotropy tensor: $\langle A\rangle = \varepsilon \begin{pmatrix} \frac{(2n+1)}{2\sqrt{2}(n+1)} & \frac{(2n+1)}{2\sqrt{2}(n+1)} \\ \frac{(2n+1)}{2\sqrt{2}(n+1)} & \frac{(2n-1)}{2\sqrt{2}(n+1)} \end{pmatrix}$, where, $\varepsilon = \frac{(n+1)\sqrt{2}\pi R^2}{L\times W}$

Anisotropy tensor for β_α^2

Volume of the element: $V_\alpha = \frac{L}{2}\times\frac{L}{2}\times W$

Total volume of the pores inside the elemental volume: $V_\alpha^p = \pi R^2\sqrt{2}(m+1)\frac{L}{2}$, for

$$m = \frac{n-1}{2}$$

The ODF

$$f(\theta,\phi,\ell) = \frac{4\pi}{\sqrt{2}(m+1)\frac{L}{2}}\delta\left(\theta-\frac{\pi}{2}\right)\delta\left(\phi-\frac{\pi}{4}\right)\left[\ell\delta\left(\ell-\sqrt{2}\frac{L}{2}\right)+2\sum_{i=1}^{m}\ell\delta\left(\ell-\frac{\sqrt{2}i}{(m+1)}\frac{L}{2}\right)\right]$$

The anisotropy tensor: $\langle A\rangle = \varepsilon \begin{pmatrix} \frac{(2m+1)}{2\sqrt{2}(m+1)} & \frac{(2m+1)}{2\sqrt{2}(m+1)} \\ \frac{(2m+1)}{2\sqrt{2}(m+1)} & \frac{(2m+1)}{2\sqrt{2}(m+1)} \end{pmatrix}$.

where, $\varepsilon = \frac{(m+1)\sqrt{2}\pi R^2}{L/2\times W} = \frac{(n+1)\sqrt{2}\pi R^2}{L\times W}$.

Anisotropy tensor for β_α^3

Volume of the element: $V_\alpha = L\times\frac{L}{2}\times W$

Total volume of the pores inside the elemental volume: $V_\alpha^p = \pi R^2\sqrt{2}(m+1)L$, where

$$m = \frac{n-1}{2}.$$

The ODF:

$$f(\theta,\phi,\ell)=\frac{4\pi}{\sqrt{2}(m+1)L}\delta\left(\theta-\frac{\pi}{2}\right)\delta\left(\phi-\frac{\pi}{4}\right)\left[(m+2)\ell\delta\left(\ell-\sqrt{2}\frac{L}{2}\right)+2\sum_{i=1}^{m}\ell\delta\left(\ell-\frac{\sqrt{2}i}{(m+1)}\frac{L}{2}\right)\right]$$

The anisotropy tensor: $\langle A\rangle=\varepsilon\begin{pmatrix}\frac{(3m+2)}{2\sqrt{2}(m+1)} & \frac{(3m+2)}{2\sqrt{2}(m+1)}\\ \frac{(3m+2)}{4\sqrt{2}(m+1)} & \frac{(3m+2)}{4\sqrt{2}(m+1)}\end{pmatrix}$

Where , $\varepsilon=\frac{(m+1)\sqrt{2}\pi R^2}{\frac{L}{2}\times W}=\frac{(n+1)\sqrt{2}\pi R^2}{L\times W}$.

Anisotropy tensor for β_α^4

Volume of the element $V_\alpha=L\times\frac{L}{2}\times W$

Total volume of the pores inside the elemental volume: $V_\alpha^p=\pi R^2\sqrt{2}(m+1)L$

where, $m=\frac{n-1}{2}$.

The ODF:

$$f(\theta,\phi,\ell)=\frac{4\pi}{\sqrt{2}(m+1)L}\delta\left(\theta-\frac{\pi}{2}\right)\delta\left(\phi-\frac{\pi}{4}\right)\left[(m+2)\ell\delta\left(\ell-\sqrt{2}\frac{L}{2}\right)+2\sum_{i=1}^{m}\ell\delta\left(\ell-\frac{\sqrt{2}i}{(m+1)}\frac{L}{2}\right)\right]$$

The anisotropy tensor: $\langle A\rangle=\varepsilon\begin{pmatrix}\frac{(3m+2)}{4\sqrt{2}(m+1)} & \frac{(3m+2)}{4\sqrt{2}(m+1)}\\ \frac{(3m+2)}{2\sqrt{2}(m+1)} & \frac{(3m+2)}{2\sqrt{2}(m+1)}\end{pmatrix}$

Where, $\varepsilon=\frac{(m+1)\sqrt{2}\pi R^2}{\frac{L}{2}\times W}=\frac{(n+1)\sqrt{2}\pi R^2}{L\times W}$

ORIENTATION 3 (O3)

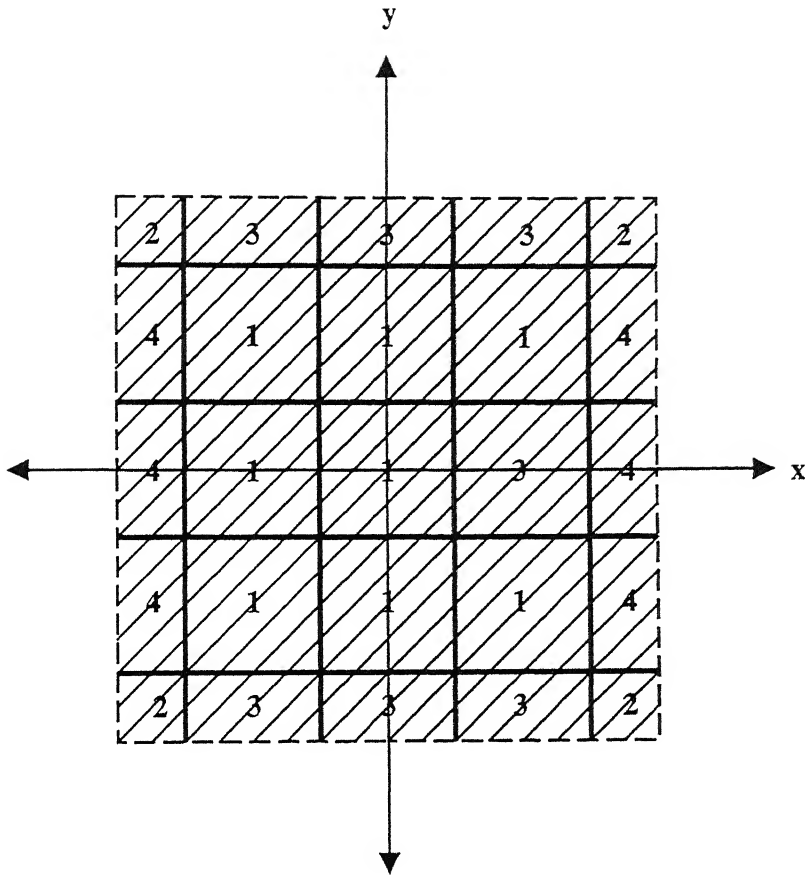

Fig D.3 Schematic diagram of alignment of pore network O3 with $\phi = 45^0$ in entire preform.

Fig. D.3 represents pore network similar to the O2, except symmetry requirement about both the axes is relaxed.

The anisotropy tensor obtained for different elemental volumes are same as in O2.

ORIENTATION 4 (O4)

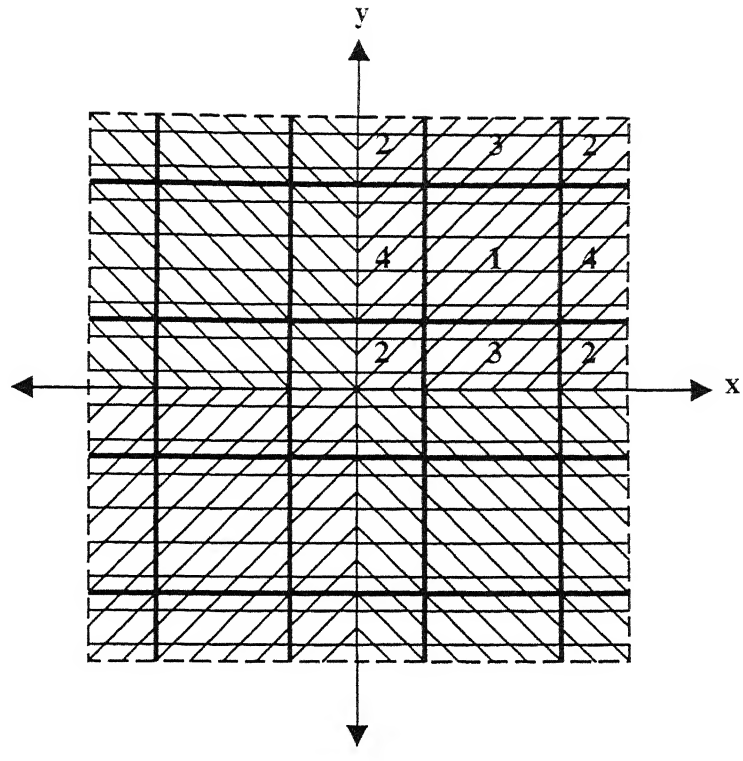

Fig. D.4 Schematic diagram of alignment of pore network in O4 $\phi = 0^0$ and 45^0.

Anisotropy tensor for β_α^1

Volume of the element is $V_\alpha = L \times L \times W$ and total volume of the pores in the elemental volume is $V_\alpha^p = \left(1+\sqrt{2}\right)(n+1)\pi R^2 L$, where n represents the number of pores oriented at an angle of $\phi = 45^0$, below the diagonal pore and n+1 is the total number of pores parallel to the **x**-axis.

The ODF:

$$f(\theta,\phi,\ell) = \frac{4\pi}{\left(1+\sqrt{2}\right)(n+1)L}\delta\left(\theta-\frac{\pi}{2}\right)$$
$$\times\left\{\delta(\phi)[(n+1)\ell\delta(\ell-L)]+\delta\left(\phi-\frac{\pi}{4}\right)\left[\ell\delta\left(\ell-\sqrt{2}L\right)+2\sum_{i=1}^{n}\ell\delta\left(\ell-\frac{\sqrt{2}i}{(n+1)}L\right)\right]\right\}$$

The anisotropy tensor: $\langle A\rangle=\varepsilon\begin{pmatrix}\frac{(4n+3)}{2(1+\sqrt{2})(n+1)} & \frac{(2n+1)}{2(1+\sqrt{2})(n+1)}\\ \frac{(2n+1)}{2(1+\sqrt{2})(n+1)} & \frac{(2n-1)}{2(1+\sqrt{2})(n+1)}\end{pmatrix}$

Where, $\varepsilon=\frac{(n+1)(1+\sqrt{2})\pi R^2}{L\times W}$

Anisotropy tensor for β_α^2

Volume of the element: $V_\alpha=\frac{L}{2}\times\frac{L}{2}\times W$

Total volume of the pores inside the elemental volume: $V_\alpha^p=\pi R^2(1+\sqrt{2})(m+1)\frac{L}{2}$

where $m=\frac{n-1}{2}$.

The ODF:

$$f(\theta,\phi,\ell)=\frac{4\pi}{(1+\sqrt{2})(m+1)\frac{L}{2}}\delta\left(\theta-\frac{\pi}{2}\right)$$

$$\left\{\delta(\phi)\left[(m+1)\ell\delta\left(\ell-\frac{L}{2}\right)\right]+\delta\left(\phi-\frac{\pi}{4}\right)\left[\ell\delta\left(\ell-\sqrt{2}\frac{L}{2}\right)+2\sum_{i=1}^{m}\ell\delta\left(\ell-\frac{\sqrt{2}i}{(m+1)}\frac{L}{2}\right)\right]\right\}$$

The anisotropy tensor. $\langle A\rangle=\varepsilon\begin{pmatrix}\frac{(4m+3)}{2(1+\sqrt{2})(m+1)} & \frac{(2m+1)}{2(1+\sqrt{2})(m+1)}\\ \frac{(2m+1)}{2(1+\sqrt{2})(m+1)} & \frac{(2m+1)}{2(1+\sqrt{2})(m+1)}\end{pmatrix}$

Where, $\varepsilon=\frac{(m+1)(1+\sqrt{2})\pi R^2}{\frac{L}{2}\times W}=\frac{(n+1)(1+\sqrt{2})\pi R^2}{L\times W}$.

Anisotropy tensor for β_α^3

Volume of the element: $V_\alpha=L\times\frac{L}{2}\times W$

Total volume of the pores inside the elemental volume: $V_\alpha^p = \pi R^2\left(1+\sqrt{2}\right)(m+1)L$,

where $m = \dfrac{n-1}{2}$.

The ODF:

$$f(\theta,\phi,\ell) = \frac{4\pi}{\left(1+\sqrt{2}\right)(m+1)L}\delta\left(\theta-\frac{\pi}{2}\right)$$
$$\left\{\delta(\phi)[(m+1)\ell\delta(\ell-L)]+\delta\left(\phi-\frac{\pi}{4}\right)\left[(m+2)\ell\delta\left(\ell-\sqrt{2}\frac{L}{2}\right)+2\sum_{i=1}^{m}\ell\delta\left(\ell-\frac{\sqrt{2}i}{(m+1)}\frac{L}{2}\right)\right]\right\}$$

The anisotropy tensor : $\langle A\rangle = \varepsilon\begin{pmatrix} \dfrac{(5m+4)}{2\left(1+\sqrt{2}\right)(m+1)} & \dfrac{(3m+2)}{2\left(1+\sqrt{2}\right)(m+1)} \\ \dfrac{(3m+2)}{4\left(1+\sqrt{2}\right)(m+1)} & \dfrac{(3m+2)}{4\left(1+\sqrt{2}\right)(m+1)} \end{pmatrix}$

Where, $\varepsilon = \dfrac{(m+1)\left(1+\sqrt{2}\right)\pi R^2}{\frac{L}{2}\times W} = \dfrac{(n+1)\left(1+\sqrt{2}\right)\pi R^2}{L\times W}$.

Anisotropy tensor for β_α^4

Volume of the elemental: $V_\alpha = L\times\dfrac{L}{2}\times W$

Total volume of the pores inside the elemental volume: $V_\alpha^p = \pi R^2\left(1+\sqrt{2}\right)(m+1)L$,

where $m = \dfrac{n-1}{2}$.

The ODF:

$$f(\theta,\phi,\ell) = \frac{4\pi}{\left(1+\sqrt{2}\right)(m+1)L}\delta\left(\theta-\frac{\pi}{2}\right)$$
$$\left\{\delta(\phi)\left[2(m+1)\ell\delta\left(\ell-\frac{L}{2}\right)\right]+\delta\left(\phi-\frac{\pi}{4}\right)\left[(m+2)\ell\delta\left(\ell-\sqrt{2}\frac{L}{2}\right)+2\sum_{i=1}^{m}\ell\delta\left(\ell-\frac{\sqrt{2}i}{(m+1)}\frac{L}{2}\right)\right]\right\}$$

The anisotropy tensor $\langle A \rangle = \varepsilon \begin{pmatrix} \frac{(7m+6)}{4(1+\sqrt{2})(m+1)} & \frac{(3m+2)}{4(1+\sqrt{2})(m+1)} \\ \frac{(3m+2)}{2(1+\sqrt{2})(m+1)} & \frac{(3m+2)}{2(1+\sqrt{2})(m+1)} \end{pmatrix}$

where, $\varepsilon = \frac{(m+1)(1+\sqrt{2})\pi R^2}{\frac{L}{2} \times W} = \frac{(n+1)(1+\sqrt{2})\pi R^2}{L \times W}$

ORIENTATION 5 (O5)

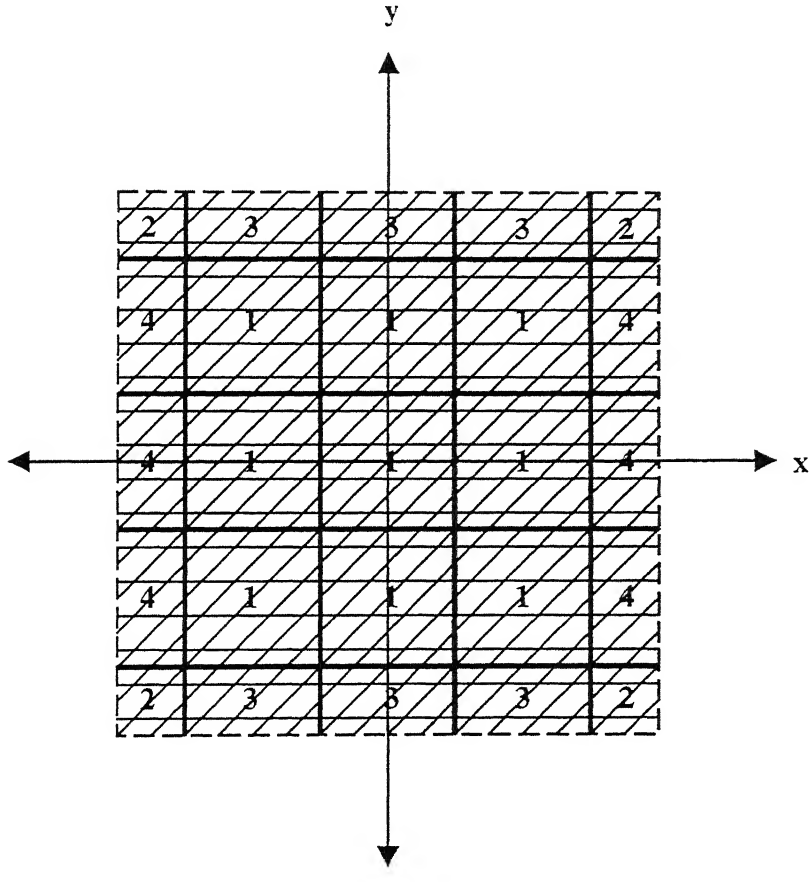

Fig. D.5. O5 pore orientation; pores as in O4 without symmetry required both the axes.

The anisotropy tensor obtained for different elemental volumes are same as in the previous case.

ORIENTATION 6 (O6)

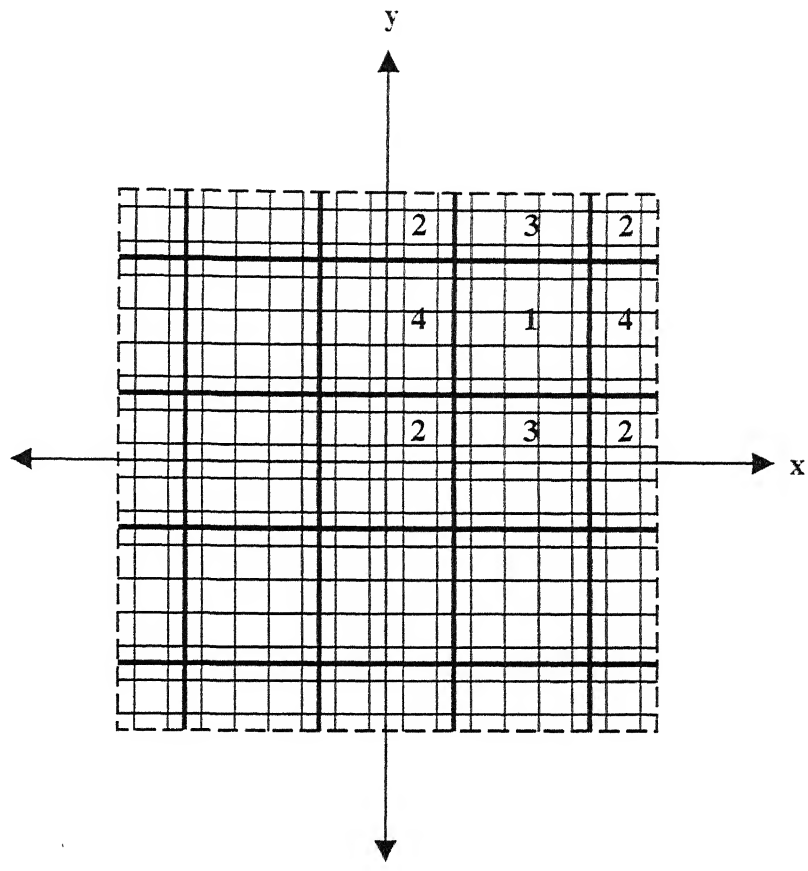

Fig. D.6: Schematic diagram of alignment of pore network in O6. $\phi = 0^0$ and 90^0.

Anisotropy tensor for β_{α}^{1}

Volume of the element is $V_\alpha = L \times L \times W$ and total volume of the pores inside the elemental volume is $V_\alpha^p = \pi R^2 2(n+1)L$, where (n+1) represents number of pores in each direction.

The ODF:

$$f(\theta,\phi,\ell) = \frac{4\pi}{2(n+1)L}\delta\left(\theta-\frac{\pi}{2}\right)\left\{\delta(\phi)[(n+1)\ell\delta(\ell-L)]+\delta\left(\phi-\frac{\pi}{2}\right)[(n+1)\ell\delta(\ell-L)]\right\}.$$

The anisotropy tensor: $\langle A\rangle=\varepsilon\begin{pmatrix}\frac{1}{2} & 0\\ 0 & \frac{1}{2}\end{pmatrix}$, where, $\varepsilon=\frac{2(n+1)\pi R^2}{L\times W}$

Anisotropy tensor for β_α^2

Volume of the element: $V_\alpha=\frac{L}{2}\times\frac{L}{2}\times W$

Total volume of the pores inside the elemental volume: $V_\alpha^p=\pi R^2(m+1)L$, where

$m=\frac{n-1}{2}$

The ODF:

$$f(\theta,\phi,\ell)=\frac{4\pi}{(m+1)L}\delta\left(\theta-\frac{\pi}{2}\right)\left\{\delta(\phi)\left[(m+1)\ell\delta\left(\ell-\frac{L}{2}\right)\right]+\delta\left(\phi-\frac{\pi}{2}\right)\left[(m+1)\ell\delta\left(\ell-\frac{L}{2}\right)\right]\right\}$$

The anisotropy tensor: $\langle A\rangle=\varepsilon\begin{pmatrix}\frac{1}{2} & 0\\ 0 & \frac{1}{2}\end{pmatrix}$, where, $\varepsilon=\frac{2(m+1)\pi R^2}{L/2\times W}=\frac{2(n+1)\pi R^2}{L\times W}$.

Anisotropy tensor for β_α^3

Volume of the element. $V_\alpha=L\times\frac{L}{2}\times W$

Total volume of the pores inside the elemental volume: $V_\alpha^p=\pi R^2 2(m+1)L$, where,

$m=\frac{n-1}{2}$

The ODF:

$$f(\theta,\phi,\ell)=\frac{4\pi}{2(m+1)L}\delta\left(\theta-\frac{\pi}{2}\right)\left\{\delta(\phi)[(m+1)\ell\delta(\ell-L)]+\delta\left(\phi-\frac{\pi}{2}\right)\left[2(m+1)\ell\delta\left(\ell-\frac{L}{2}\right)\right]\right\}$$

The anisotropy tensor. $\langle A\rangle=\varepsilon\begin{pmatrix}\frac{1}{2} & 0\\ 0 & \frac{1}{2}\end{pmatrix}$, Where, $\varepsilon=\frac{2(m+1)\pi R^2}{\frac{L}{2}\times W}=\frac{2(n+1)\pi R^2}{L\times W}$

Anisotropy tensor for β_α^4

volume of the element: $V_\alpha=L\times\frac{L}{2}\times W$

Total volume of the pores inside the elemental volume: $V_\alpha^p=\pi R^2 2(m+1)L$, where,

$m=\frac{n-1}{2}$

The ODF·

$$f(\theta,\phi,\ell)=\frac{4\pi}{2(m+1)L}\delta\left(\theta-\frac{\pi}{2}\right)\left\{\delta(\phi)\left[2(m+1)\ell\delta\left(\ell-\frac{L}{2}\right)\right]+\delta\left(\phi-\frac{\pi}{2}\right)\left[(m+1)\ell\delta(\ell-L)\right]\right\}$$

The anisotropy tensor. $\langle A\rangle=\varepsilon\begin{pmatrix}\frac{1}{2} & 0\\ 0 & \frac{1}{2}\end{pmatrix}$, Where, $\varepsilon=\frac{2(m+1)\pi R^2}{\frac{L}{2}\times W}=\frac{2(n+1)\pi R^2}{L\times W}$

ORIENTATION 7 (O7)

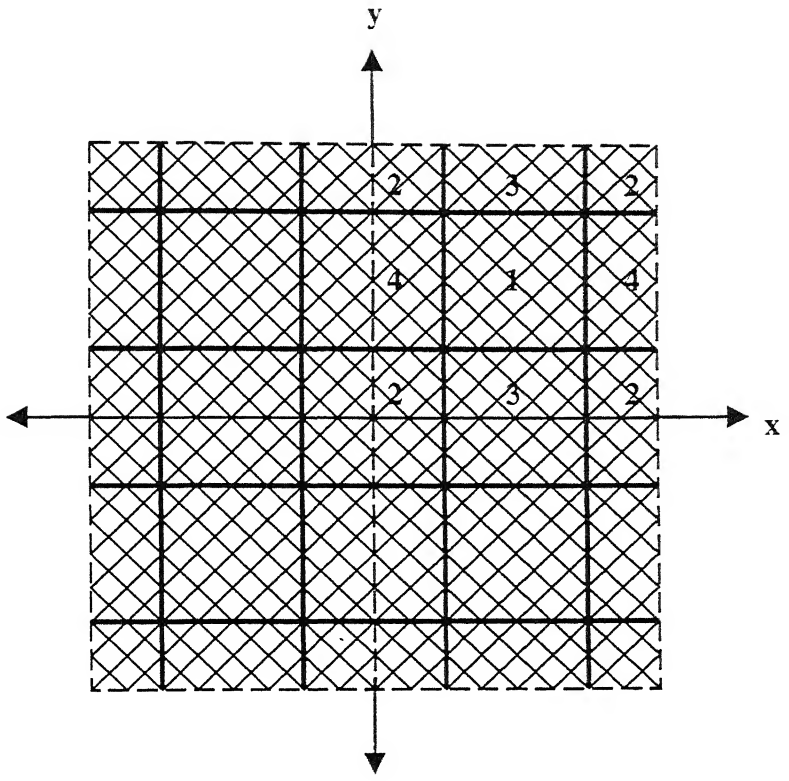

D.7· Schematic diagram of alignment of pore network in O7. $\phi = 45^0$ and 135^0

Anisotropy tensor for β_α^1

Volume of the element is $V_\alpha = L \times L \times W$ and total volume of the pores in the elemental volume is $V_\alpha^p = \pi R^2 2\sqrt{2}(n+1)L$, where n represents the number of pores below the either diagonal.

The ODF·

$$f(\theta,\phi,\ell)=\frac{4\pi}{2\sqrt{2}(n+1)L}\delta\left(\theta-\frac{\pi}{2}\right)\left\{\begin{array}{l}\delta\left(\phi-\frac{\pi}{4}\right)\left[\ell\delta\left(\ell-\sqrt{2}L\right)+2\sum_{i=1}^{n}\ell\delta\left(\ell-\frac{\sqrt{2}i}{(n+1)}L\right)\right]\\+\delta\left(\phi-\frac{3\pi}{4}\right)\left[\ell\delta\left(\ell-\sqrt{2}L\right)+2\sum_{i=1}^{n}\ell\delta\left(\ell-\frac{\sqrt{2}i}{(n+1)}L\right)\right]\end{array}\right\}$$

The anisotropy tensor: $\langle A\rangle=\varepsilon\begin{pmatrix}\frac{(2n+1)}{2\sqrt{2}(n+1)} & 0\\ 0 & \frac{(2n+1)}{2\sqrt{2}(n+1)}\end{pmatrix}$,

where, $\varepsilon=\frac{(n+1)2\sqrt{2}\pi R^2}{L\times W}$

Anisotropy tensor for β_α^2

Volume of the element: $V_\alpha=\frac{L}{2}\times\frac{L}{2}\times W$

Total volume of the pores inside the elemental volume: $V_\alpha^p=\pi R^2 2\sqrt{2}(m+1)\frac{L}{2}$,

where, $m=\frac{n-1}{2}$.

TheODF:

$$f(\theta,\phi,\ell)=\frac{4\pi}{2\sqrt{2}(m+1)\frac{L}{2}}\delta\left(\theta-\frac{\pi}{2}\right)\left\{\begin{array}{l}\delta\left(\phi-\frac{\pi}{4}\right)\left[\ell\delta\left(\ell-\sqrt{2}\frac{L}{2}\right)+2\sum_{i=1}^{m}\ell\delta\left(\ell-\frac{\sqrt{2}i}{(m+1)}\frac{L}{2}\right)\right]\\ +\delta\left(\phi-\frac{3\pi}{4}\right)\left[\ell\delta\left(\ell-\sqrt{2}\frac{L}{2}\right)+2\sum_{i=1}^{m}\ell\delta\left(\ell-\frac{\sqrt{2}i}{(m+1)}\frac{L}{2}\right)\right]\end{array}\right\}$$

The anisotropy tensor: $\langle A\rangle=\varepsilon\begin{pmatrix}\frac{(2m+1)}{2\sqrt{2}(m+1)} & 0\\ 0 & \frac{(2m+1)}{2\sqrt{2}(m+1)}\end{pmatrix}$,

where $\varepsilon=\frac{(m+1)2\sqrt{2}\pi R^2}{L/2\times W}=\frac{(n+1)2\sqrt{2}\pi R^2}{L\times W}$

Anisotropy tensor for β_α^3

Volume of the element: $V_\alpha=L\times\frac{L}{2}\times W$

Total volume of the pores inside the elemental volume: $V_\alpha^p = \pi R^2 2\sqrt{2}(m+1)L$.

where,

$$m = \frac{n-1}{2}$$

The ODF:

$$f(\theta,\phi,\ell) = \frac{4\pi}{2\sqrt{2}(m+1)L}\delta\left(\theta-\frac{\pi}{2}\right)\left\{\begin{array}{l}\delta\left(\phi-\frac{\pi}{4}\right)\left[(m+2)\ell\delta\left(\ell-\sqrt{2}\frac{L}{2}\right)+2\sum_{i=1}^{m}\ell\delta\left(\ell-\frac{\sqrt{2}i}{(m+1)}\frac{L}{2}\right)\right] \\ +\delta\left(\phi-\frac{3\pi}{4}\right)\left[(m+2)\ell\delta\left(\ell-\sqrt{2}\frac{L}{2}\right)+2\sum_{i=1}^{m}\ell\delta\left(\ell-\frac{\sqrt{2}i}{(m+1)}\frac{L}{2}\right)\right]\end{array}\right\}$$

The anisotropy tensor. $\langle A\rangle = \varepsilon\begin{pmatrix}\frac{(3m+2)}{2\sqrt{2}(m+1)} & 0 \\ 0 & \frac{(3m+2)}{4\sqrt{2}(m+1)}\end{pmatrix}$,

where $\varepsilon = \frac{(m+1)2\sqrt{2}\,\pi R^2}{\frac{L}{2}\times W} = \frac{(n+1)2\sqrt{2}\,\pi R^2}{L\times W}$

Anisotropy tensor for β_α^4

Volume of the element: $V_\alpha = L\times\frac{L}{2}\times W$

Total volume of the pores inside the elemental volume: $V_\alpha^p = \pi R^2 2\sqrt{2}(m+1)L$.

where, $m = \frac{n-1}{2}$.

The ODF.

$$f(\theta,\phi,\ell)=\frac{4\pi}{2\sqrt{2}(m+1)L}\delta\left(\theta-\frac{\pi}{2}\right)\left\{\begin{array}{l}\delta\left(\phi-\frac{\pi}{4}\right)\left[(m+2)\ell\delta\left(\ell-\sqrt{2}\frac{L}{2}\right)+2\sum_{i=1}^{m}\ell\delta\left(\ell-\frac{\sqrt{2}i}{(m+1)}\frac{L}{2}\right)\right] \\ +\delta\left(\phi-\frac{3\pi}{4}\right)\left[(m+2)\ell\delta\left(\ell-\sqrt{2}\frac{L}{2}\right)+2\sum_{i=1}^{m}\ell\delta\left(\ell-\frac{\sqrt{2}i}{(m+1)}\frac{L}{2}\right)\right]\end{array}\right\}$$

The anisotropy tensor: $\langle A\rangle=\varepsilon\begin{pmatrix}\frac{(3m+2)}{4\sqrt{2}(m+1)} & 0\\ 0 & \frac{(3m+2)}{2\sqrt{2}(m+1)}\end{pmatrix}$,

where $\varepsilon=\frac{(m+1)2\sqrt{2}\pi R^2}{\frac{L}{2}\times W}=\frac{(n+1)2\sqrt{2}\pi R^2}{L\times W}$

ORIENTATION 8 (O8)

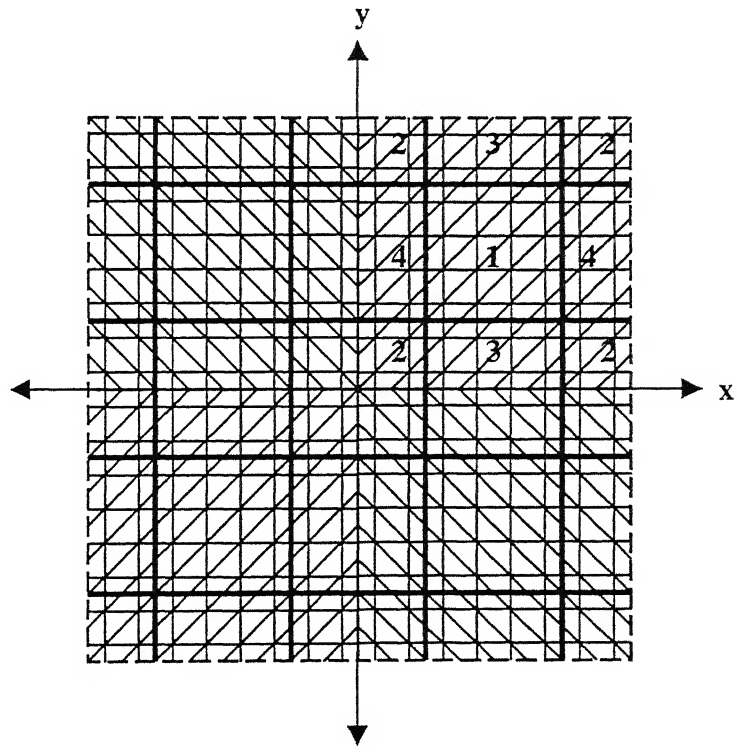

Fig. D.8: Schematic diagram of alignment of pore network in O8. $\phi = 0^0$ and 45^0.

Anisotropy tensor for β_α^1

Volume of the element is $V_\alpha = L \times L \times W$ and total volume of the pores in the elemental volume is $V_\alpha^p = \left(2+\sqrt{2}\right)(n+1)\pi R^2 L$, where n represents the number of pores oriented at an angle of $\phi = 45^0$,below the diagonal.

The ODF:

$$f(\theta,\phi,\ell)=\frac{4\pi}{\left(2+\sqrt{2}\right)(n+1)L}\delta\left(\theta-\frac{\pi}{2}\right)\left\{\begin{array}{l}\delta(\phi)[(n+1)\ell\delta(\ell-L)]+\delta\left(\phi-\frac{\pi}{2}\right)[(n+1)\ell\delta(\ell-L)] \\ +\delta\left(\phi-\frac{\pi}{4}\right)\left[\ell\delta\left(\ell-\sqrt{2}L\right)+2\sum_{i=1}^{n}\ell\delta\left(\ell-\frac{\sqrt{2}i}{(n+1)}L\right)\right]\end{array}\right\}$$

The anisotropy tensor: $\langle A\rangle=\varepsilon\begin{pmatrix}\frac{(4n+3)}{2\left(2+\sqrt{2}\right)(n+1)} & \frac{(2n+1)}{2\left(2+\sqrt{2}\right)(n+1)} \\ \frac{(2n+1)}{2\left(2+\sqrt{2}\right)(n+1)} & \frac{(4n+3)}{2\left(2+\sqrt{2}\right)(n+1)}\end{pmatrix}$,

where, $\varepsilon = \dfrac{(n+1)\left(2+\sqrt{2}\right)\pi R^2}{L\times W}$

Anisotropy tensor for β_α^2

Volume of the element: $V_\alpha = \dfrac{L}{2}\times\dfrac{L}{2}\times W$

Total volume of the pores inside the elemental volume: $V_\alpha^p = \pi R^2\left(2+\sqrt{2}\right)(m+1)\dfrac{L}{2}$,

where $m = \dfrac{n-1}{2}$

The ODF.

$$f(\theta,\phi,\ell)=\frac{4\pi}{\left(2+\sqrt{2}\right)(m+1)\frac{L}{2}}\delta\left(\theta-\frac{\pi}{2}\right)\begin{Bmatrix}\delta(\phi)\left[(m+1)\ell\delta\left(\ell-\frac{L}{2}\right)\right]+\delta\left(\phi-\frac{\pi}{2}\right)\left[(m+1)\ell\delta\left(\ell-\frac{L}{2}\right)\right]\\ \delta\left(\phi-\frac{\pi}{4}\right)\left[\ell\delta\left(\ell-\sqrt{2}\frac{L}{2}\right)+2\sum_{i=1}^{m}\ell\delta\left(\ell-\frac{\sqrt{2}i}{(m+1)}\frac{L}{2}\right)\right]\end{Bmatrix}$$

The anisotropy tensor. $\langle A\rangle=\varepsilon\begin{pmatrix}\frac{(4m+3)}{2\left(2+\sqrt{2}\right)(m+1)} & \frac{(2m+1)}{2\left(2+\sqrt{2}\right)(m+1)}\\ \frac{(2m+1)}{2\left(2+\sqrt{2}\right)(m+1)} & \frac{(4m+3)}{2\left(2+\sqrt{2}\right)(m+1)}\end{pmatrix}$,

where, $\varepsilon=\frac{(m+1)\left(2+\sqrt{2}\right)\pi R^2}{L/2\times W}=\frac{(n+1)\left(2+\sqrt{2}\right)\pi R^2}{L\times W}$

Anisotropy tensor for β_α^3

Volume of the element. $V_\alpha=L\times\frac{L}{2}\times W$

Total volume of the pores inside the elemental volume· $V_\alpha^p=\pi R^2\left(2+\sqrt{2}\right)(m+1)L$,

where, $m=\frac{n-1}{2}$.

The ODF:

$$f(\theta,\phi,\ell)=\frac{4\pi}{\left(2+\sqrt{2}\right)(m+1)L}\delta\left(\theta-\frac{\pi}{2}\right)\begin{Bmatrix}\delta(\phi)[(m+1)\ell\delta(\ell-L)]+\delta\left(\phi-\frac{\pi}{2}\right)\left[2(m+1)\ell\delta\left(\ell-\frac{L}{2}\right)\right]+\\ \delta\left(\phi-\frac{\pi}{4}\right)\left[(m+2)\ell\delta\left(\ell-\sqrt{2}\frac{L}{2}\right)+2\sum_{i=1}^{m}\ell\delta\left(\ell-\frac{\sqrt{2}i}{(m+1)}\frac{L}{2}\right)\right]\end{Bmatrix}$$

The anisotropy tensor: $\langle A\rangle=\varepsilon\begin{pmatrix}\frac{(5m+4)}{2\left(2+\sqrt{2}\right)(m+1)} & \frac{(3m+2)}{2\left(2+\sqrt{2}\right)(m+1)}\\ \frac{(3m+2)}{4\left(2+\sqrt{2}\right)(m+1)} & \frac{(7m+6)}{4\left(1+\sqrt{2}\right)(m+1)}\end{pmatrix}$.

where, $\varepsilon=\frac{(m+1)\left(2+\sqrt{2}\right)\pi R^2}{\frac{L}{2}\times W}=\frac{(n+1)\left(2+\sqrt{2}\right)\pi R^2}{L\times W}$

Anisotropy tensor for β_α^4

Volume of the element $V_\alpha = L \times \frac{L}{2} \times W$

Total volume of the pores inside the elemental volume: $V_\alpha^p = \pi R^2 (2+\sqrt{2})(m+1)L$,

where, $m = \frac{n-1}{2}$.

The ODF:

$$f(\theta,\phi,\ell) = \frac{4\pi}{(2+\sqrt{2})(m+1)L}\delta\left(\theta-\frac{\pi}{2}\right)\left\{\begin{array}{l}\delta(\phi)\left[2(m+1)\ell\delta\left(\ell-\frac{L}{2}\right)\right]+\delta\left(\phi-\frac{\pi}{2}\right)[(m+1)\ell\delta(\ell-L)]+ \\ \delta\left(\phi-\frac{\pi}{4}\right)\left[(m+2)\ell\delta\left(\ell-\sqrt{2}\frac{L}{2}\right)+2\sum_{i=1}^{m}\ell\delta\left(\ell-\frac{\sqrt{2}\,i}{(m+1)}\frac{L}{2}\right)\right]\end{array}\right\}$$

The anisotropy tensor: $\langle A\rangle = \varepsilon\begin{pmatrix}\frac{(7m+6)}{4(2+\sqrt{2})(m+1)} & \frac{(3m+2)}{4(2+\sqrt{2})(m+1)} \\ \frac{(3m+2)}{2(2+\sqrt{2})(m+1)} & \frac{(5m+4)}{2(2+\sqrt{2})(m+1)}\end{pmatrix}$

Where, $\varepsilon = \frac{(m+1)(2+\sqrt{2})\pi R^2}{\frac{L}{2}\times W} = \frac{(n+1)(2+\sqrt{2})\pi R^2}{L\times W}$

ORIENTATION 9 (O9)

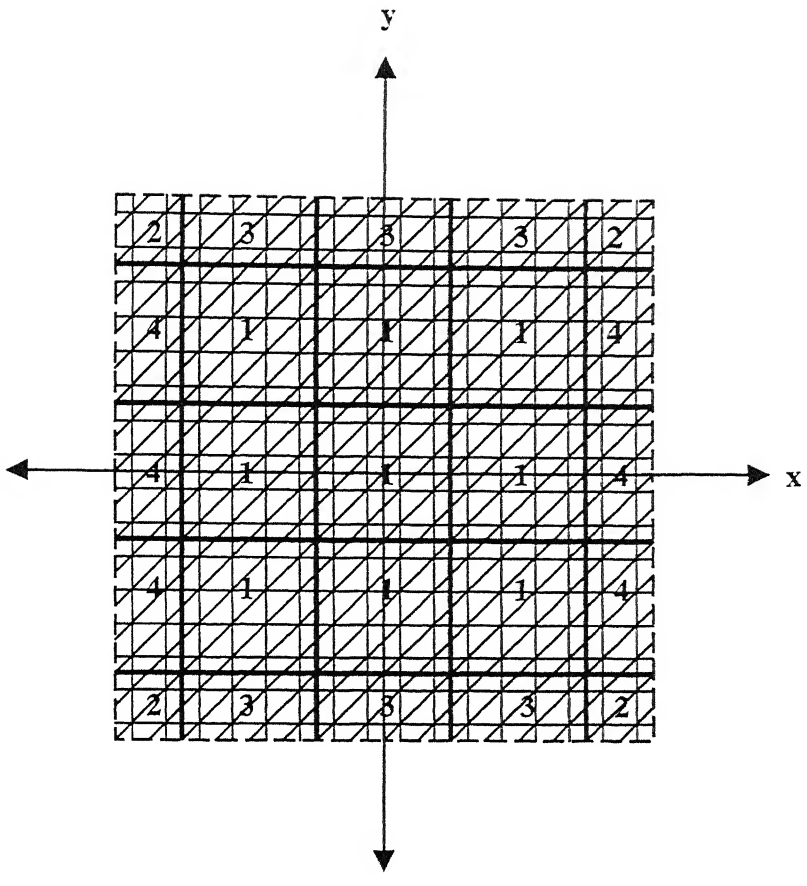

Fig. D.9: Schematic diagram of alignment of pore network O9 with $\phi = 0^0$, 45^0 and 90^0 in entire preform.

The anisotropy tensor obtained for different elemental volumes are same as in the previous case.

ORIENTATION 10 (O10)

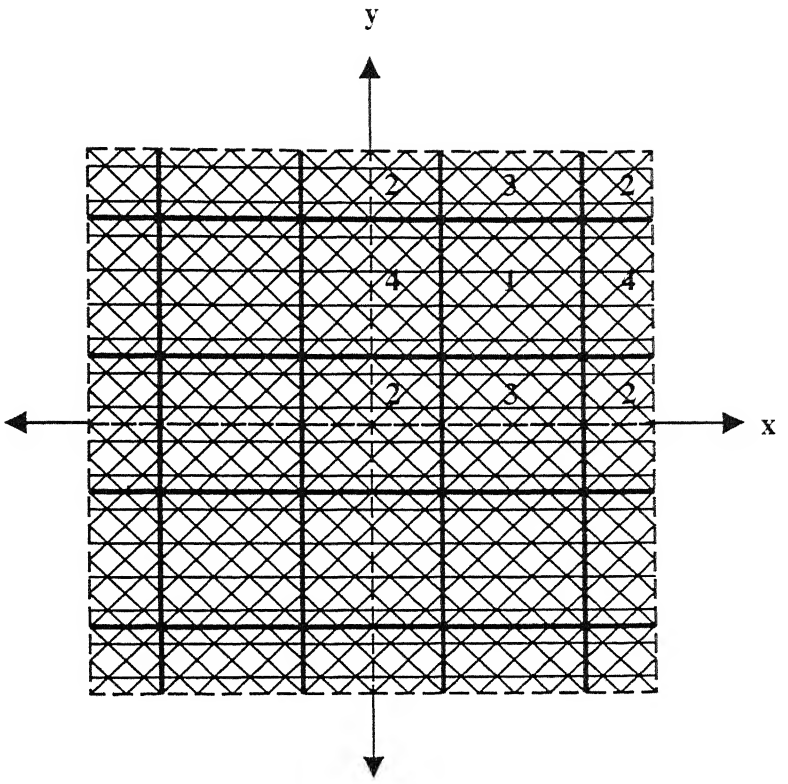

Fig. D.10: Schematic diagram of alignment of pore network in O10. ($\phi = 0^0$, 45^0, and 135^0.

Anisotropy tensor for β_α^1

Volume of the element is $V_\alpha = L \times L \times W$ and total volume of the pores in the elemental volume is $V_\alpha^p = \left(1+2\sqrt{2}\right)(n+1)\pi R^2 L$, where n represents the number of pores oriented at an angle of $\phi = 45^0$ or 135^0,below the either diagonal and (n+1) are pores parallel to x-axis.

The ODF

$$f(\theta,\phi,\ell)=\frac{4\pi}{(1+2\sqrt{2})(n+1)L}\delta\left(\theta-\frac{\pi}{2}\right)\begin{Bmatrix}\delta(\phi)\left[(n+1)\ell\delta(\ell-L)\right]+\\ \delta\left(\phi-\frac{\pi}{4}\right)\left[\ell\delta(\ell-\sqrt{2}L)+2\sum_{i=1}^{n}\ell\delta\left(\ell-\frac{\sqrt{2}i}{(n+1)}L\right)\right]+\\ \delta\left(\phi-\frac{3\pi}{4}\right)\left[\ell\delta(\ell-\sqrt{2}L)+2\sum_{i=1}^{n}\ell\delta\left(\ell-\frac{\sqrt{2}i}{(n+1)}L\right)\right]\end{Bmatrix}$$

The anisotropy tensor: $\langle A\rangle=\varepsilon\begin{pmatrix}\frac{(3n+2)}{(1+2\sqrt{2})(n+1)} & 0\\ 0 & \frac{(2n+1)}{(1+2\sqrt{2})(n+1)}\end{pmatrix}$,

where, $\varepsilon=\frac{(n+1)(1+2\sqrt{2})\pi R^2}{L\times W}$

Anisotropy tensor for β_α^2

Volume of the element: $V_\alpha=\frac{L}{2}\times\frac{L}{2}\times W$

Total volume of the pores inside the elemental volume: $V_\alpha^p=\pi R^2(1+2\sqrt{2})(m+1)\frac{L}{2}$.

where, $m=\frac{n-1}{2}$.

The ODF:

$$f(\theta,\phi,\ell)=\frac{4\pi}{(1+2\sqrt{2})(m+1)\frac{L}{2}}\delta\left(\theta-\frac{\pi}{2}\right)\begin{Bmatrix}\delta(\phi)\left[(m+1)\ell\delta\left(\ell-\frac{L}{2}\right)\right]+\\ \delta\left(\phi-\frac{\pi}{4}\right)\left[\ell\delta\left(\ell-\sqrt{2}\frac{L}{2}\right)+2\sum_{i=1}^{m}\ell\delta\left(\ell-\frac{\sqrt{2}i}{(m+1)}\frac{L}{2}\right)\right]+\\ \delta\left(\phi-\frac{3\pi}{4}\right)\left[\ell\delta\left(\ell-\sqrt{2}\frac{L}{2}\right)+2\sum_{i=1}^{m}\ell\delta\left(\ell-\frac{\sqrt{2}i}{(m+1)}\frac{L}{2}\right)\right]\end{Bmatrix}$$

The anisotropy tensor: $\langle A\rangle=\varepsilon\begin{pmatrix}\frac{(3m+2)}{(1+2\sqrt{2})(m+1)} & 0\\ 0 & \frac{(2m+1)}{(1+2\sqrt{2})(m+1)}\end{pmatrix}$,

where, $\varepsilon = \dfrac{(m+1)(1+2\sqrt{2})\pi R^2}{\frac{L}{2}\times W} = \dfrac{(n+1)(1+2\sqrt{2})\pi R^2}{L\times W}$.

Anisotropy tensor for β_α^3

Volume of the element: $V_\alpha = L\times\dfrac{L}{2}\times W$

Total volume of the pores inside the elemental volume: $V_\alpha^p = \pi R^2(1+2\sqrt{2})(m+1)L$.

where, $m = \dfrac{n-1}{2}$

TheODF.

$$f(\theta,\phi,\ell) = \frac{4\pi}{(1+2\sqrt{2})(m+1)L}\delta\left(\theta-\frac{\pi}{2}\right)\left\{\begin{aligned}&\delta(\phi)\left[(m+1)\delta(\ell-L)\right]\\&+\delta\left(\phi-\frac{\pi}{4}\right)\left[(m+2)\ell\delta\left(\ell-\sqrt{2}\frac{L}{2}\right)+2\sum_{i=1}^{m}i\,\delta\left(\ell-\frac{\sqrt{2}i}{(m+1)}\frac{L}{2}\right)\right]\\&+\delta\left(\phi-\frac{3\pi}{4}\right)\left[(m+2)\ell\delta\left(\ell-\sqrt{2}\frac{L}{2}\right)+2\sum_{i=1}^{m}i\,\delta\left(\ell-\frac{\sqrt{2}i}{(m+1)}\frac{L}{2}\right)\right]\end{aligned}\right\}$$

The anisotropy tensor. $\langle A\rangle = \varepsilon\begin{pmatrix}\dfrac{(4m+3)}{(1+2\sqrt{2})(m+1)} & 0\\ 0 & \dfrac{(3m+2)}{2(1+2\sqrt{2})(m+1)}\end{pmatrix}$,

where, $\varepsilon = \dfrac{(m+1)(1+2\sqrt{2})\pi R^2}{\frac{L}{2}\times W} = \dfrac{(n+1)(1+2\sqrt{2})\pi R^2}{L\times W}$

Anisotropy tensor for β_α^4

Volume of the element. $V_\alpha = L\times\dfrac{L}{2}\times W$

Total volume of the pores inside the elemental volume $V_\alpha^p = \pi R^2(1+2\sqrt{2})(m+1)L$.

where, $m = \dfrac{n-1}{2}$.

The ODF:

$$f(\theta,\phi,\ell)=\frac{4\pi}{(1+2\sqrt{2})(m+1)L}\delta\left(\theta-\frac{\pi}{2}\right)\left\{\begin{array}{l}\delta(\phi)\left[2(m+1)\ell\delta\left(\ell-\frac{L}{2}\right)\right]\\ +\delta\left(\phi-\frac{\pi}{4}\right)\left[(m+2)\ell\delta\left(\ell-\sqrt{2}\frac{L}{2}\right)+2\sum_{i=1}^{m}\ell\delta\left(\ell-\frac{\sqrt{2}i}{(m+1)}\frac{L}{2}\right)\right]+\\ \delta\left(\phi-\frac{3\pi}{4}\right)\left[(m+2)\ell\delta\left(\ell-\sqrt{2}\frac{L}{2}\right)+2\sum_{i=1}^{m}\ell\delta\left(\ell-\frac{\sqrt{2}i}{(m+1)}\frac{L}{2}\right)\right]\end{array}\right\}$$

The anisotropy tensor: $\langle A\rangle=\varepsilon\begin{pmatrix}\frac{(5m+4)}{2(1+2\sqrt{2})(m+1)} & 0\\ 0 & \frac{(3m+2)}{(1+2\sqrt{2})(m+1)}\end{pmatrix}$,

where, $\varepsilon=\frac{(m+1)(1+2\sqrt{2})\pi R^2}{\frac{L}{2}\times W}=\frac{(n+1)(1+2\sqrt{2})\pi R^2}{L\times W}$.

ORIENTATION.11 (O11)

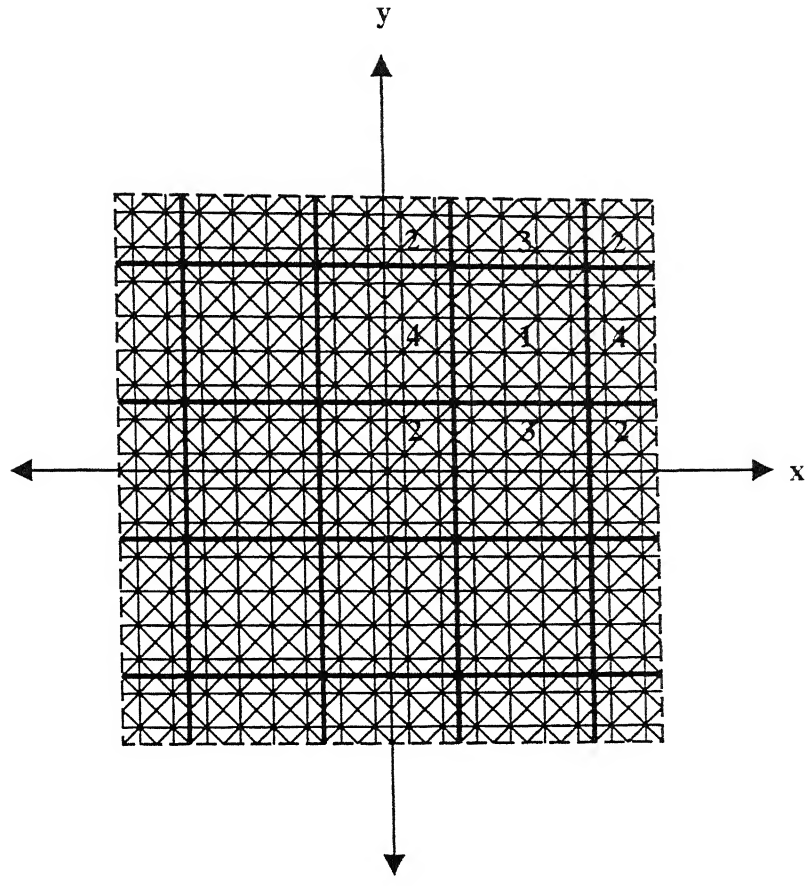

Fig. D.11: Schematic diagram of alignment of pore network in O11 $\phi = 0^0, 45^0, 90^0$ and 135^0.

Anisotropy tensor for β_α^1

Volume of the elemental volume is $V_\alpha = L \times L \times W$ and total volume of the pores in the elemental volume is $V_\alpha^p = \left(2+2\sqrt{2}\right)(n+1)\pi R^2 L$, where n represents the number of pores oriented at an angle of $\phi = 45^0$ or 135^0,below the either diagonal and (n+1) are the pores parallel to each axis.

The ODF:

$$f(\theta,\phi,\ell)=\frac{4\pi}{2\left(1+\sqrt{2}\right)(n+1)L}\delta\left(\theta-\frac{\pi}{2}\right)\left\{\begin{array}{l}\delta(\phi)\left[(n+1)\ell\delta(\ell-L)\right]+\delta\left(\phi-\frac{\pi}{2}\right)\left[(n+1)\ell\delta(\ell-L)\right]+\\ \delta\left(\phi-\frac{\pi}{4}\right)\left[\ell\delta\left(\ell-\sqrt{2}L\right)+2\sum_{i=1}^{n}\ell\delta\left(\ell-\frac{\sqrt{2}i}{(n+1)}L\right)\right]+\\ \delta\left(\phi-\frac{3\pi}{4}\right)\left[\ell\delta\left(\ell-\sqrt{2}L\right)+2\sum_{i=1}^{n}\ell\delta\left(\ell-\frac{\sqrt{2}i}{(n+1)}L\right)\right]\end{array}\right\}$$

The anisotropy tensor $\langle A\rangle=\varepsilon\begin{pmatrix}\frac{(3n+2)}{2\left(1+\sqrt{2}\right)(n+1)} & 0\\ 0 & \frac{(3n+2)}{2\left(1+\sqrt{2}\right)(n+1)}\end{pmatrix}$

Where, $\varepsilon=\frac{(n+1)2\left(1+\sqrt{2}\right)\pi R^2}{L\times W}$

Anisotropy tensor for β_α^2

Volume of the element. $V_\alpha=\frac{L}{2}\times\frac{L}{2}\times W$

Total volume of the pores inside the elemental volume: $V_\alpha^p=\pi R^2\left(2+2\sqrt{2}\right)(m+1)\frac{L}{2}$,

where, $m=\frac{n-1}{2}$.

The ODF:

$$f(\theta,\phi,\ell)=\frac{4\pi}{2\left(1+\sqrt{2}\right)(m+1)\frac{L}{2}}\delta\left(\theta-\frac{\pi}{2}\right)\left\{\begin{array}{l}\delta(\phi)\left[(m+1)\ell\delta\left(\ell-\frac{L}{2}\right)\right]+\delta\left(\phi-\frac{\pi}{2}\right)\left[(m+1)\ell\delta\left(\ell-\frac{L}{2}\right)\right]+\\ \delta\left(\phi-\frac{\pi}{4}\right)\left[\ell\delta\left(\ell-\sqrt{2}\frac{L}{2}\right)+2\sum_{i=1}^{m}\ell\delta\left(\ell-\frac{\sqrt{2}i}{(m+1)}\frac{L}{2}\right)\right]+\\ \delta\left(\phi-\frac{3\pi}{4}\right)\left[\ell\delta\left(\ell-\sqrt{2}\frac{L}{2}\right)+2\sum_{i=1}^{m}\ell\delta\left(\ell-\frac{\sqrt{2}i}{(m+1)}\frac{L}{2}\right)\right]\end{array}\right\}$$

The anisotropy tensor. $\langle A\rangle=\varepsilon\begin{pmatrix}\frac{(3m+2)}{2\left(1+\sqrt{2}\right)(m+1)} & 0\\ 0 & \frac{(3m+2)}{2\left(1+\sqrt{2}\right)(m+1)}\end{pmatrix}$,

where, $\varepsilon = \dfrac{(m+1)2(1+\sqrt{2})\pi R^2}{\frac{L}{2}\times W} = \dfrac{(n+1)2(1+\sqrt{2})\pi R^2}{L\times W}$.

Anisotropy tensor for β_α^3

Volume of the element: $V_\alpha = L\times\dfrac{L}{2}\times W$

Total volume of the pores inside the elemental volume: $V_\alpha^p = \pi R^2(2+2\sqrt{2})(m+1)L$,

where, $m = \dfrac{n-1}{2}$.

The ODF:

$$f(\theta,\phi,\ell) = \frac{4\pi}{2(1+\sqrt{2})(m+1)L}\delta\left(\theta-\frac{\pi}{2}\right)\left\{\begin{array}{l}\delta(\phi)\left[(m+1)\ell\delta(\ell-L)\right]+\delta\left(\phi-\frac{\pi}{2}\right)\left[2(m+1)\ell\delta\left(\ell-\frac{L}{2}\right)\right]+\\ \delta\left(\phi-\frac{\pi}{4}\right)\left[(m+2)\ell\delta\left(\ell-\sqrt{2}\frac{L}{2}\right)+2\sum_{i=1}^{m}\ell\delta\left(\ell-\frac{\sqrt{2}i}{(m+1)}\frac{L}{2}\right)\right]+\\ \delta\left(\phi-\frac{3\pi}{4}\right)\left[(m+2)\ell\delta\left(\ell-\sqrt{2}\frac{L}{2}\right)+2\sum_{i=1}^{m}\ell\delta\left(\ell-\frac{\sqrt{2}i}{(m+1)}\frac{L}{2}\right)\right]\end{array}\right\}$$

The anisotropy tensor $\langle A\rangle = \varepsilon\begin{pmatrix}\dfrac{(4m+3)}{2(1+\sqrt{2})(m+1)} & 0\\ 0 & \dfrac{(5m+4)}{4(1+\sqrt{2})(m+1)}\end{pmatrix}$,

where, $\varepsilon = \dfrac{(m+1)2(1+\sqrt{2})\pi R^2}{\frac{L}{2}\times W} = \dfrac{(n+1)2(1+\sqrt{2})\pi R^2}{L\times W}$.

Anisotropy tensor for β_α^4

Volume of the element: $V_\alpha = L\times\dfrac{L}{2}\times W$

Total volume of the pores inside the elemental volume: $V_\alpha^p = \pi R^2(2+2\sqrt{2})(m+1)L$,

where,. $m = \dfrac{n-1}{2}$

The ODF

$$f(\theta,\phi,\ell)=\frac{4\pi}{2\left(1+\sqrt{2}\right)(m+1)L}\delta\left(\theta-\frac{\pi}{2}\right)\begin{cases}\delta(o)\left[2(m+1)\delta\left(\ell-\frac{L}{2}\right)+\delta\left(o-\frac{\pi}{2}\right)\left[(m+1)\delta(\ell-L)\right]-\right.\\ \delta\left(\phi-\frac{\pi}{4}\right)\left[(m+2)\delta\left(\ell-\sqrt{2}\frac{L}{2}\right)+2\sum_{i=1}^{\tilde{}}\ell\delta\left(\ell-\frac{\sqrt{2}i}{(m+1)}\frac{L}{2}\right)\right]+\\ \left.\delta\left(\phi-\frac{3\pi}{4}\right)\left[(m+2)\delta\left(\ell-\sqrt{2}\frac{L}{2}\right)+2\sum_{i=1}^{m}\ell\delta\left(\ell-\frac{\sqrt{2}i}{(m+1)}\frac{L}{2}\right)\right]\right\}$$

The anisotropy tensor: $\langle A\rangle=\varepsilon\begin{pmatrix}\frac{(5m+4)}{4\left(1+\sqrt{2}\right)(m+1)} & 0\\ 0 & \frac{(4m+3)}{2\left(1+\sqrt{2}\right)(m+1)}\end{pmatrix}$,

where, $\varepsilon=\frac{(m+1)2\left(1+\sqrt{2}\right)\pi R^2}{\frac{L}{2}\times W}=\frac{(n+1)2\left(1+\sqrt{2}\right)\pi R^2}{L\times W}$

LIST OF REFERENCES

1 W. J. Lackey and T. L Starr, "Fabrication of fiber reinforced ceramic composites by chemical vapor infiltration: Processing, Structure and properties." pp. 397-450 in fiber reinforced composites. Edited by K. S Mazdiyansi Noyes publications. Park Ridge, NJ, 1990.

2. P. J. Lamicq, G. A Benhart, M. M. Dauchier, and J. G. Mace, "SiC SiC composite ceramics," Am. Ceram. Bull. Vol. 65, No 2, 1986, pp. 336-338

3. E. Fitzer and R Gadow, "Fiber reinforced Silicon carbide," Ceram Bull Vol 65, No 2, 1986, pp. 326-335.

4 R Naslain, F Langlais, and R. Fedou, "The CVI-processing of ceramic matrix composities," J De Physique, Colloque C5, supplement au n^0 5, Tome 50, 1989, pp. c5-191-c5-207.

5. G. S. Fishman and W. T. Petuskey, "Thermodynamic analysis and kinetic implications of chemical vapor deposition of SiC from Si-C-Cl-H gas system," J Am. Ceram. Soc. Vol. 68, No. 4, 1985, pp. 185-190.

6. Fitzer, W. Remmele, and S. Schoch, "Preparation of SiC-whiskers reinforced cvd-SiC," J. De Physique, Colloque C5, supplement au n^0 5, Tome 50, 1989, pp. c5-209-c5-217.

7. R. D. Veltri, D. A. Condit, and F S. Galasso, "Chemical vapor deposited SiC matrix composites," J. Am. Ceram. Soc. Vol. 72, No. 3, 1989, pp. 478-480.

8. T. M Besmann, R. A. Lowden, D. P. Stinton, and T L. Starr, "A method for rapid chemical vapor infiltration of ceramic composites," J. De Physique, Colloque C5, supplement au n^0 5, Tome 50, 1989, pp. c5-229-c5-239.

9. D. P. Stinton, A. J. Caputo, and R. A Lowden, "Synthesis of fiber-reinforced SiC composites by chemical vapor infiltration," Am. Ceram. Bull. Vol. 66, No 2. 1987, pp. 368-372.

10 K Sugiyama and T Nakamura "Pulse CVI of porous carbon," J Mater Sci Letters. Vol 6, 1987, pp 331-333.

11 M Sahimi, G. R. Gavalas, and T. T Tsotsis, "Statistical and continuum models of fluid-solid reactions in porous media," Chem Engng. Sci Vol. 45, No 6, 1990, pp. 1443-1502.

12. S. Reyes and K. F. Jenson, "Estimation of effective coefficients in porous solids based on percolation concepts," Chem Engng Sci Vol 40, No 9, 1985, pp 1723-1734

13. R Landaur, "The electrical resistance of binary metallic mixtures," J App. Phys Vol. 23, No. 7, 1952, pp.779-784.

14. S. Kirckpatrick, "Classical transport in diordered media: Scaling and effective medium theories," Phys. Rev. Lett. Vol. 27, No. 25, 1971, pp. 1722-1725

15. C. K. Harris, "Application of generalised effective-medium theory to transport in porous media," Transport in porus media. Vol. , No. 5, 1990, pp. 517-542.

16. V. N. Burganos and S. V Sotirchos, "Diffuison in pore networks: Effective medium theory and smooth field approximation," AIChe Journal. Vol. 33, No. 10, 1987, pp. 1678-1689.

17. S. V. Sotrichos, "Multicomponent diffusion and convection in capillary structure," AIChe Journal. Vol. 35, No 12, 1989, pp. 1953-1961.

18. P. G. Toledo, H. Ted Davis, and L. E. Scriven, "Transport properties of anisotropic porous media: Effective medium theory," Chem. Engng. Sci. Vol 47, No. 2, 1992, pp. 391-405.

19 B. Evans, III, G M Watson, and E. A. Mason, "Gaseous diffusion in porous media at uniform pressure," J. Chem. Phys Vol. 6, No. 12, 1961, pp 2076-2083

20. E A Mason, and A. P Malinauskas, "Gas transport in porous media, the dusty gas model," Chem. Eng. Monographs No 17, Elsevier Science Publishers, 1983

21 R. Jackson, in Transport in porous catalysis, chem. Engng Monographs, Vol 4, 1977.

22 C. Feng and W. E Stewart, "Practical models for isothermal diffusion and flow of gases in porous solids," Ind Eng. Chem. Fundam Vol 12,No. 2, 1973, pp. 143-147.

23. E A. Efthimiadis and S. V. Sotirchos, "A partially overlapping grain model for gas-solid reactions," Chem. Engng. Sci. Vol 48, No 7, 1993, pp 1201-1212.

24. J. Kim, J. Alberto ochoa, and S. Whitaker, "Diffusion in anisotropic porous media," Transport in porous media. Vol , No. 2, 1987, pp. 327-356.

25 M. P Hollewand and L. F Gladden, "Modelling of diffusion and reaction in porous catalyst using a random three-dimensional network model," Chem. Engng Sci. Vol. 47, No. 7, 1992, pp. 1761-1770.

26. M. P. Hollewand and L F. Gladden, "Representation of porous catalyst using random pore networks," Chem. Engng. Sci. Vol. 47, No. 9-11, 1992, pp. 2757-2762.

27. C. Rieckmann and F. J. Keil, "Multicomponent diffusion and reaction in three dimensional network. General kinetics," Ind Eng. Chem Res. Vol. 36, 1997, pp. 3275-3281.

28. B. Fuertes and G. Marban, "Modelling gasification reactions including the percolation phenomenon," Chem. Engng. Sci. Vol. 49, No. 22, 1994, pp. 3813-3821.

29 L. Zhang and N. A. Seaton, "The application of continuum equation to diffusion and reaction in pore networks," Chem. Engng. Sci Vol 49, No 1, 1994, pp 41-50

30 P. Rajniak and R. T. Yang, "Unified network model for diffusion of condensable vapors in porous media," AIChe Journal. Vol. 42, No 2, 1996, pp. 319-329

31 S M. Gupte and J. A Tsamopoulos, "Densification of porous materials by chemical vapor infiltration," J Electrochem. Soc. Vol 136, No 2, 1989, pp. 555-561.

32 G. Q Lu, "Modelling the densification of porous structures in CVI ceramic composites processing," Journal of Materials Processing Technology, Vol 37, 1993, pp. 487-498.

33. G. Y. Chung, B. J. McCoy, and M. Smith, "Chemical vapor infiltration: Modelling solid matrix deposition for ceramic composites reinforced with layered woven fabrics," Chem Engng. Sci. Vol. 47, No. 2, 1992, pp. 311-323.

34. D. Gupta and J. W. Evans, "Mathematical model for chemical vapor infiltration in a microwave-heated preform," J. Am. Ceram. Soc Vol. 76, No 8, 1993, pp. 1924-1929.

35. M. Kawasa, Y. Ikuta, T. Tago, Takao Masuda, and Kenji Hashimoto, "Modelling of a thermal-gradient chemical vapor iniltration process for production of silicon carbide whisker/Alumina composite," Chem. Engng Sci. Vol. 49, No. 24A, 1994, pp. 4861-4870.

36. H. Chang, T. F. Morse, and B. W. Sheldon, "Minimizing infiltration time during isothermal chemical vapor inilftration with methyltrichlorosilane," J. Am. Ceram. Soc. Vol. 80, No.7, 1997, pp. 1805-1811.

37. N. Tai, T Chou, and C M Ma, "Effects of deposition mechanisms in the modeling of Forced-flow /temperature –gradient chemical vapor infiltration." J Am. Ceram. Soc Vol. 77, No. 3, 1994, pp. 849-851

38 J Y Ofori and S. V Sotirchos, "Multicomponent mass transport in chemical vapor infiltration," Ind Eng. Chem. Res. Vol. 35, 1996, pp 1275-1287

39. J. Y Ofori and S V. Sotirchos, "Multidimensional modeling of chemical vapor infiltration. application to isobaric CVI," Ind. Eng. Chem. Res Vol. 36, 1997, pp 357-367.

40. J. Y. Ofori and S. V. Sotirchos, "Optimal pressure and temperature for isobaric, isothermal chemical vapor infiltration," AIChe Journal Vol 42, No 10, 1996, pp 2828-2840.

41. J. Y. Ofori and S. V. Sotirchos, "Structural model effects on the predication of chemical vapor infiltration models," J. Electrochem Soc. Vol. 143, No. 6, 1996, pp. 1962-1973.

42 J. O. Herschfelder, C. F. Curtiss and R. B Bird, in Molecular Theory of Gases and Liquids, John Wiley, New York, 1964.

43. R. B. Bird, W. E. Stewart, and E. N. Lightfoot, in Transport Phenomena, Wiley, New York, 1960.

44. J. W. Evans and D.Gupta, " Mathematical modelling of the production of composites by CVI," in Materials Processing in computer Age, Ed. V. R Voller, M. S. Stachowicz and B. G. Thomas, Proceedings Of Int. Symp. Sponsered by TMS, Feb 17 – Feb – 21, 1991, New Orleans, pp 111-122

A 130847

Date Slip

This book is to be returned on the date last stamped.